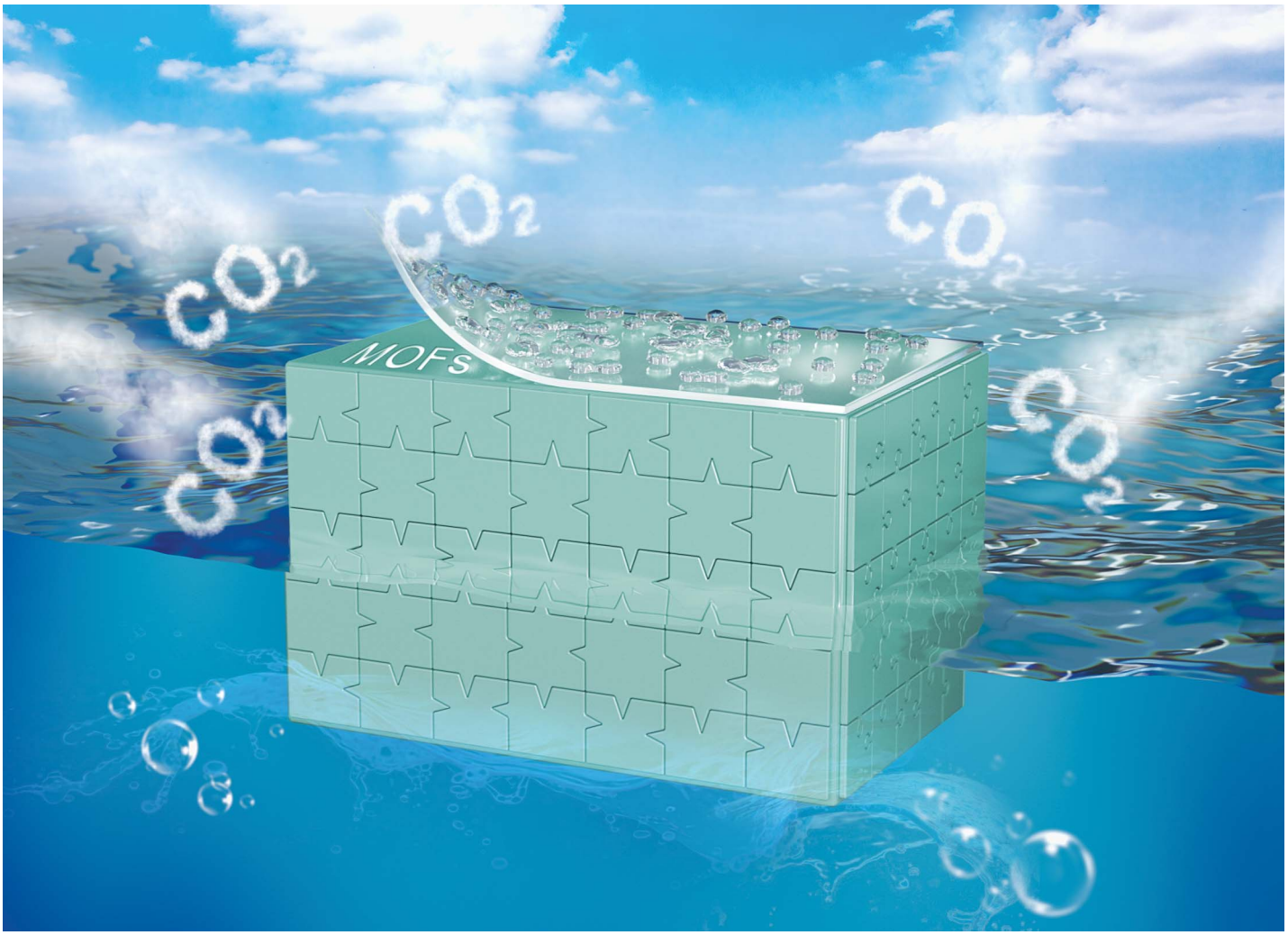

Showcasing research from Professor Hong's laboratory, Fujian Institute of Research on the Structure of Matter, Chinese Academy of Sciences, China.

Water-stable metal-organic frameworks (MOFs): rational construction and carbon dioxide capture

To prepare water-stable MOFs, several important strategies such as increasing the bonding strength of building units and introducing hydrophobic units have been proposed. Many water-stable MOFs have been prepared for capturing carbon dioxide in various scenarios, including flue gas decarbonization, direct air capture, and purified crude natural gas. Here, the design and synthesis of water-stable MOFs, as well as their applications in carbon capture are highlighted.

As featured in:

See Qihui Chen, Maochun Hong *et al.*, *Chem. Sci.*, 2024, **15**, 1570.

ROYAL SOCIETY OF CHEMISTRY

rsc.li/chemical-science

Registered charity number: 207890

Chemical Science

ROYAL SOCIETY OF CHEMISTRY

REVIEW

View Article Online
View Journal | View Issue

Cite this: *Chem. Sci.*, 2024, **15**, 1570

Water-stable metal–organic frameworks (MOFs): rational construction and carbon dioxide capture

Cao Xiao,[ab] Jindou Tian,[a] Qihui Chen *[ab] and Maochun Hong *[ab]

Received 13th November 2023
Accepted 3rd January 2024

DOI: 10.1039/d3sc06076d

rsc.li/chemical-science

Metal–organic frameworks (MOFs) are considered to be a promising porous material due to their excellent porosity and chemical tailorability. However, due to the relatively weak strength of coordination bonds, the stability (*e.g.*, water stability) of MOFs is usually poor, which severely inhibits their practical applications. To prepare water-stable MOFs, several important strategies such as increasing the bonding strength of building units and introducing hydrophobic units have been proposed, and many MOFs with excellent water stability have been prepared. Carbon dioxide not only causes a range of climate and health problems but also is a by-product of some important chemicals (*e.g.*, natural gas). Due to their excellent adsorption performances, MOFs are considered as a promising adsorbent that can capture carbon dioxide efficiently and energetically, and many water-stable MOFs have been used to capture carbon dioxide in various scenarios, including flue gas decarbonization, direct air capture, and purified crude natural gas. In this review, we first introduce the design and synthesis of water-stable MOFs and then describe their applications in carbon dioxide capture, and finally provide some personal comments on the challenges facing these areas.

1. Introduction

Metal–organic frameworks (MOFs) are a kind of organic–inorganic hybrid material with intramolecular pores formed by coordination self-assembly of organic ligands and metal ions/clusters.[1] Compared with traditional porous materials (such as porous carbons and zeolite molecular sieves), the pore size and pore surface of MOFs can be precisely regulated by reasonable design of building elements and modification of pores.[2–17] In addition, the structure of MOFs is long-range ordered, which enables the structure–activity relationships of MOFs easy to be revealed by single crystal X-ray diffraction (SCXRD).[18–21] In this context, MOFs have been widely used in various fields, such as gas adsorption and separation,[22–37] pollutant capture,[38–40] electrical/ionic conduction,[41–43] selective recognition,[44–46] and heterogeneous catalysis.[47–50] At the initial stage, scientists mainly focused on the synthesis of MOFs with novel structures and the exploration of new functions of MOFs. However, if MOFs are to be used in the real world as practical materials rather than just as potential materials, they must meet the requirements of practical applications, such as economy, processability and stability.[51] Given the ubiquity of water vapor in the real world, water stability is the first hurdle to be overcome in the practical applications of MOFs. Over the past

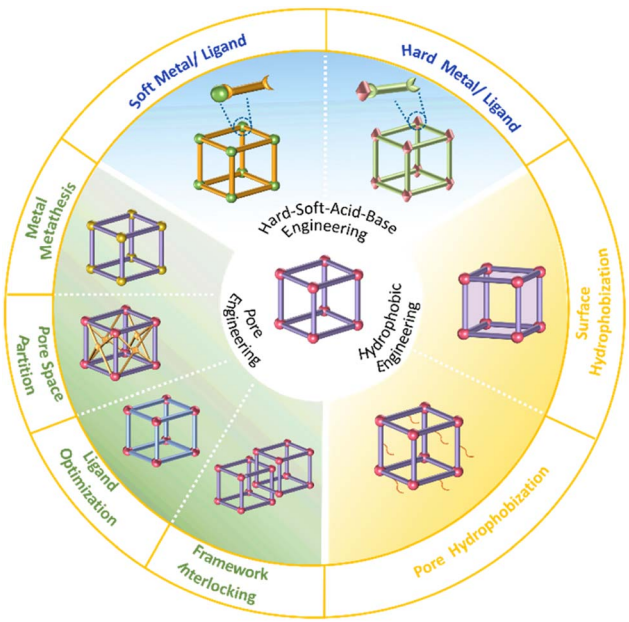

Scheme 1 Water stable MOFs based on different strategies. (a) Hard–Soft-Acid–Base engineering (direct preparation of water stable MOFs from hardness matching metals and ligands). (b) Pore engineering (improving the water stability of MOFs through pore modification, including metal metathesis, pore space partition, ligand optimization, and framework interlocking). (c) Hydrophobic engineering (improving the water stability of MOFs through introducing hydrophobic units, including pore hydrophobization and surface hydrophobization).

[a]*State Key Laboratory of Structural Chemistry, Fujian Institute of Research on the Structure of Matter, Chinese Academy of Sciences, Fuzhou, 350002, P. R. China. E-mail: chenqh@fjirsm.ac.cn; hmc@fjirsm.ac.cn*

[b]*University of Chinese Academy of Sciences, Beijing, 100049, P. R. China*

Table 1 Summary of the water stability of some representative MOFs[a]

MOFs	Metal	Ligands	Testing condition	Time	Ref.
MIL-101(Cr)	Cr(III)	BDC	Aqueous solution (pH = 0–12)	2 months	76
MIL-101(Fe)	Fe(III)	BDC	Aqueous solution (pH = 1–12)	1 day	77
MIL-53(Cr)	Cr(III)	BDC	Water 0.07 M HCl aqueous solution 0.07 M NaOH aqueous solution	2 days	78
MIL-53(Al)	Al(III)	BDC	Water Aqueous solution (pH = 4–12)	2 months 3 days	78
In_2S_3@MIL-101	Cr(III)	BDC	Water Aqueous solution (pH = 3–8)	—	79
NH_2-MIL-53(Al)	Al(III)	BDC-NH_2	Water Aqueous solution (pH = 4, 12)	2 months	80
MIL-101-Fe-NH_2	Fe(III)	BDC-NH_2	Aqueous solution (pH = 1–12)	1 day	81
MIL-100(Cr)	Cr(III)	BTC	Water	12 months	82
MIL-100(Fe)	Fe(III)	BTC	Water	—	83
MIL-100(Al)	Al(III)	BTC	Water	—	84
BUT-18	Al(III)	H_3CTTA	Water, boiling water Aqueous solution (pH = 1) Aqueous solution (pH = 10)	24 h	85
BUT-8(Cr)	Cr(III)	$H_2NDC(SO_3H)_2$	10 M H_2SO_4 aqueous solution Concentrated HCl solution	1 week	86
UiO-66	Zr(IV)	BDC	Aqueous solution (pH = 0–12)	2 months	87
NH_2-UiO-66	Zr(IV)	BDC	Water 12 M HCl and 16 M HNO_3	2 months	80
UiO-67	Zr(IV)	BPDC	Water Aqueous solution (pH = 4) Aqueous solution (pH = 12)	2 months 3 days 2 months	87
UiO-67-4Me	Zr(IV)	BPDC-4Me	Water Aqueous solution (pH = 2, 12) at 80 °C	14 days	88
UiO-67-4Me–NH_2-38%	Zr(IV)	H_2DABPDC	Water Aqueous solution (pH = 2, 12) at 80 °C	14 days	88
PCN-56(Zr)	Zr(IV)	TPDC-2CH_3	Aqueous solution (pH = 2) Aqueous solution (pH = 11)	2 days 1 day	89
PCN-57(Zr)	Zr(IV)	TPDC-4CH_3	Aqueous solution (pH = 2) Aqueous solution (pH = 11)	4.5 days 2 days	89
PCN-58(Zr)	Zr(IV)	TPDC-2CH_2N_3	Water Aqueous solution (pH = 2) Aqueous solution (pH = 11)	24 h 24 h 15 h	89
PCN-59(Zr)	Zr(IV)	TPDC-4CH_2N_3	Water Aqueous solution (pH = 2) Aqueous solution (pH = 11)	72 h 20 h 24 h	89
PCN-223	Zr(IV)	H_2TCPP	Aqueous solution (pH = 0–10)	24 h	90
PCN-225(Zr)	Zr(IV)	H_2TCPP	Boiling water Aqueous solution (pH = 0–12)	12 h	146
PCN-228(Zr)	Zr(IV)	H_4TCP-1	Water Aqueous solution (pH = 0) Aqueous solution (pH = 12)	1 day	91
PCN-229(Zr)	Zr(IV)	H_4TCP-2	Water Aqueous solution (pH = 0) Aqueous solution (pH = 12)	1 day	91
PCN-230(Zr)	Zr(IV)	H_4TCP-2	Aqueous solution (pH = 0–12)	1 day	91
OPA-PCN-222(Zr)	Zr(IV)	H_2TCPP	Water Aqueous solution (pH = 11)	1 month 7 days	92
BUT-12	Zr(IV)	H_3CTTA	Boiling water HCl solutions (2 M, 6 M, and concentrated HCl) Aqueous solution (pH = 10)	24 h	93
BUT-13	Zr(IV)	H_3TTNA	Boiling water HCl solutions (2 M, 6 M, and concentrated HCl) Aqueous solution (pH = 10)	24 h	93
BUT-14	Zr(IV)	BCQD	Boiling water Concentrated HCl aqueous solution Aqueous solution (pH = 10)	48 h	94

Table 1 (*Contd.*)

MOFs	Metal	Ligands	Testing condition	Time	Ref.
BUT-15	Zr(IV)	PBPTT	Boiling water Concentrated HCl aqueous solution Aqueous solution (pH = 10)	48 h	94
BUT-17	Zr(IV)	H_4CPTTA	Boiling water Concentrated HCl aqueous solution Aqueous solution (pH = 12)	—	95
BUT-44	Zr(IV)	H_4BTEB	Water Aqueous solution (pH = 10) Aqueous solutions (1 M HCl)	72 h 1 day 1 day	96
BUT-66	Zr(IV)	H_2BDB	Water Aqueous solution (pH = 1–10)	1 month	97
BUT-67	Zr(IV)	H_2NDB	Water Aqueous solution (pH = 1–10)	48 h	97
MOF-808	Zr(IV)	BTC	Boiling water	24 h	98
NU-1100	Zr(IV)	L_4H H_2BPDC	Water	24 h	99
ISO-NU-1000	Zr(IV)	H_4TBAPy-2	Water	24 h	100
MIP-207	Ti(IV)	BTC	Water	3 days	101
MIP-208	Ti(IV)	5-Aa-IPA	Boiling water Aqueous solution (pH = 0–10)	8 h	102
BUT-172	In(III)	H_3CTTA	Boiling water Aqueous solution (pH = 3, 10)	1 day	103
BUT-173	In(III)	H_3CTTA	Water Aqueous solution (pH = 3, 10)	1 day	103
In(tcpp)	In(III)	H_4TCPP	Aqueous solution (pH = 2, 12) Water	24 h	104
USTC-8(In)	In(III)	H_2TCPP	Aqueous solution (pH = 0–11)	12 h	105
Y-BTC	Y(III)	BTC	Water	—	106
Y-pek-MOF-1	Y(III)	BTBA	Water at 85 °C	24 h	107
$[(CH_3)_2NH_2]_2[Tb_6(\mu_3\text{-}OH)_8(FTZB)_6(H_2O)_6]\cdot(H_2O)_{22}$	Y(III)	H_2FTZB	Water	24 h	108
Tb-BTC	Tb(III)	H_2FTZB	Water	—	106
Tb-pek-MOF-1	Tb(III)	BTBA	Water at 85 °C	24 h	107
$[(CH_3)_2NH_2]_2[Y_6(\mu_3\text{-}OH)_8(FTZB)_6(H_2O)_6]\cdot(H_2O)_{52}$	Tb(III)	H_2FTZB	Water	24 h	108
La-BTN	La(III)	H_3BTN	Water Aqueous solution (pH = 2) at 100 °C Aqueous solution (pH = 12)	1 day	109
La-BTB	La(III)	H_3BTB	Water at 60 °C and 100 °C Aqueous solution (pH = 2–14)	3 days	110
Eu-1,4-NDC-fcu-MOF	Eu(III)	1,4-H_2NDC	Boiling water Aqueous solution (pH = 3.5–10)	24 h	111
PCN-202	Ni(II)	1,4-H_2NDC	Aqueous solution (pH = 12)	1 day	112
PCN-600(Fe)	Fe(III)	1,4-H_2NDC	Aqueous solution (pH = 2–11)	24 h	113
ZIF-8/MAF-4	Zn(II)	MeIM	Boiling water	7 days	114 and 115
MAF-23	Zn(II)	H_2btm	Water	7 days	116
MAF-stu-1	Zn(II)	H_2imPim	Boiling water Aqueous solution (pH = 2, 11)	9 days	117
Zn(1,4-BDP)	Zn(II)	1,4-BDP	Water at 40 °C	—	118
Zn(1,3-BDP)	Zn(II)	1,3-BDP	Boiling water	3 days	118
ZIF-11	Zn(II)	bIM	Water	7 days	119
ZIF-61	Zn(II)	IM, MeIM	Boiling water	7 days	120
ZIF-68	Zn(II)	bIm, nIM	Boiling water	7 days	120
ZIF-69	Zn(II)	cbIM, nIM	Boiling water	7 days	120
ZIF-70	Zn(II)	IM, nIM	Boiling water	7 days	120
ZIF-90	Zn(II)	ICA	Water	7 days	120
ZIF-67	Co(II)	MeIM	Boiling water	7 days	120
MFU-1	Co(II)	H_2bdpb	Water	6 months	121
MAF-X27-Cl	Co(II)	H_2bbta	Acidic solution (0.001 M HCl) Alkaline solution (1.0 M KOH)	1 week	122
FJI-H30	Co(II)	TPMA	Water Aqueous solution (pH = 2–12)	5 days	123

Table 1 (*Contd.*)

MOFs	Metal	Ligands	Testing condition	Time	Ref.
ZJU-75	Co(II)	pyz-NH_2	Water Aqueous solution (pH = 1–12)	3 days	124
Co-btz-ht	Co(II)	btz	Aqueous solution (pH = 1–12)	20 h	125
PCN-601	Ni(II)	H_4TPP	Saturated NaOH solution at 100 °C 0.1 mM HCl aqueous solution	24 h	126
PCN-602(Ni)	Ni(II)	H_4TPPP	0.1 mM HCl aqueous solution 1 M NaOH aqueous solution	24 h	127
$Ni_3(BTP)_2$	Ni(II)	H_3BTP	Boiling water Boiling aqueous solution (pH = 2–14)	2 weeks	128
Ni-btz-ht	Ni(II)	btz	Aqueous solution (pH = 1–12)	20 h	125
BUT-32	Ni_4 clusters	H_3TPTA	Boiling water Aqueous solution (pH = 3) NaOH aqueous solution (4 M)	24 h	129
BUT-33	Ni_4 clusters	H_3TPTA	Boiling water Aqueous solution (pH = 3) NaOH aqueous solution (4 M)	24 h	129
Cu-BTTri	Cu(II)	H_3BTTri	Boiling water Aqueous solution (pH = 3)	3 days 1 day	130
MAF-2	Cu(I)	Hetz	Water	—	131
MAF-41	Cu(I)	H_2fbdim	Water Boiling water Aqueous solution (pH = 3–14)	One week One week 3 days	132
Cu_2TBPZ	Cu(I)	TBPZ	Water Aqueous solution (pH = 3, 12)	24 h	133
$[Ag_2(o\text{-Hmpba})_2(o\text{-}H_2mpba)_2]$	Ag(I)	*o*-H_2mpba	Water Aqueous solution (pH = 2–13)	8 months 1 week	135
FJI-H14	Cu(II)	H_2BTTA	Aqueous solution (pH = 2–12) at 100 °C	24 h	136
FJI-H25Fe	Fe(III)	H_2BTTA	Aqueous solution (pH = 8–12)	—	137
FJI-H29	Zn(II)	H_2DTBDA	Water Aqueous solution (pH = 2–13)	2 days	138
$[Zn_4(\mu_4\text{-O})\text{-}(\mu_4\text{-4-carboxy-3,5-dimethyl-4-carboxy-pyrazolato})_3]$	Zn(II)	H_2dmcapz	Water 0.001 M HNO_3 aqueous solution	—	139
USTC-7	Zn(II)	H_3TZBPDC	Aqueous solution (pH = 2–12)	12 h	140
FJI-H36	Ni(II)	H_2DTBDA	Water Aqueous solution (pH = 2–12)	—	141

[a] Linkers are abbreviated as: BDC = terephthalate; BDC-NH_2 = 2-aminoterephthalate; BTC = benzene-1,3,5-tricarboxylate; $H_2NDC(SO_3H)_2$ = 4,8-disulfonaphthalene-2,6-dicarboxylatlate; H4tcpp = 2,3,5,6-tetrakis(4-carboxyphenyl)pyrazine; BPDC = biphenyl-4,4′-dicarboxylate; BCQD = 5′,5‴-bis(4-carboxyphenyl)-[1,1′:3′,1″:4″,1‴:3‴,1⁗-quinquephenyl]-4,4⁗-dicarboxylate, PBPTT = 4,4′,4″,4‴-(4,4′-(1,4-phenylene)bis(pyridine-6,4,2-triyl)) tetrabenzoate, H_4BTEB = 4,4′,4″,4‴-(benzene-1,2,4,5-tetrayltetrakis(ethyne-2,1-diyl)) tetrabenzoic acid, H_4CPTTA = 5′-(4-carboxyphenyl)-[1,1′:3′,1″-terphenyl]-3,4″,5-tricarboxylic acid, TPDC-$2CH_3$ = 2′,5′-dimethyl-terphenyl-4,4″-dicarboxylic acid, TPDC-$4CH_3$ = 2′,3′,5′,6′-tetramethyl-terphenyl-4,4″-dicarboxylic acid, TPDC-$4CH_2N_3$- = 2′,3′,5′,6′-tetra(azidomethyl)-[1,1′:4′,1″-terphenyl]- 4,4″-dicarboxylate, H_2dmcapz = 3,5-dimethyl-4-carboxypyrazole, H_2TCPP = tetrakis(4-carboxyphenyl)porphyrin, H_3TZBPDC = 4′-(1*H*-tetrazol-5-yl)-[1,1′-biphenyl]-3,5-dicarboxylic acid, Hetz = 3,5-diethyl-1,2,4-triazole, H_2btm = bis(5-methyl-1H-1,2,4-triazol-3-yl)methane; btz = 1,4-bis(4*H*-1,2,4-triazol-4-yl)benzene; H_3BTN = 1,3,5-tri(6-hydroxycarbonylnaphthalen-2-yl)benzene); H_3BTB = 1,3,5-tris(4-carboxyphenyl)benzene); H_2imPim = 2-(1*H*-imidzol-2-yl)-3*H*-imidazo[4,5-*c*]pyridine; 1,4-BDP = 1,4-benzenedi(4′-pyrazolyl); 1,3-BDP = 1,3-benzenedi(4′-pyrazolyl); H_2bdpb = 1,4-bis[(3,5-dimethyl)-pyrazol-4-yl] benzene; H_3BTP = 1,3,5-tris(1*H*-pyrazol-4-yl)benzene; H_3TPTA = 2,4,6-tris(4-(pyrazolate-4-yl)phenyl)-1,3,5-triazine; H_3BTTri = 1,3,5-tris(1*H*-1,2,3-triazol-5-yl)benzene; H_2fbdim = 2,6-ditrifluoromethyl-benzodiimidazole; H_2DTBDA = 3′,5′-di(1*H*-1,2,4-triazol1-yl)-[1,1′-biphenyl]-3,5-dicarboxylic acid; H_3CTTA = dimethyl-5′-(4-(methoxycarbonyl)phenyl)-2′,4′,6′-trimethyl-[1,1′:3′,1″- terphenyl]-4,4″-dicarboxylic acid; BPDC-4Me = 3,3′,5,5′-tetramethyl-1,1′-biphenyl; TPDC-$2CH_2N_3$ = 2′,5′-bis(azidomethyl)-[1,1′:4′,1″-terphenyl]-4,4″-dicarboxylic acid; H_3TTNA = 6,6′,6″-(2,4,6-trimethylbenzene-1,3,5-triyl)tris(2-naphthoic acid)); H_2BDB = [1,1′:3′,1″-terphenyl]-4,4″-dicarboxylic acid; H_4TCPB-Br_2 = (1,4-dibromo-2,3,5,6-tetrakis(4-carboxyphenyl)benzene; BTBA = biphenyl-3,4,5-tricarboxylic acid; H_2FTZB = 2-fluoro-4-(1*H*-tetrazol-5-yl)benzoic acid; 1,4-H_2NDC = 1,4-naphthalenedicarboxylate; MeIM = 2-methyl-1*H*-imidazole; bIM = 1*H*-benzo[*d*]imidazole; IM = 2*H*-imidazole; nIM = 2-nitro-1*H*-imidazole; cbIM = 6-chloro-1*H*-benzo[*d*]imidazole; ICA = imidazolate-2-carboxyaldehyde; H_2bbta = 1*H*,5*H*-benzo(1,2-*d*:4,5-*d*′)bistriazole); TPMA = tris(pyridin4-ylmethyl)amine; pyz-NH_2 = 2-aminopyrazine; H_4TPP = 5,10,15,20-tetra(1*H*-pyrazol-4-yl)porphyrin; H_4TPPP = 5,10,15,20-tetra(pyrazolate-4-yl)porphyrin; TBPZ = 3,3′,5,5′-tetraethyl-4,4′-bipyrazolate; *o*-H_2mpba = 2-(3,5-dimethyl-1H-pyrazol-4-yl)benzoic acid; 1,2,4-TAZT = 1,2,4-triazolate; H_4DH_3PhDC = 2′,5′-dimethyl-3,3″-dihydroxy-[1,1′:4′,1″-terphenyl]-4,4″-dicarboxylic acid; dtp = 3,6-di(4-pyridyl)-1,2,4,5-tetrazine; pyr = pyrazine; HQc = quinoline-5-carboxylic acid; dobpdc = 4,4′-dioxido-3,3′-biphenyldicarboxylate; TABZ = 3,3′,5,5′-tetramethyl-1*H*,1′*H*-4,4′-bipyrazole; F-pymo = 5-fluoropyrimidin-2-olate, HINO = isonicotinic acid N-oxide; H_4TBAPy-2 = 1,2,7,8-tetrakis(*p*-benzoic-acid) pyrene]; L_4H = 4-[2-[3,6,8-tris[2-(4-carboxyphenyl) ethynyl]-pyren-1-yl]ethynyl]-benzoic acid; 5-Aa-IPA = 5-acetamidoisophthalate.

decade, hundreds of water-stable MOFs have been prepared (Scheme 1 and Table 1), such as famous MILs, UiOs, PCNs, BUTs, ZIFs, and MAFs. With the successful synthesis of more and more water-stable MOFs, the understanding of the water stability of MOFs has also been deepened.[52–62] For instance, the selection of suitable metals and ligands with matching softness/

hardness can effectively construct water-stable MOFs, and the introduction of hydrophobic groups into the pores or surfaces of MOFs can further improve their water stability. Recently, a series of water-stable MOFs have been successfully constructed, and a timely summary can provide a guide for the controllable construction of more stable MOFs that can be used in a harsher environment.

The continued increase of atmospheric carbon dioxide (CO_2) has led to a number of serious climate problems, including rising sea levels and rising temperatures. In addition to causing climate change, high levels of atmospheric CO_2 can also cause a range of health problems for humans in confined spaces (*e.g.*, submarines and airplanes). Furthermore, as an undesired concomitant of many important fine chemicals (*e.g.*, natural gas), CO_2 has greatly affected their production and transportation. Therefore, there is an urgent need to develop efficient and economical carbon capture technologies to trap unwanted CO_2 from air and fine chemicals. Due to their high adsorption capacity and relatively low recovery energy, MOFs have proven to be a kind of promising adsorbent for carbon capture and have been widely used in a variety of scenarios, including flue gas decarbonization, direct air capture, and purified natural gas.[63–75]

Considering that water vapor is widely present in flue gas, air, and crude natural gas, a practical MOF-based CO_2 adsorbent should first have good water stability. To date, many water-stable MOFs that can realize efficient CO_2 capture have been reported; and a timely collation of these advances can help scientists design and synthesize MOFs that can be used to capture CO_2 in industry.

In this review, we begin with a brief introduction to the importance of water-stable MOFs and the urgency of carbon capture. Then, the definition of stability (including thermodynamic stability and kinetic stability), synthetic strategies (from universal strategies to specific approaches), and important progress (*e.g.*, classic examples and recent advances) of water-stable MOFs are introduced in detail. In addition, the applications of water-stable MOFs in different scenarios (*e.g.*, flue gas decarbonization, direct air capture, and purified natural gas) are systematically discussed. Finally, some personal comments on the challenges facing these areas are presented. Despite our best efforts, we have only been able to cover a small fraction of the many studies on water-stable MOFs. However, we also hope that our review will provide a useful reference for researchers interested in designing water-stable MOFs for CO_2 capture.

2. Design and synthesis of water-stable MOFs

2.1. The definition and characterization of water stability of MOFs

Water stability is used to describe the extent to which a substance is affected by water, also known as water resistance. With regard to MOFs, their water stability refers to the ability to maintain their structure when exposed to water. For a given MOF, if it is exposed to water for a long time, its ordered structure will not be damaged, and its porous properties can be maintained, and it can be considered water-stable. In this context, the water stability of MOFs is usually evaluated by powder X-ray diffraction (PXRD) tests and gas adsorption experiments; in which PXRD analysis is used to determine whether the ordered structure of MOFs is destroyed, and a gas adsorption experiment is used to evaluate whether the porosity of MOFs is effectively maintained. It must be pointed out that the characterization of the water stability of MOFs is directly related to their application scenarios. For example, the use of MOFs in aqueous solutions may lead to the dissolution of partial MOFs. At this time, other tests (*e.g.*, nuclear magnetic resonance (NMR) and inductive coupled plasma emission spectrometer (ICP)) are needed to accurately evaluate their water stability.

2.2. The thermodynamic stability of MOFs

The hydrolysis of MOFs is a complex chemical transformation, in which the nucleophilic H_2O will attack the electrophilic metal ions, and the incompletely dissociated organic ligands will in turn continue to bond with the metal ions; only after a series of complex reactions, the hydrolytic products which are favourable both in kinetics and thermodynamics will be formed. For a given MOF, its thermodynamic stability to water refers to the ΔG of the hydrolysis reaction (Scheme 2). If the ΔG is greater than 0, then its hydrolysis cannot occur spontaneously and it can be considered water-stable. According to the Gibbs equation $\Delta G = \Delta H - T\Delta S$, if ΔG is to be greater than 0, it must be ensured that ΔH is much greater than 0, because hydrolysis of MOFs is a process of entropy increasing ($\Delta S > 0$). This means that the metal–ligand interactions of a water-stable MOF should be greater than the corresponding metal–oxygen interactions formed by hydrolysis. Thus, only the coordination

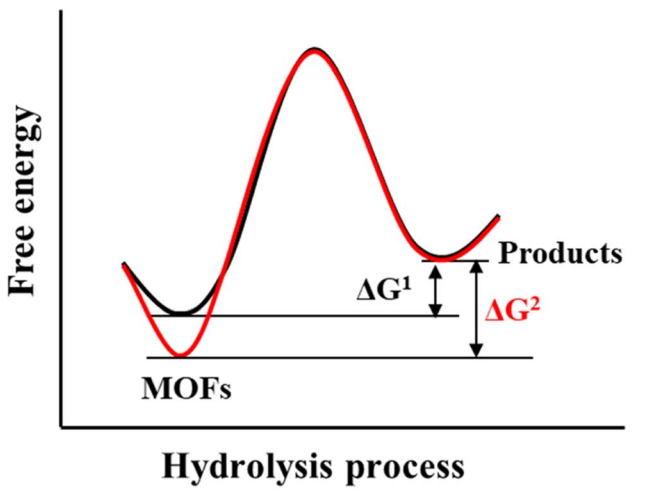

Scheme 2 The definition and optimization of the thermodynamic stability of MOFs to water. Black line represents the thermodynamic stability of a given MOF to water, which refers to the ΔG^1 of the hydrolysis reaction. The red line represents the optimized thermodynamic stability of the MOF through enhancing its bonding strength ($\Delta G^2 > \Delta G^1$).

elements with strong enough interaction (generally greater than the corresponding metal–water interaction) can be used to synthesize water-stable MOFs.

To optimize the thermodynamic stability of MOFs in water, it is necessary to increase the bonding strength of metal ions and organic ligands as much as possible. For any MOF, the organic ligand acts as a Lewis base that provides electrons, while the metal ion acts as a Lewis acid that accepts electrons. According to Hard–Soft-Acid–Base (HSAB) theory, Lewis acids/bases can be divided into three categories, including hard acids/bases, soft acids/bases, and borderline acids/bases. Hard acids/bases refer to particles with a high charge density and small radius, which have low polarizability but high polarity. Soft acids/bases are those particles with a low charge density and large radius, which have high polarizability but low polarity. Thermodynamically stable complexes are preferentially constructed from hard acids and hard bases or from soft acids and soft bases. In this regard, water-stable MOFs can be directly constructed from hard metals (*e.g.*, Al^{3+}, Zr^{4+}, In^{3+}, Ti^{4+}, Hf^{4+}, Fe^{3+}, and Cr^{3+})/ligands (carboxylic acid ligands or other ligands that contain free oxygen atoms) and soft metals (*e.g.*, Zn^{2+} and Cu^{+})/ligands (*e.g.*, imidazolyl derivatives, triazolyl derivatives, and tetrazolyl derivatives). In addition, post-synthesis modification (PSM) can also be used to improve the water stability of the as-prepared MOFs.

2.3. The kinetic stability of MOFs

The thermodynamics of a given reaction can only reveal whether it can occur spontaneously. Whether the reaction can proceed smoothly also depends on its kinetics. For a thermodynamically unstable MOF, the hydrolysis reaction is also difficult to occur if the activation energy of hydrolysis is very high (Scheme 3). Therefore, the kinetic stability of a given MOF to water is related to its hydrolytic activation energy.

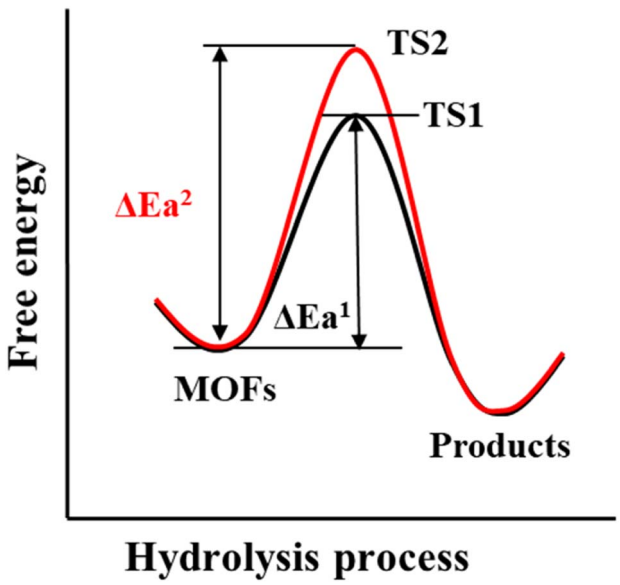

Scheme 3 The definition and optimization of the kinetic stability of MOFs to water. Black line represents the kinetic stability of a given MOF to water, which refers to the ΔEa^1 (activation energy) of its hydrolysis reaction. The red line represents the optimized kinetic stability of the MOF through enhancing its activation energy ($\Delta Ea^2 > \Delta Ea^1$).

To improve the kinetic stability of a MOF to water, the activation energy of hydrolysis should be increased as much as possible. The hydrolysis of the MOF is so complex that its activation energy is difficult to calculate.[142,143] In this case, inhibition of the hydrolysis kinetics of a MOF can only be qualitatively analyzed by reaction rate theory. According to such theory, the hydrolysis reaction of MOFs can be inhibited by preventing the effective collision between H_2O molecules and the metal ions of MOFs. In this regard, introducing enough hydrophobic groups on the surface of a MOF can effectively prevent the contact between H_2O and the MOF. In addition, the introduction of appropriate hydrophobic groups into the pores of MOFs can effectively prevent the diffusion of water in the pores.

2.4. Reported water-stable MOFs

2.4.1. Water-stable MOFs based on hard metal ions/ligands. As described above, water-stable MOFs can be reasonably constructed from hard metal ions and hard ligands, and many water-stable MOFs based on this strategy have been reported. In 2005, Férey and co-workers first reported a water-stable MOF (MIL-101(Cr)) based on μ_3-oxocentered tri-nuclear chromium (Fig. 1g).[76] Due to the strong bond energy of the Cr(III)–O bond, it could remain stable for two months in both strong acid solutions (pH = 0) and strong base solutions (pH = 12). Isomorphic MIL-101(Fe) and MIL-101-Fe–NH_2 based on the same inert Fe–O motifs also showed excellent water/acid/base resistance.[77,81] Then a series of water-stable MOFs (*e.g.*, MIL-53, MIL-100, BUT-18, and BUT-8) based on various hard metal ions (Cr^{3+}, Fe^{3+}, and Al^{3+}) and different carboxylate ligands were synthesized (Fig. 1).[78,82–85] Notably, the framework of BUT-8(Cr) could remain stable even in concentrated H_2SO_4, meaning that BUT-8(Cr) is one of the reported MOFs with the best acid resistance.[86] It could be found that the formation of multiple M–O bonds was beneficial in improving the water stability of MOFs. For MOFs with the same framework, the introduction of substituents such as amine groups on the ligands had little effect on their water stability, but the introduction of In_2S_3 nanoparticles would significantly reduce the chemical stability of the framework. This might be because the polar In_2S_3 facilitated the diffusion of water into the pores of MOFs.[79]

The Zr–O unit with very strong bond energy is another building block that is widely used in the synthesis of water-stable MOFs. UiO-66, as a representative example, constructed from 12-coordinated $Zr_6O_4(OH)_4(CO_2)_{12}$ clusters and linear terephthalic acid (H_2BDC) ligands, was reported by Lillerud and co-workers in 2008 (Fig. 2).[87,145] Due to the extremely strong interactions between Zr^{4+} ions and O anions, UiO-66 not only displayed excellent water/acid/base resistance but also resisted various common organic solvents. Then other water-stable UiO series (*e.g.*, UiO-67 and UiO-68) based on the same strategy were prepared by using other linear carboxylate ligands. Very recently, through the modification of ligands and the mixing of modified ligands, Su's group has achieved the controllable

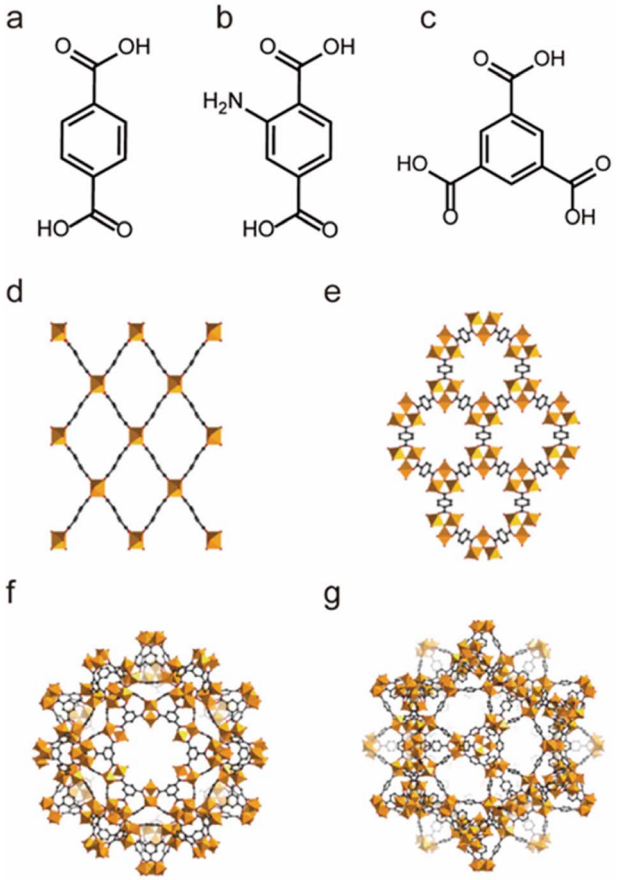

Fig. 1 The structures of the MIL series and the used ligands. (a) The H_2BDC ligand. (b) The H_2BDC-NH_2 ligand. (c) The 1,3,5-BTC ligand. (d) MIL-53. (e) MIL-88. (f) MIL-100. (g) MIL-101. Reproduced from ref. 144 with permission from Wiley, Copyright 2018.

construction of UiO-67-4Me-R_2-x% with excellent acid–base stability and adjustable hydrophilicity and hydrophobicity.[88]

Based on suitable Zr–O clusters and different carboxylate ligands, Zhou's group also reported a series of water-stable MOFs (PCN series) (Fig. 3). They first used single or mixed linear dicarboxylic acids bearing methyl or azide groups (Fig. 3a–c) to prepare three isoreticular MOFs, PCN-56, PCN-57 and PCN-58 with different functional groups.[89] Notably, such as-prepared functionalized MOFs could keep their framework and crystallinity well for a long time in diluted HCl solution (pH = 2) and NaOH solution (pH = 11). Then they synthesized a series of more stable MOFs (PCN-225, PCN-228, PCN-229 and PCN-230) using porphyrin-derived tetracarboxylate ligands and zirconium salts. These newly prepared materials had better acid tolerance and their framework could be stabilized in 1 M HCl solution. This may be because porphyrin groups can also react with hydrogen ions.[91,146,147]

Li's group also prepared a series of water-stable Zr-based MOFs based on suitable polycarboxylate ligands (Fig. 4). All these reported porous materials possessed excellent chemical stability. For example, BUT-17 not only displayed strong stability in boiling water but also resisted concentrated HCl solution and NaOH aqueous solution (pH = 12).[95] Notably,

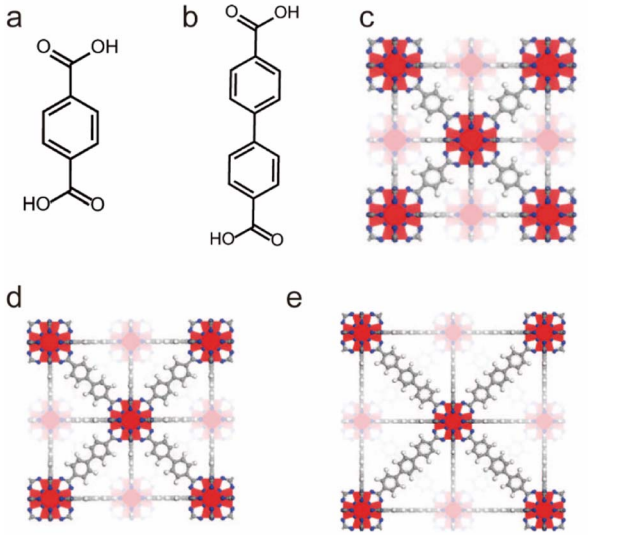

Fig. 2 The structures of the UiO series and the used ligands. (a) The H_2BDC ligand. (b) The H_2BPDC ligand. (c) UiO-66. Reproduced from ref. 87 with permission from the American Chemical Society, Copyright 2008. (d) UiO-67. Reproduced from ref. 87 with permission from the American Chemical Society, Copyright 2008. (e) UiO-68. Reproduced from ref. 87 with permission from the American Chemical Society, Copyright 2008.

several of them (*e.g.*, BUT 12–15 and 17) could resist concentrated HCl, which makes them one of the most acid-resistant MOFs.[93,96,97]

In addition to Zr^{4+}, Ti^{4+} ions can also be used to construct water-stable Ti-based MOFs. Since the ionic radius of Ti^{4+} is smaller than that of Zr^{4+}, it can react with various oxygen-containing ligands more vigorously, making the preparation of crystalline Ti-based MOFs more challenging. Recently, the Serre team used pre-prepared titanium-oxygen clusters (Ti_8AF) to self-assemble with H_3BTC ligands to achieve the controlled synthesis of Ti-MOF (MIP-207) (Fig. 5a and c), which could be stable in water for more than 3 days.[101] By reacting a two-arm carboxylate ligand 5-acetamidoisophthalate (5-Aa-IPA) with Ti_8AF clusters, they synthesized a more stable MOF (MIP-208) (Fig. 5b and d), which could be stable in boiling water and aqueous solutions with pH 0–10, representing the most stable Ti-MOFs reported to date.[102] The enhanced stability was thought to come from the infinite titanium–oxygen chains in its structure.

Besides tetravalent Zr^{4+}/Ti^{4+}, trivalent In^{3+} can also be used to construct water-stable MOFs (Fig. 6).[103–105] Based on tritopic carboxylate ligands, Li *et al.* successfully obtained two isomeric In(III)-MOFs, BUT-172 and BUT-173, which had slightly different three-dimensional (3D) open framework structures but the same secondary building units (SBUs) (Fig. 6a, d and e). These two In(III)-MOFs were highly stable in water at room temperature due to the relatively strong In–O bonds. However, only BUT-172 could maintain its structural integrity in aqueous solutions with pH between 3 and 10 at ambient temperature or in boiling water. Such unusual stability discrepancy may result from their distinct structural symmetries. Using a π-conjugated ligand, tetrakis (4-carboxyphenyl)porphyrin (TCPP), an indium-based

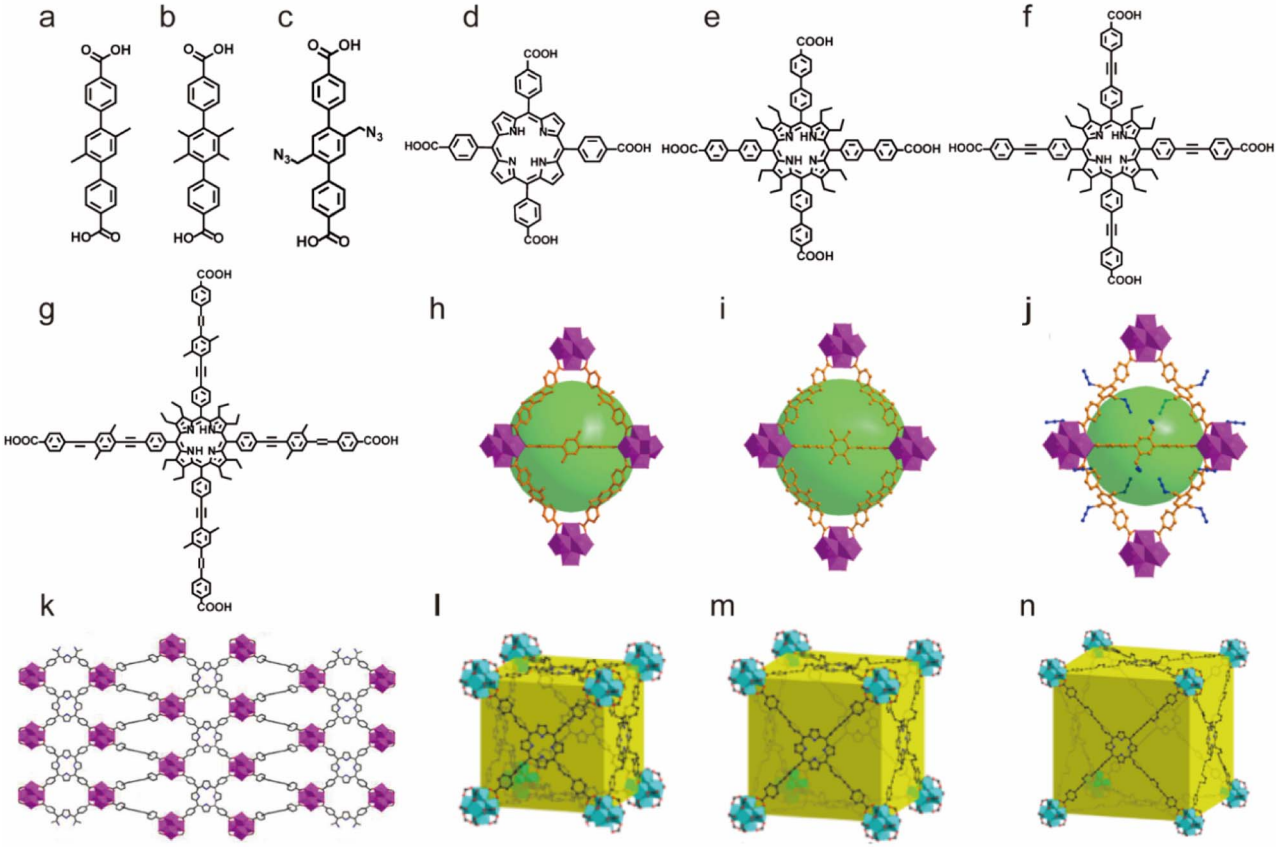

Fig. 3 The structures of the PCN series and the used ligands. (a) The TPDC-2CH_3 ligand. (b) The TPDC-4CH_3 ligand. (c) The TPDC-2CH_2N_2 ligand. (d) The H_2TCPP ligand. (e) The H_4TCP-1 ligand. (f) The H_4TCP-2 ligand. (g) The H_4TCP-3 ligand. (h) PCN-56. Reproduced from ref. 89 with permission from the American Chemical Society, Copyright 2012. (i) PCN-57. Reproduced from ref. 89 with permission from the American Chemical Society, Copyright 2012. (j) PCN-58. Reproduced from ref. 89 with permission from the American Chemical Society, Copyright 2012. (k) PCN-225. Reproduced from ref. 146 with permission from the American Chemical Society, Copyright 2013. (l) PCN-228. Reproduced from ref. 91 with permission from the American Chemical Society, Copyright 2015. (m) PCN-229. Reproduced from ref. 91 with permission from the American Chemical Society, Copyright 2015. (n) PCN-230. Reproduced from ref. 91 with permission from the American Chemical Society, Copyright 2015.

porphyrinic MOF, USTC-8, was successfully synthesized by Jiang's group (Fig. 6c and g).[105] As anticipated, USTC-8 proved its exceptional water stability by maintaining the framework integrity in pH = 1–12 aqueous solutions for 12 h. To detect the pollutant in the aqueous solution, Li's group reported a novel luminous MOF (In(tcpp)) by combining the chromophore ligand 2,3,5,6-tetrakis(4-carboxyphenyl)pyrazine (H_4tcpp) and In(III) salts (Fig. 6b and f).[104] The as-prepared sample could remain stable in water, acidic solution (pH = 2), and alkaline solution (pH = 12), confirming its practicability for detecting pollutants in water.

Due to the high coordination numbers and the strong metal–oxygen interaction, rare-earth (RE) salts are another class of metal ions that are widely used for the synthesis of water-stable MOFs.[148] By employing 1,3,5-benzenetricarboxylate (BTC) as the organic linker, a series of microporous lanthanide-organic framework enantiomers (Y-BTC and Tb-BTC) were prepared by Jiang and co-workers (Fig. 7a and g).[106] The as-synthesized Ln-BTC not only could retain its framework in water but also exhibit excellent thermal stability (450 °C). Kitagawa's group synthesized a La(III)-framework (La-BTB) based on the H_3BTB (H_3BTB = 1,3,5-tris(4-carboxyphenyl)benzene) ligand (Fig. 7e and i), and it could maintain its framework integrity even after being soaked in boiling water, in hot (60 °C) HCl solution (pH = 2) and NaOH solution (pH = 14) for three days.[110] Based on the 1,3,5-tri(6-hydroxycarbonylnaphthalen-2-yl)benzene) (H_3BTN) ligand, another La(III)-MOF(La-BTN) was further reported by Kitagawa *et al.* (Fig. 7f and h).[109] La-BTN was able to retain its structural integrity not only in a boiling acidic solution (pH = 2) but also in a strongly alkaline solution (pH = 12) for over 1 day. Eddaoudi *et al.* prepared a series of RE-fcu-MOFs (RE = Y(III) or Tb(III)) with fcu topology based on the 2-fluoro-4-(1*H*-tetrazol-5-yl)benzoic acid (H_2-FTZB) ligand (Fig. 7c and l),[108] in which an unusual metal cluster $[RE_6(\mu_3\text{-}OH)_8(O_2C\text{–})_6(N_4C\text{–})_6]^{2-}$ was *in situ* generated and served as a 12-connected metal node for MOFs' construction. Both isomeric MOFs show favourable water and thermal stability. After that, they reported another two La(III)-MOFs (pek-MOF-1 and 2) that were constructed from biphenyl-3,4,5-tricarboxylic acid (Fig. 7d) and 5-(4-carboxybenzyloxy)isophthalic acid, in which two different metal nodes (Fig. 7k), including a 12-connected nonnuclear and an 8-connected hexanuclear RE(III)-cluster, were also *in situ* formed.[107] Both of them

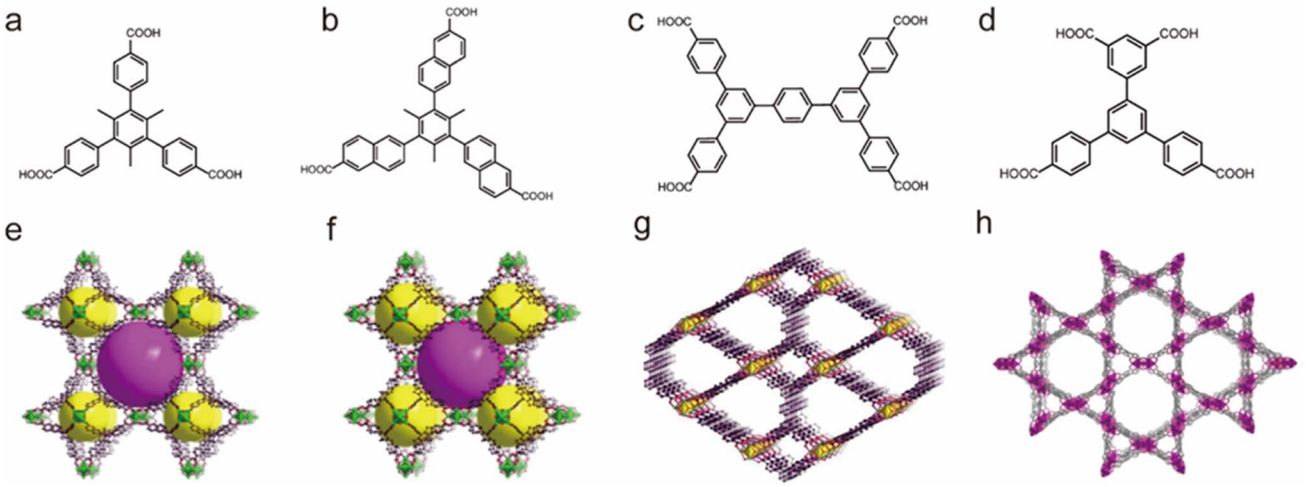

Fig. 4 The structures of the BUT series and the used ligands. (a) The H_3CTTA ligand. (b) The H_3TTNA ligand. (c) The BCQD ligand. (d) The H_4CPTTA ligand. (e) BUT-12. Reproduced from ref. 93 with permission from the American Chemical Society, Copyright 2016. (f) BUT-13. Reproduced from ref. 93 with permission from the American Chemical Society, Copyright 2016. (g) BUT-14. Reproduced from ref. 94 with permission from the American Chemical Society, Copyright 2017. (h) BUT-17. Reproduced from ref. 95 with permission from Springer Nature, Copyright 2019.

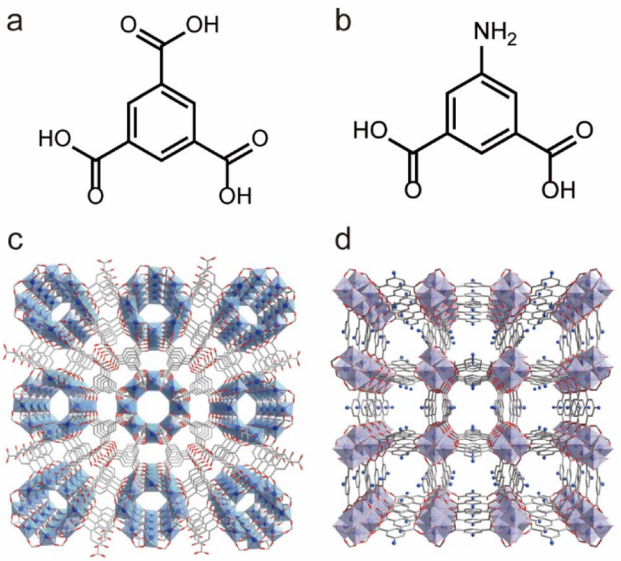

Fig. 5 The structures of Ti-MOFs and the used ligands. (a) The 1,3,5-BTC ligand. (b) 5-Aa-IPA ligand. (c) The structures of MIP-207. Reproduced from ref. 101 with permission from Elsevier, Copyright 2020. (d) The structures of MIP-208. Reproduced from ref. 102 with permission from Elsevier, Copyright 2020.

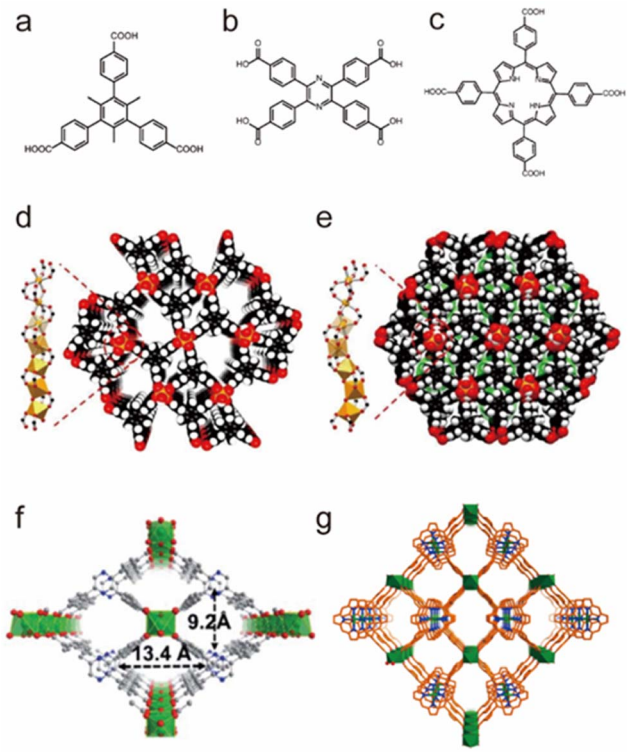

Fig. 6 The structures of representative In(III)-MOFs and the used ligands. (a) The H_3CTTA ligand. (b) The H_4TCPP ligand. (c) The H_2TCPP ligand. (d) BUT-172. Reproduced from ref. 103 with permission from the Royal Society of Chemistry, Copyright 2020. (e) BUT-173. Reproduced from ref. 103 with permission from the Royal Society of Chemistry, Copyright 2020. (f) In(tcpp). Reproduced from ref. 104 with permission from the Royal Society of Chemistry, Copyright 2021. (g) USTC-8. Reproduced from ref. 105 with permission from the American Chemical Society, Copyright 2018.

exhibited good water resistance and thermal stability. Furthermore, they used commercial 1,4-naphthalenedicarboxylic acid to prepare a series of isostructural fcu-MOFs (Fig. 7b and j).[111] Owing to the 12-connected $[RE_6(\mu_3\text{-}OH)_8(O_2C\text{–})_{12}]$ node, Eu-1,4-NDC-fcu-MOF could maintain its structural integrity in boiling water for at least 24 h.

In short, many water-stable MOFs were successfully prepared from various hard metal ions and carboxylate-based ligands, including famous MILs, UIOs, PCNs, and BUTs. Due to the very strong metal–oxygen interaction, many of them also exhibit

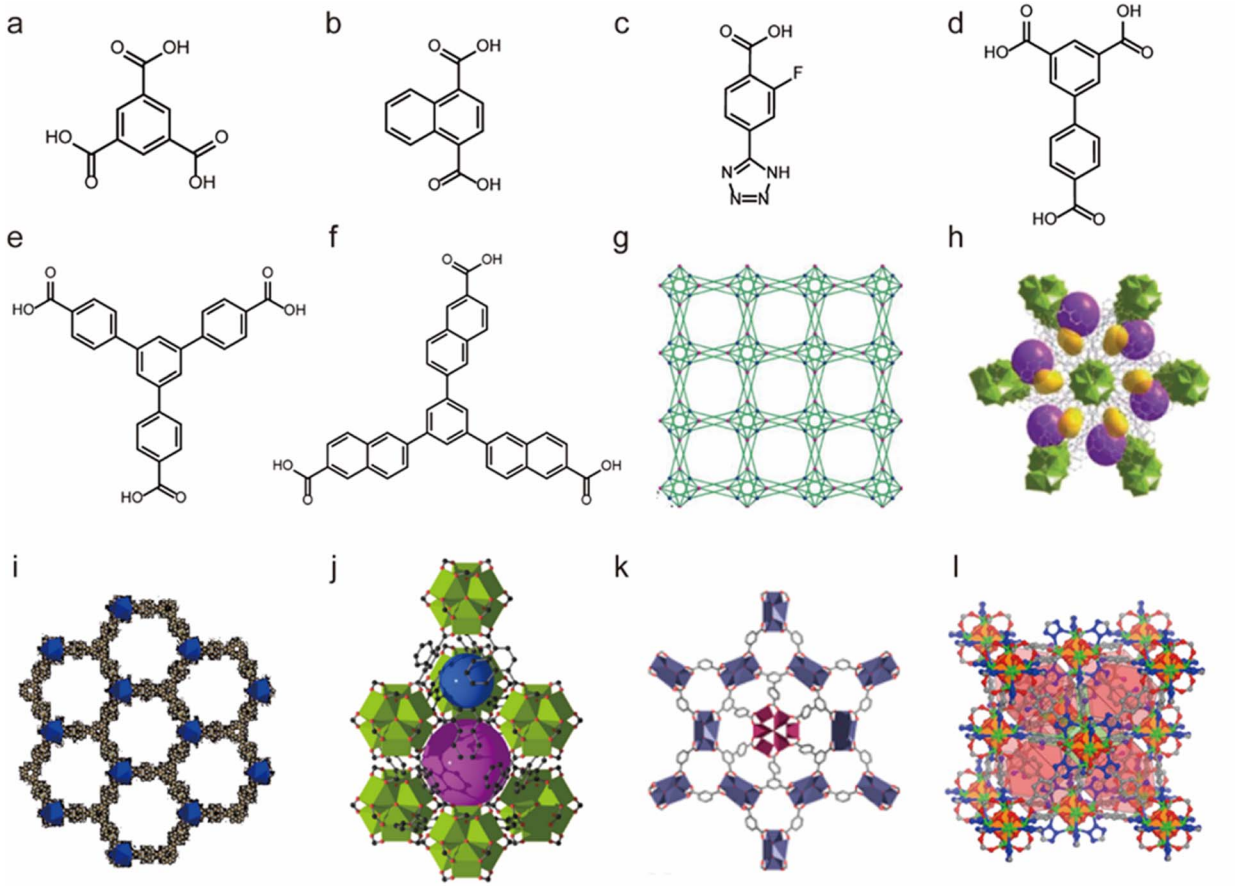

Fig. 7 The structures of representative rare-earth MOFs and the used ligands. (a) The 1,3,5-BTC ligand. (b) The 1,4-H_2NDC ligand. (c) The H_2FTZB ligand. (d) The BTBA ligand. (e) The BTB ligand. (f) The BTN ligand. (g) Y-BTC. Reproduced from ref. 106 with permission from the American Chemical Society, Copyright 2010. (h) La-BTN. Reproduced from ref. 109 with permission from the Royal Society of Chemistry, Copyright 2014. (i) La-BTB. Reproduced from ref. 110 with permission from Wiley, Copyright 2013. (j) Eu-1,4-NDC-fcu-MOF. Reproduced from ref. 111 with permission from the American Chemical Society, Copyright 2015. (k) pek-MOF-1. Reproduced from ref. 107 with permission from the American Chemical Society, Copyright 2015. (l) $[(CH_3)_2NH_2]_2[Tb_6(\mu_3\text{-}OH)_8(FTZB)_6(H_2O)_6]\cdot(H_2O)_{22}$. Reproduced from ref. 108 with permission from the American Chemical Society, Copyright 2013.

excellent acid/base resistance and thermal stability. It is noteworthy that BUT-8(Cr) even can retain its structural integrity in concentrated H_2SO_4.

2.4.2. Water-stable MOFs based on soft metal ions/ligands. According to HSAB theory, thermodynamically stable MOFs also can be rationally prepared from soft metal ions and soft ligands,

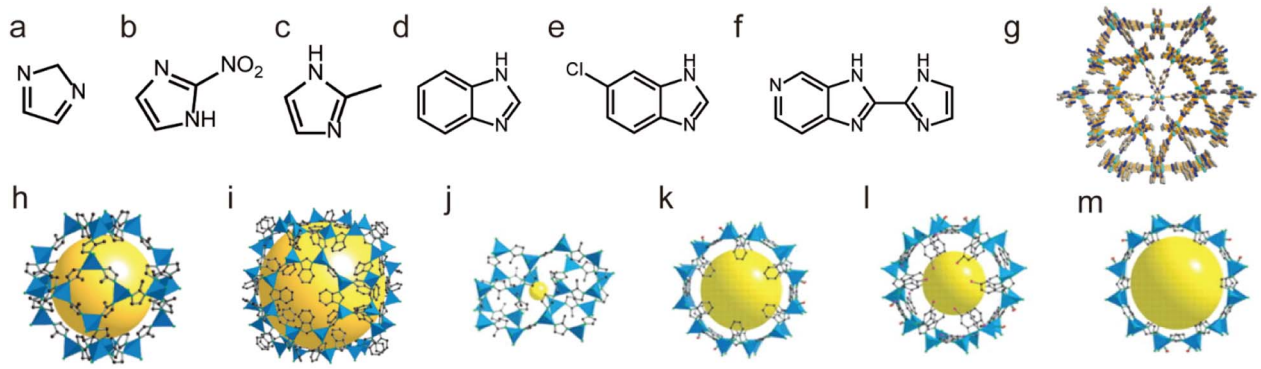

Fig. 8 The structures of representative Zn(II)-MOFs and the used ligands. (a) The IM ligand. (b) The nIM ligand. (c) The MeIM ligand. (d) The PhIM ligand. (e) The cbIM ligand. (f) The H_2imPim ligand. (g) MAF-stu-1. Reproduced from ref. 117 with permission from Wiley, Copyright 2019. (h) ZIF-8 (MAF-4). Reproduced from ref. 111 with permission from the National Academy of Sciences of the USA, Copyright 2006. (i) ZIF-11. Reproduced from ref. 111 with permission from the National Academy of Sciences of the USA, Copyright 2006. (j) ZIF-61. (k) ZIF-68. (l) ZIF-69. (m) ZIF-70. Reproduced from ref. 120 with permission from The American Association for the Advancement of Science, Copyright 2008.

and many water-stable MOFs based on this strategy have been developed. For example, the famous zeolitic imidazolate framework (ZIF-8) (also called MAF-4), assembled from soft Zn(II) ions and soft imidazolate ligands, could maintain its structure in boiling water for 7 days (Fig. 8a and l).[114,115] Besides ZIF-8, Yaghi and co-workers also synthesized a series of water-stable ZIFs (*e.g.*, ZiF-11, ZIF-68, ZIF-69, and ZIF-70) (Fig. 8), and all of them have high thermal stability and excellent water-resistance.[120] Recently, another water-stable Zn(II)-MOF (MAF-stu-1) based on the 2-(1*H*-imidzol-2-yl)-3*H*-imidazo[4,5-*c*]pyridine (H_2imPim) ligand was reported.[117] MAF-stu-1 maintained its full crystallinity following 9 days of submerging the bulk samples in boiling water, acidic/basic solutions (pH = 2, 13), or various organic solvents. Moreover, it displayed record thermal stability (up to 680 °C). These results confirm that combinations of Zn(II) ions and suitable N-containing ligands can lead to MOFs with excellent chemical stability (*e.g.* base stability and thermal stability).

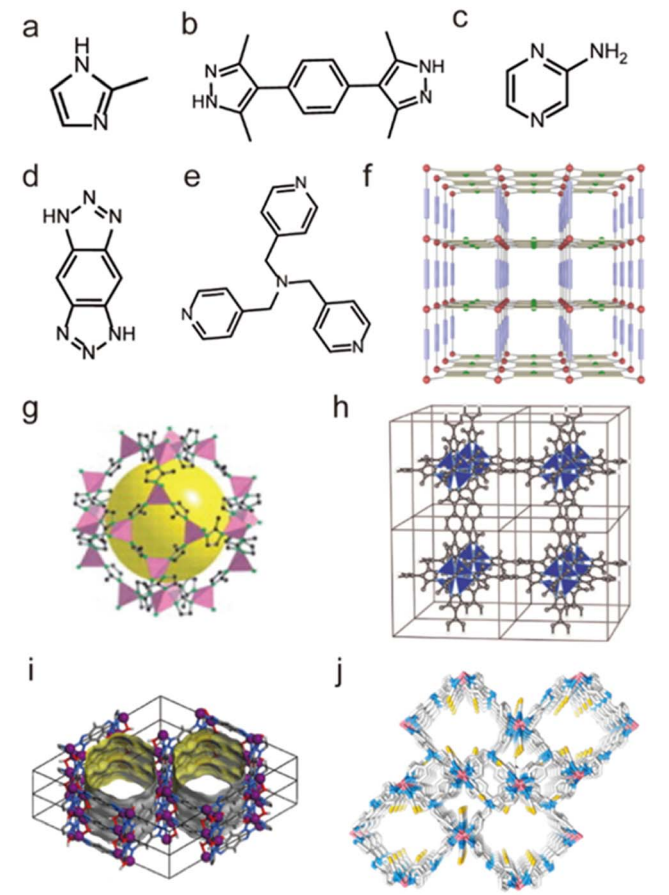

Fig. 9 The structures of representative Co(II)-MOFs and the used ligands. (a) The MeIM ligand. (b) The H_2bdpb ligand. (c) The pyz-NH_2 ligand. (d) The H_2bbta ligand. (e) The TPMA ligand. (f) ZJU-75. Reproduced from ref. 124 with permission from Wiley, Copyright 2023. (g) ZIF-67. Reproduced from ref. 120 with permission from The American Association for the Advancement of Science, Copyright 2008. (h) MFU-1. Reproduced from ref. 121 with permission from Wiley, Copyright 2009. (i) MAF-X27-Cl. Reproduced from ref. 122 with permission from the American Chemical Society, Copyright 2016. (j) FJI-H30. Reproduced from ref. 123 with permission from the American Chemical Society, Copyright 2020.

Not limited to Zn^{2+}, other low-valent metal ions such as Co^{2+}, Ni^{2+}, Cu^{2+}, and Ag^{+} can also be regarded as soft acids to prepare water-stable MOFs with appropriate N-containing linkers (soft bases). For instance, Yaghi *et al.* prepared a water-stable Co(II)-MOF (ZIF-67) based on Co(II) salt and the 2-methylimidazolate (MeIM) ligand (Fig. 9a and g).[120] ZIF-67 could retain its structure after being soaked in water for 7 days. Based on Co(II) salts and 1,4-bis[(3,5-dimethyl)-pyrazol-4-yl]benzene (H_2bdpb), Volkmer *et al.* developed a novel MOF (MFU-1). Due to the inert [$CoON_3$] units, MFU-1 did not decompose even when exposed to humid air for more than six months (Fig. 9b and h).[121] In 2016, Chen *et al.* found that MAF-X27-Cl, composed of 1*H*,5*H*-benzo-(1,2-*d*:4,5-*d*)bistriazole and Co(II) (Fig. 9d and i), showed exceptional chemical stability and could retain its original crystallinity in acidic (0.001 M HCl) or strongly alkaline (1.0 M KOH) solution for at least 1 week.[122] Recently, we prepared a flexible framework (FJIH-30) (Fig. 9e and j) through combining the tris(pyridin4-ylmethyl)amine (TPMA) ligand with $Co(SCN)_2$. Its framework could be retained not only in water for 5 days but also in aqueous solution with a wide pH range (from 2 to 12).[123] Very recently, Li's group developed a microporous framework (ZJU-75) by using the pyz-NH_2 ligand, $Co(NO_3)_2 \cdot 6H_2O$ and $K_2[Ni(CN)_4] \cdot nH_2O$ (Fig. 9c and f).[124] ZJU-75 also displayed high chemical stability; it could maintain its structural integrity after being submerged in water and aqueous solutions of pH 1 and 12 for three days or exposed to air for three months.

The self-assembly based on Ni^{2+} and N-containing linkers can also lead to water-stable MOFs. In 2011, Long and co-workers used 1,3,5-tris(1*H*-pyrazol-4-yl)benzene (H_3BTP) and Ni(II) salt to prepare a microporous pyrazolate-bridged MOF ($Ni_3(BTP)_2$) (Fig. 10c and i).[128] Remarkably, the framework of $Ni_3(BTP)_2$ was stable in boiling water, boiling HCl or HNO_3 aqueous solutions at pH 2, and a boiling NaOH aqueous solution at pH 14, and maintained both its crystallinity and porosity after 14 days of uninterrupted tests. By isoreticular expansion, another two water-stable Ni(II)-pyrazolate MOFs (BUT-32 and BUT-33) were synthesized from a conformation-matched elongated pyrazolate ligand, 2,4,6-tris(4-(pyrazolate-4-yl)phenyl)-1,3,5-triazine (H_3TPTA) (Fig. 10d, g and h) by Li's group in 2020.[129] Given the network interpenetration in BUT-32, the two MOFs possessed the same topology but had different pore sizes. Both the thermodynamic product BUT-32 and the kinetic product BUT-33 could retain their structure in boiling water for 24 hours, a HCl aqueous solution (pH = 3), and NaOH aqueous solution (4 M) at room temperature, respectively. Guided by a top-down topological analysis, Zhou's group rationally synthesized a water-stable Ni(II)-MOF (PCN-601) from a pyrazolate-based 5,10,15,20-tetra(1H-pyrazol-4-yl)porphyrin ligand (H_4TPP) (Fig. 10a and e).[126] PXRD and N_2 adsorption further revealed its extraordinary base resistance; PCN-601 was the first identified MOF that could retain its crystallinity and porosity in saturated NaOH solution (~20 mol L^{-1}) both at room temperature and 100 °C. Such excellent chemical stability was believed to come from the high connectivity numbers between the porphyrinic ligands and ($[Ni_8(OH)_4(H_2O)_2Pz_{12}]$, Pz = pyrazolate)

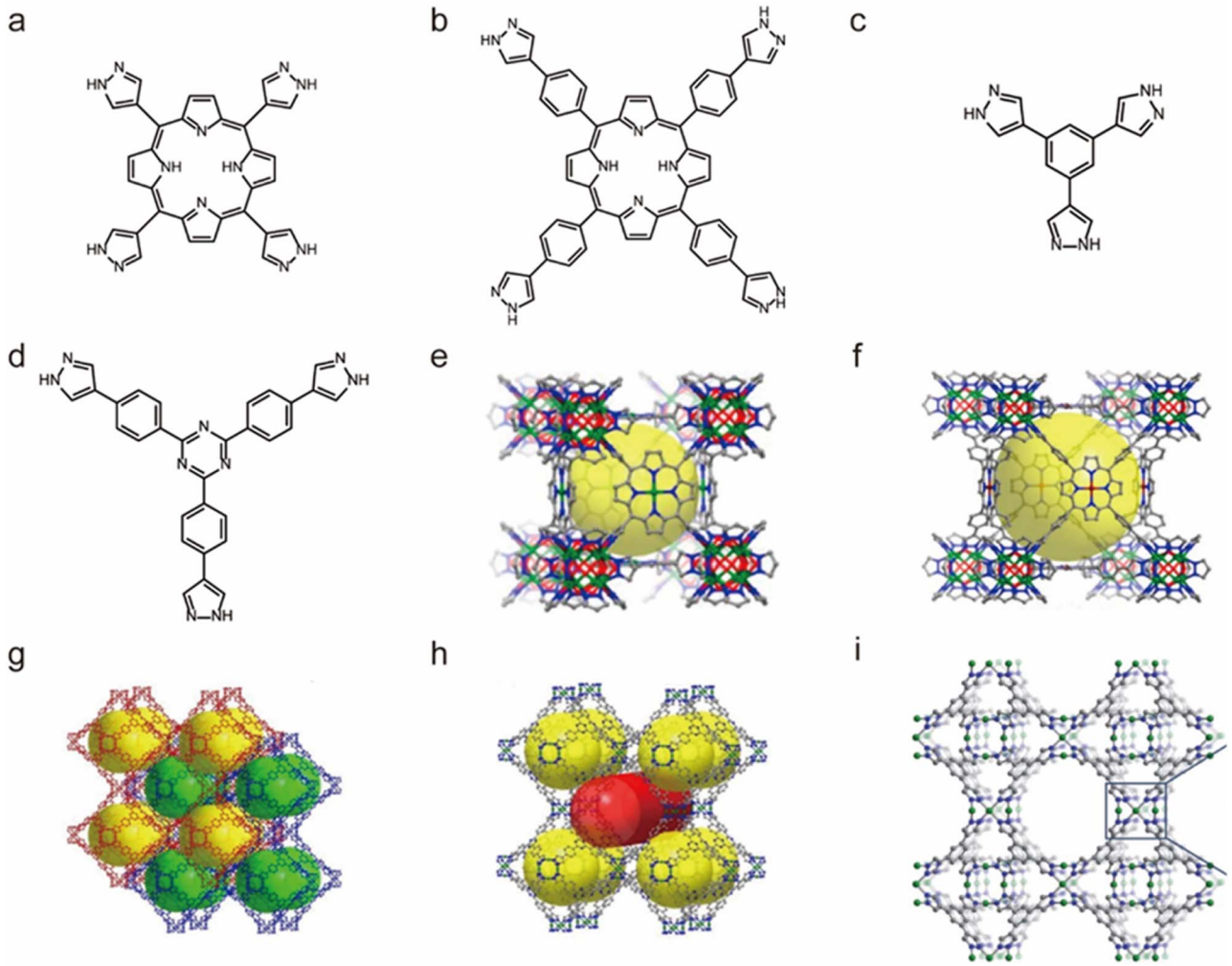

Fig. 10 The structures of representative Ni(II)-MOFs and the used ligands. (a) The H_4TPP ligand. (b) The H_4TPPP ligand. (c) The H_3BTP ligand. (d) The H_3TPTA ligand. (e) PCN-601. Reproduced from ref. 126 with permission from the American Chemical Society, Copyright 2016. (f) PCN-602. Reproduced from ref. 127 with permission from the American Chemical Society, Copyright 2017. (g) BUT-32. Reproduced from ref. 129 with permission from the American Chemical Society, Copyright 2020. (h) BUT-33. Reproduced from ref. 129 with permission from the American Chemical Society, Copyright 2020. (i) $Ni_3(BTP)_2$. Reproduced from ref. 128 with permission from the Royal Society of Chemistry, Copyright 2011.

clusters, robust Ni(II)–N bonds and a relatively short length of the ligand. Based on a longer 5,10,15,20-tetrakis(4-(pyrazolate-4-yl)phenyl)porphyrin (H_4TPPP) ligand and the same 12-connected $[Ni_8(OH)_4(H_2O)_2Pz_{12}]$ cluster, Zhou's group synthesized another water-stable Ni(II)-MOF (PCN-602) (Fig. 10b and f).[127] Although PCN-602 has the same secondary building units and topology as PCN-601, its base stability was significantly reduced and it could only remain stable in 1 M NaOH solution. This may be because its pore size is larger than that of PCN-601, which is conducive to the diffusion of hydroxide anions.

Additionally, there are also many water-stable MOFs constructed from Cu(I), Cu(II), and Ag(I) ions and N-containing ligands. For example, based on an azolate ligand Hetz (Hetz = 3,5-diethyl-1,2,4-triazole), Chen's group reported a NbO type Cu(I)-framework (MAF-2), which showed good water vapor tolerance (Fig. 11c and i).[131] Another water-stable Cu(I)-MOF, namely Cu_2TBPZ (TBPZ = 3,3′,5,5′-tetraethyl-4,4′-bipyrazolate) (Fig. 11b and h), was synthesized through a stepwise method by Li's group.[133] Cu_2TBPZ could maintain its structural integrity after being soaked in various boiling solvents (*e.g.*, THF, toluene, hexane, and DMSO), water, and even in acidic (0.001 M HCl) or basic (0.001 M NaOH) aqueous solutions for 24 h. In 2019, Zhang and co-workers synthesized a new Cu(I)-MOF(MAF-41) based on a linear ligand, 2,6-ditrifluoromethyl-benzodiimidazole (H2fbdim) (Fig. 11d and j).[132] After complete guest removal below 150 °C, MAF-41 displayed good chemical stability in boiling water for at least one week, in aqueous solutions with a wide range of pH (3–14) at room temperature for at least 3 days. In addition, the structural integrity of MAF-41 could be maintained for at least 6 months when exposed to humid air (~70 RH%). Their team also developed a water-stable Ag(I)-MOF$[Ag_2(o\text{-Hmpba})_2(o\text{-}H_2mpba)_2]$ by using the 2-(3,5-dimethyl-1*H*-pyrazol-4-yl)benzoic acid (o-H_2mpba) ligand (Fig. 11e and f).[135] Due to its hydrophobicity, the as-prepared Ag(I)-MOF could remain intact and keep its color unchanged in the air for at least 8 months, and

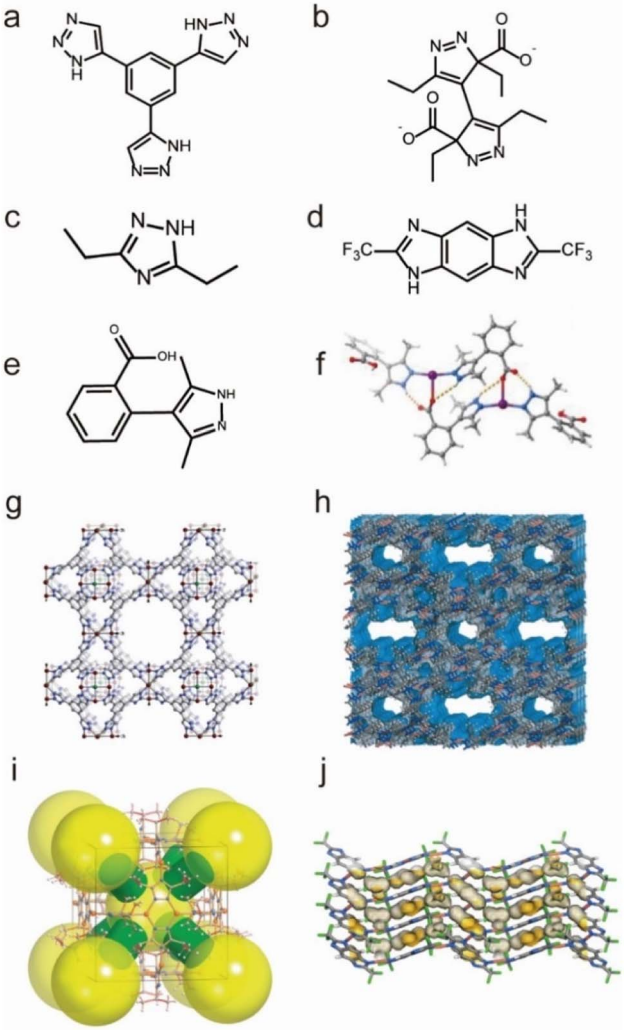

Fig. 11 The structures of representative Cu/Ag-MOFs and the used ligands. (a) The H_3BTTri ligand. (b) The TBPZ ligand (TBPZ = 3,3′,5,5′-tetraethyl-4,4′-bipyrazolate). (c) The Hetz ligand. (d) The H_2fbdim ligand. (e) The *o*-H_2mpba ligand. (f) [Ag_2(*o*-Hmpba)$_2$(*o*-H_2mpba)$_2$]. Reproduced from ref. 135 with permission from Wiley, Copyright 2020. (g) Cu-BTTri. Reproduced from ref. 130 with permission from the American Chemical Society, Copyright 2009. (h) Cu_2TBPZ. Reproduced from ref. 133 with permission from Wiley, Copyright 2014. (i) MAF-2. Reproduced from ref. 131 with permission from the American Chemical Society, Copyright 2008. (j) MAF-41. Reproduced from ref. 132 with permission from Springer Nature, Copyright 2019.

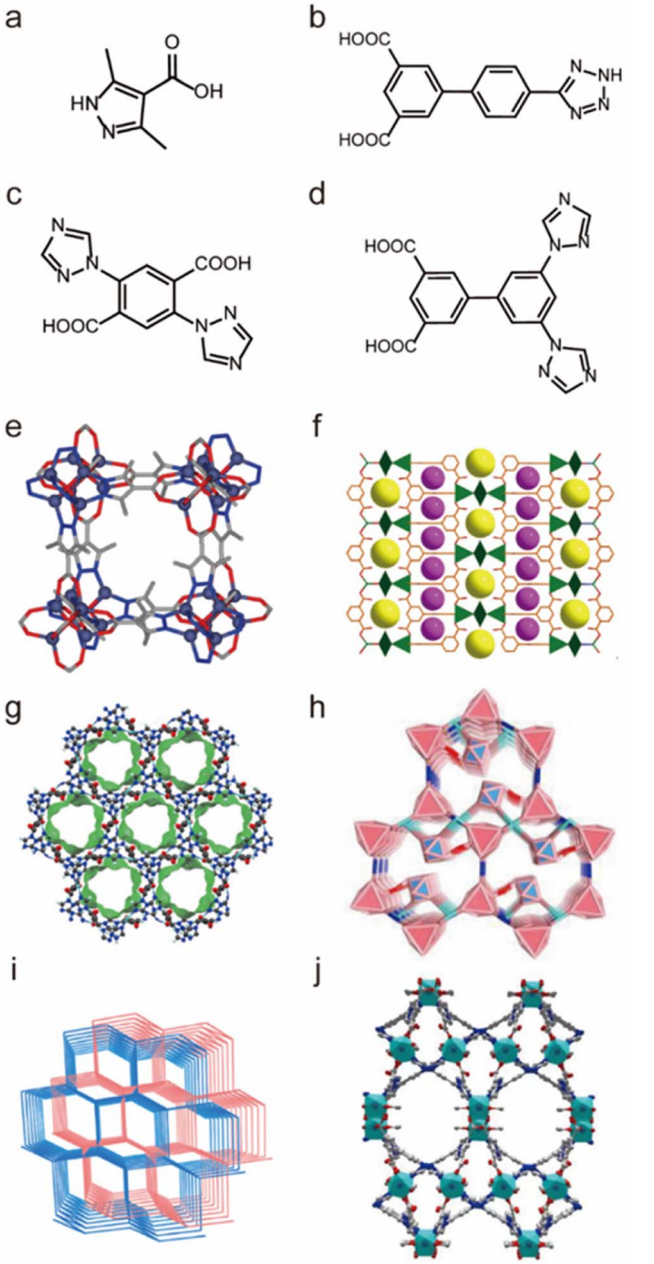

Fig. 12 The structures of representative MOFs based on N-containing carboxylate ligands and the used ligands. (a) The H_2dmcapz ligand. (b) The H_3TZBPDC ligand. (c) The H_2BTTA ligand. (d) The H_2DTBDA ligand. (e) [$Zn_4(\mu_4$-O)-(μ_4-4-carboxy-3,5-dimethyl-4-carboxy-pyrazolato)$_3$]. Reproduced from ref. 139 with permission from the American Chemical Society, Copyright 2011. (f) USTC-7. Reproduced from ref. 140 with permission from the Royal Society of Chemistry, Copyright 2016. (g) FJI-H14. Reproduced from ref. 136 with permission from Springer Nature, Copyright 2017. (h) FJI-H25Fe. Reproduced from ref. 137 with permission from Wiley, Copyright 2020. (i) FJI-H29. Reproduced from ref. 138 with permission from the American Chemical Society, Copyright 2020. (j) FJI-H36. Reproduced from ref. 141 with permission from Wiley, Copyright 2023.

also in aqueous solution with a wide range of pH (2–13) for at least 1 week. Based on the Cu(II) ion and triazolate ligand 1,3,5-tris(1*H*-1,2,3-triazol-5-yl)benzene (H_3BTTri), Long's group prepared a water-stable MOF (Cu-BTTri) (Fig. 11a and g),[130] which also exhibited strong resistance for both acidic solutions (pH = 3) and boiling water.

As previously indicated, chemically stable MOFs can be rationally prepared from soft low-valent metal ions and soft N-containing ligands. However, due to the very strong coordination interaction, the assembly between these soft coordination units usually leads to powder (*e.g.*, microcrystals and amorphous solids) unsuitable for SCXRD analysis. Due to the reversibility of coordination bonds, high-quality single crystals of MOFs can be self-assembled by selecting coordination units with weak coordination (*e.g.*, selecting soft acids and hard

bases), but MOFs constructed from weak coordination units are usually less stable. By self-assembling the ligands containing both soft and hard coordination atoms with soft metal ions, both the crystallinity and stability of MOFs can be balanced well. In this context, many water-stable MOFs based on ligands containing both N and O atoms were prepared. For example, Navarro and co-workers prepared a water-stable MOF [$Zn_4(\mu_4$-O)-(μ_4-4-carboxy-3,5-dimethyl-4-carboxy-pyrazolato)$_3$] based on a N-containing carboxylate ligand 3,5-dimethyl-4-carboxypyrazole (H_2dmcapz) ligand and Zn(II) ion, which could retain its framework integrity in water and boiling MeOH/benzene for 24 hours (Fig. 12a and e).[139] Then Jiang's group synthesized a water-stable MOF (USTC-7) by using the N-containing carboxylate ligand 4′-(1*H*-tetrazol-5-yl)-[1,10-biphenyl]-3,5dicarboxylic acid (H_3TZBPDC) and Zn(II) salt (Fig. 12b and f).[140] USTC-7 exhibited its exceptional stability not only in various boiling solvents but also in pH = 2–12 aqueous solutions for 12 h. Based on N-containing carboxylate ligands, our group designed and synthesized a series of water-stable MOFs with good crystallinity, such as FJI-H14, FJI-H25Fe, FJI-H29 and FJI-H36.[136,141] Through the reaction of 2,5-di(1*H*-1,2,4-triazol-1-yl)terephthalic acid (H_2BTTA) with $Cu(NO_3)_2$, a water-stable MOF (FJI-H14) was first prepared (Fig. 12c and g). FJI-H14 not only could retain its framework in the pH = 2–12 aqueous solutions at 373 K for 24 hours but also displayed excellent thermal stability (503 K). Structural analyses demonstrate that such excellent stability results from its CuN_2O_3 units with strong coordination and abundant free N atoms that can react with hydrogen ions. Combining the same ligand (H_2BTTA) with other metal nodes, [$Fe_3(\mu_3$-O)($CH_3COO)_6$] clusters and Co-doped [$Fe_2Co(\mu_3O)(CH_3COO)_6$] clusters, two isomeric MOFs (FJI-H25Fe and FJI-H25FeCo) with distinct water stability were further prepared (Fig. 12c and h).[137] The Fe-MOF could retain its framework even in a pH = 12 aqueous solution while FeCo-MOF would quickly hydrolyse in the pH = 10 aqueous solution. The base stability of FeCo-MOF is lower than that of Fe-MOF due to partial substitution of Co; since the weaker Co–O units made the Co substituted framework more vulnerable to be deconstructed by OH^- anions. Based on a longer 3′,5′-di(1*H*-1,2,4-triazol1-yl)-[1,1′-biphenyl]-3,5-dicarboxylic acid (H_2DTBDA) ligand, another two water-stable MOFs (FJI-H29 and FJI-H36) were further synthesized (Fig. 12d, i and j).[138] Both of them displayed excellent acid/base resistance and good thermal stability. FJI-H29 exhibited better base stability (pH = 13) but less thermal stability (423 K), while FJI-H36 showed better thermal stability (473 K) but less base resistance (pH = 12). This means that the chemical stability (*e.g.*, base resistance and thermal stability) of MOFs can be controllably regulated by the selection of metal ions and ligands with different hardness.

In a word, many water-stable MOFs based on various soft metal ions and N-containing ligands were reported, including ZIFs, MAFs, PCNs, BUTs, and FJI-Hs. Due to the strong metal–nitrogen interaction, most of the reported MOFs also displayed good acid/base stability, especially base stability.

Notably, PCN-601 could retain its structural integrity in saturated NaOH solution (about 20 mol L^{-1}). This means that MOFs can be used normally even in a strongly alkaline environment.

2.4.3. Enhancing the thermodynamic stability of MOFs through pore engineering. In addition to directly using suitable coordination units, subsequent modification of pores of MOFs also can enhance their thermodynamic stability. Thus, many different strategies such as interlocking of the framework, increasing the rigidity of the framework, changing the distribution of charge, and pore space partition have been developed, and the water stability of many metastable MOFs has been successfully enhanced.

2.4.3.1. Enhancing stability through interlocking of frameworks. In addition to the weak coordination nodes, the relatively large pores of MOFs can also lead to their instability; this is because large pores facilitate the diffusion of small molecules that can break down their framework. For a specific MOF, the interlocking of its independent framework can not only enhance the interactions between interlocked frameworks but also reduce its pore size, so the interlocking of the framework can be used to enhance the water stability of MOFs. For example, Walton's group used the interpenetration of the framework to enhance the water stability of MOFs.[149] They prepared two isostructural MOFs DMOF [Zn(BDC)$(DABCO)_{0.5}$] and MOF-508 [Zn(BDC)$(BPY)_{0.5}$] by using different pillared ligands. The DMOF was a non-catenated pillared layer structure while MOF-508 was a two-fold interpenetrated pillared layer structure. Even though the pK_a of DABCO is significantly higher than that of BPY, the interlocked MOF-508 also exhibited better water stability than the non-interlocked DMOF. This enhanced stability is thought to be due to the higher thermodynamic stability and lower water absorption of the interlocked structure. The same enhanced effect can also be found in other interlocked MOFs (*e.g.*, Zn-BTTB-DMBPY and Co-BTTB-DMBPY).[150]

Interestingly, the water stability of MOFs can also be influenced by the direction of interpenetration. Chen and co-workers synthesized three isomeric MOFs([Zn(Hmpba)$_2$]) through a solvothermal reaction of 4-(3,5-dimethyl-1*H*-pyrazol-4-yl)benzoic acid (H_2mpba) and $Zn(NO_3)_2$.[151] Although three isomers had 4-fold interpenetrated structures, they exhibited entirely different water stability due to the different directions of interpenetration. Here, two nanoporous metastable isomers would spontaneously convert into the most stable nonporous isomer. This not only confirms that the interpenetration of the framework can improve the thermodynamic stability of MOFs but also indicates that the interpenetration with small pores is more stable than that with large pores.

2.4.3.2. Enhancing stability through pore space partition. As mentioned previously, for a metastable MOF containing large pores, its stability can be improved by the interlocking of the framework. This is because interlocking can effectively improve its thermodynamic stability and reduce its pore size. In fact, matched ligands also can be used to enhance the thermodynamic stability of a metastable MOF through pore space partition (PSP).[7] For example, Du's group prepared two water-stable MOFs (1 and 2) with comparable structural properties but distinct water stability based on an MIL-88 type Co(II)-MOF

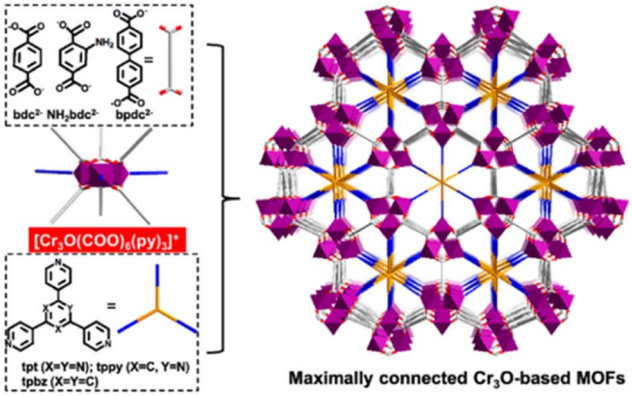

Fig. 13 The structural components, together with the framework viewed along the *c* axis. NH_2bdc^{2-} = 2-aminoterephthalate, $bpdc^{2-}$ = biphenyl-4,4′-dicarboxylate), tpt = 2,4,6-tri(4-pyridyl)-1,3,5triazine, tpbz = 1,3,5-tri(4-pyridyl)-benzene, and tppy = 2,4,6-tris(4-pyridyl) pyridine. Reproduced from ref. 153 with permission from the American Chemical Society, Copyright 2021.

through the PSP strategy.[152] After introducing two size-matching triangular blocks $[Co_2(ina)_3(H_2O)_2]^+$ and 2,4,6-tri(4-pyridyl)-1,3,5-triazine (tpt) into the pores, the moisture stability of the MOFs with tpt substitution rose dramatically. Recently, Bu and colleagues prepared a family of acid/base-resistant Cr-MOFs by dividing the large pore of the original Cr-MOFs into interconnected small pores employing triangle ligands (Fig. 13).[153] The newly formed Cr-MOFs (CPM-243(F)) could maintain their crystallinity even under very severe conditions such as HCl aqueous solution and 10 M NaOH aqueous solution. Such exceptional stability was due to the presence of the multi-binding pore-partitioning ligand, framework rigidity, and highly connected Cr_3O nodes.

Chen, Xiang, and co-workers also used the PSP strategy to realize the improvement of MOFs' stability.[154] As shown in Fig. 14, by a triangular ligand (Tripp = 2,4,6-tris(4-pyridyl) pyridine), every metal cluster in the original FJU-88 increased three coordination bonds. Due to the increased connection numbers of metal clusters, the thermal stability of the newly generated MOF (FJU-90) (up to 300 °C) was noticeably higher than that of the initial FJU-88 (durable only below 50 °C). Moreover, FJU-90 could maintain its structure even after being submerged in water for a day or exposed to air for a month, but the mother MOF (FJU-88) could not. The same improved effect

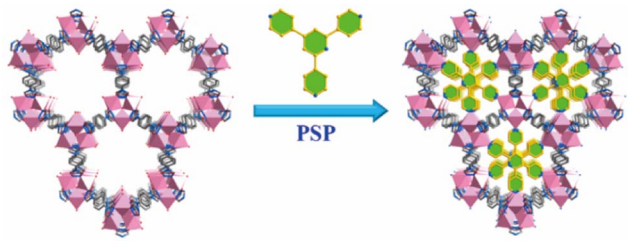

Fig. 14 Pore space partition (PSP) through symmetry- and size-matching-regulated ligand insertion. Reproduced from ref. 154 with permission from the American Chemical Society, Copyright 2019.

also can be found in $[Cu_2(obb)_2(bpy)_{0.5}(DMF)]\cdot 2DMF$ and $[Co_2(INT)_3(H_2O)_2]$.[155,156]

2.4.3.3. Enhancing stability through increasing the rigidity of the ligand. In some situations, the rigidity of organic linkers tends to reduce the structural diversity but is beneficial to construct chemically stable MOFs. For instance, Zhou, Li, and co-workers prepared 13 Zr-MOFs by combining three ligands with the same topology but different rigidity with $Zr_6O_4(OH_4)(-CO_2)_n$ units (n = 8 or 12) (Fig. 15).[157] The MOFs constructed from the less rigid ligand L_B^1 were labile while those with rigid ligands L_B^2 and L_B^3 were chemical stable, which could maintain intact in water, acidic solution (pH = 1), or weakly basic (pH = 11) aqueous solution. The enhancement of stability may be due to the fact that rigid ligands have higher deformation energy barriers than flexible ligands and tend to maintain their conformation in the framework, which significantly restricts the dissociation of M-L and improves its repair. The same improvements also could be found in other isostructural MOFs (*e.g.*, BUT-109(Zr)/BUT-110(Zr), and CoBTTBBPY/CoBTTBAZPY, and ZnBTTBBPY/ZnBTTBAZPY).[158,159]

2.4.3.4. Enhancing stability through ligand charge-separation. In addition to the strategies given above, the charge density of organic ligands also plays a significant role in framework stability. Bu's group developed a ligand charge-separation (LCS) strategy for the stabilization of MOFs with high-charge-density ligands (Fig. 16).[160] By breaking down the ligand 2,5-dioxido-1,4-benzenedicarboxylate ($dobdc^{4-}$) of MOF-74-Zn $[Zn_2(-obpdc)]$ into OH^- and $obdc^{3-}$ (H_3obdc = 2-hydroxyterephthalic acid), two new MOFs CPM-74 $[Zn_2(OH)(obpdc)]$ and CPM-75

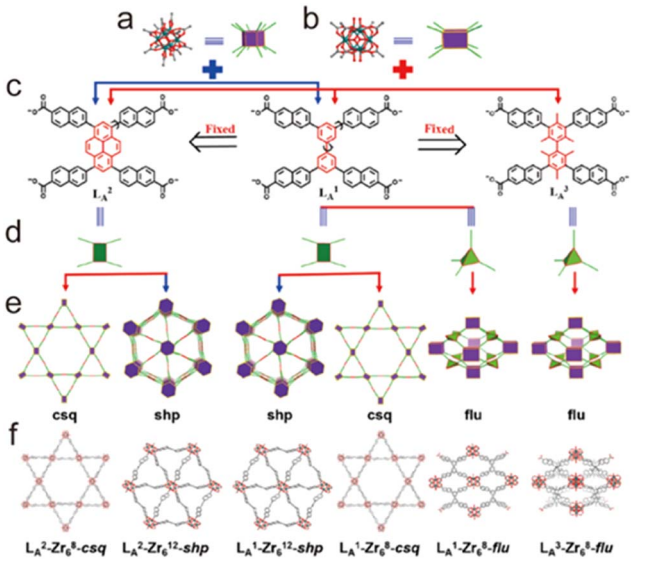

Fig. 15 Construction of a series of Zr-MOFs by using naphthoate-based tetracarboxylate ligands. (a) 12-Connected Zr_6 clusters; (b) 8-connected Zr_6 clusters; (c) different ligands LA^1, LA^2, and LA^3; (d) configuration of ligands; different topologies (e) and structures (f) of LA^2-Zr_6^8-csq (5), LA^2-Zr_6^{12}-shp (4), LA^1-Zr_6^{12}-shp (3), LA^1-Zr_6^8-csq (2), LA^1-Zr_6^8-flu (1), and LA^3-Zr_6^8-flu (6) MOFs, respectively. Reproduced from ref. 157 with permission from the American Chemical Society, Copyright 2019.

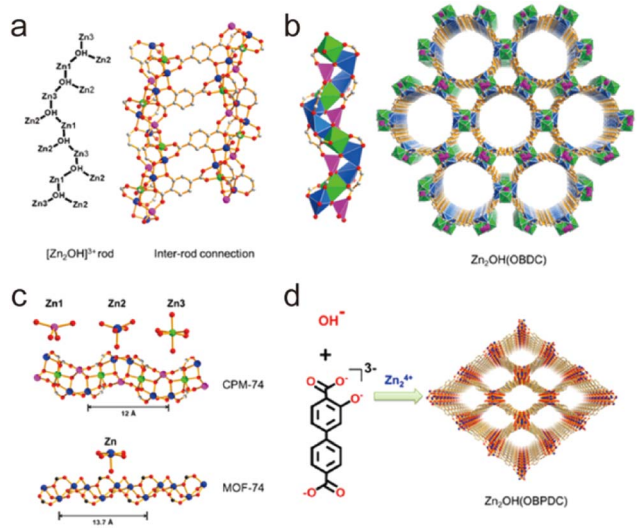

Fig. 16 (a) ChemDraw representation of $[Zn_2(OH)]^{3+}$ rod and ball-and-stick view of inter-rod connection. (b) Polyhedral view of the rod and the framework of CPM-74. (c) Comparison between the chains in CPM-74 and MOF-74. (d) Building scheme of CPM-75. Zn1, pink; Zn2, blue; Zn3, green; C, gray; O, red. Reproduced from ref. 160 with permission from the American Chemical Society, Copyright 2019.

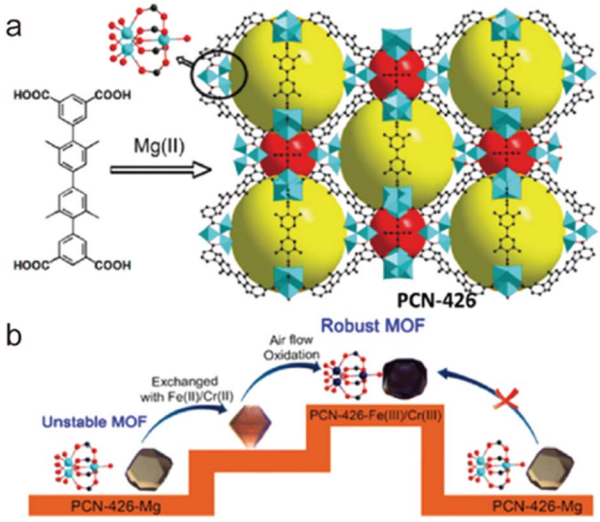

Fig. 17 (a) The ligand and the structure of PCN-426-Mg; (b) the metal exchange routes for PCN-426. Reproduced from ref. 161 with permission from the American Chemical Society, Copyright 2014.

$[Zn_2(OH)(obpdc)]$ could be obtained. Compared with parent MOF-74-Zn, the two newly prepared MOFs had the same density of metal sites and similar Zn–O chains, so they could be considered quasi-MOF-74-Zn isomers. Although MOF-74-Zn was sensitive to water, both CPM-74 and CPM-75 could stably exist in aqueous solutions with pH from 3 to 10, exceeding most reported Zn(II)-MOFs based on carboxylate ligands. This significant enhancement may be because the separated low-charge-density ligands can coordinate with Zn(II) ions more flexibly, resulting in more stable coordination configurations.

2.4.3.5. Enhancing stability through metal metathesis. Theoretically, replacing the metal ions in a labile MOF with suitable metal ions that can form stronger coordination bonds and lead to an isomeric but more stable MOF. This means that the metal metathesis can effectively improve the stability of a metastable MOF without changing its framework and pore. Through metal metathesis and oxidation, Zhou and co-workers realized the enhancement of stability of a labile Mg-based MOF (PCN-426-Mg) (Fig. 17).[161] After PSM, the as-prepared isostructural PCN-426-Cr possessed the stronger Cr(III)–O units. Although PCN-426-Mg was particularly vulnerable to humidity, the newly formed PCN-426-Cr could maintain its crystallinity even in an extremely acidic solution (4 M HCl) or a pH = 12 aqueous solution. Furthermore, Zhang and Wang developed a mild and efficient method for one-step synthesizing Cr(III)-MOFs from Fe(III)-MOFs through metal metathesis, namely solvent-assisted metal metathesis. They found that acetone could effectively improve the efficiency of metal exchange by coordinating with the Fe(III) ions of MOFs. Assisted by acetone, a series of isostructural Cr(III)-MOFs could be directly prepared from their Fe(III)-based precursors through the exchange of metal ions, and all the modified MOFs displayed enhanced stability.[162]

2.4.4. Enhancing the kinetic stability of MOFs through hydrophobic engineering. One approach to constructing MOFs with long-term water stability is increasing the strength of coordination bonds between metals and ligands (improving thermodynamic stability); the other spotlight can be turned on inhibiting the hydrolysis of MOFs (enhancing kinetic stability). The hydrolysis of MOFs in water could be considered as a competitive reaction between the ligand and H_2O toward metal clusters. To minimize the contact and affinity between MOFs and water, many different strategies, including directly using hydrophobic ligands, bonding hydrophobic groups, and forming hybrid composites have been developed.

2.4.4.1. Enhancing the kinetic stability by directly using hydrophobic ligands. Directly using hydrophobic ligands is the most commonly used method to improve the kinetic stability of MOFs in water. For example, employing hydrophobic polymer ligands and pyridine linkers, Cohen's group synthesized a series of polymer–metal–organic frameworks (polyMOFs) (Fig. 18).[163] In contrast to the parent MOF without hydrophobic units, polyMOFs could retain their crystallinity after being exposed to boiling water for 24 hours due to the cross-linking of polymer chains in the pores of polyMOFs. Apart from the polymer ligands, other hydrophobic units such as nonpolar alkyl chains and fluorine-containing groups can be introduced into organic linkers to prepare water-resistant MOFs. For instance, with the help of methyl-functionalized ligands, Li and co-workers could realize the controllable construction of a water-stable MOF based on water-unstable Cu(II) paddle wheel units (Fig. 19).[164] Through combining a ligand (H_8tdhb) functionalized with six methyl groups with Cu(II) ions, they prepared a microporous MOF (BUT-155a) with Cu(II) paddle wheel units. Even though the Cu(II) paddle wheel units are highly sensitive to water, the as-prepared BUT-155a also displayed excellent water stability due to the introduction of hydrophobic methyl groups. It could

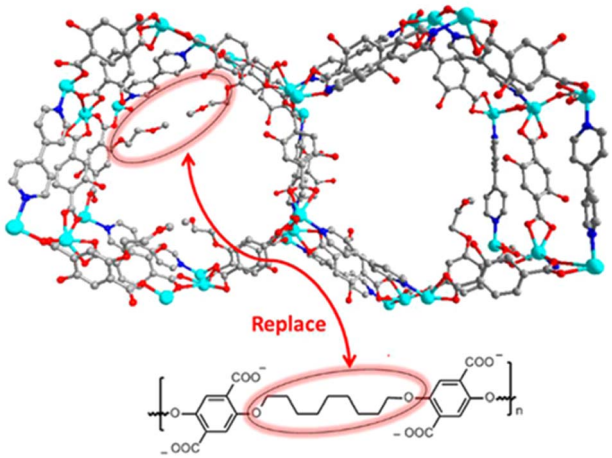

Fig. 18 Packing diagram of MOF 1 along the *c*-axis direction (top); design concept for creating a polyMOF analogue of MOF 1 *via* replacing dangling groups by polymer chains (bottom). Reproduced from ref. 163 with permission from the American Chemical Society, copyright 2016.

maintain structural integrity even in boiling water for 24 hours and the aqueous solution with a wide pH range (4s–10).

Another water-stable Cu(II)-MOF (USTC-6) was prepared by Jiang's group through using a fluorine-containing ligand (4,4′-(per-fluoropropane-2,2-diyl)diphthalic acid). Due to the strong hydrophobicity of the CF_3 groups, USTC-6 demonstrated extraordinary endurance to water and aqueous solutions (pH = 2–10), despite the fact that the majority of Cu–O coordination bonds in MOFs are susceptible to hydrolysis.[165] Similarly, Li and

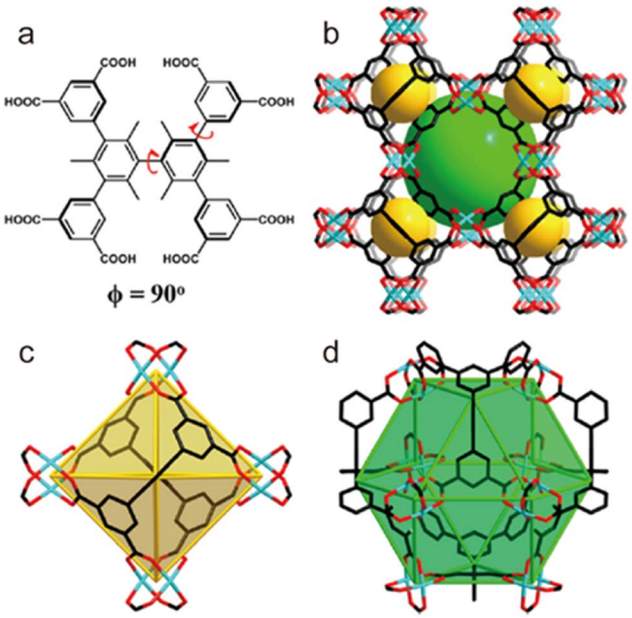

Fig. 19 (a) Structure of the ligand H_8tdhb, (b) crystal structure of BUT-155a, and (c) octahedral cage (cage A) and (d) cuboctahedral cage (cage B) in BUT-155a (color code: C, black; O, red; Cu, blue; H atoms on ligands are omitted for clarity). Reproduced from ref. 164 with permission from the American Chemical Society, copyright 2017.

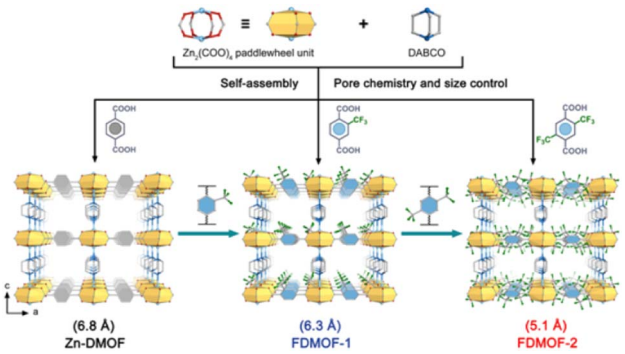

Fig. 20 Fluorinated functional group introduction into the confined pore space. Reproduced from ref. 166 with permission from Wiley, Copyright 2023.

co-workers realized the construction of a water-stable Zn(II) paddle wheel-based MOF by using fluorine-containing ligands. Through separately reacting the ligand 2-(trifluoromethyl) terephthalic acid (BDC-CF_3) and 2, 5-bis(trifluoromethyl) terephthalic acid (BDC-$(CF_3)_2$) with Zn(II) salt, they constructed two fluorinated Zn-DMOFs (named FDMOF-1 and FDMOF-2) (Fig. 20).[166] FDMOF-1 and FDMOF-2 exhibited ultrahigh structural stability due to the introduction of fluorinated functional groups into the confined pore space. Even at 70% relative humidity, they could maintain their structural integrity well for a period of six months.

In order to explore the effect of the length of hydrophobic chains on the water stability of MOFs, a series of isostructural NbO-type MOFs were synthesized by Zhou's group.[167] They found that the water stability of the resulting Cu(II)-MOFs increased significantly while their thermal stability reduced as the length of the hydrophobic chains increased. Besides the length of hydrophobic groups, the distance between metal nodes and hydrophobic groups is another key parameter for influencing the chemical stability of MOFs. A reasonable comparison between MOF-508 and its two analogues (SCUTC-18 and SCUTC-19) was made by Ma's group.[168] In contrast to the unsubstituted bipyridine ligands of MOF-508, two methyl groups were introduced into the ortho- and meso-sites of the bipyridine ligands in SCUTC-18 and SCUTC-19, respectively. Only SCUTC-18 protected by the closer methyl groups could retain its porous structure after being exposed to humid air for 30 days.

2.4.4.2. Enhancing the kinetic stability by bonding hydrophobic groups. As mentioned above, since hydrophobic groups can effectively block the contact between water and metal nodes, kinetically stable MOFs can be directly constructed by using hydrophobic ligands. Besides directly using hydrophobic ligands, introducing suitable hydrophobic groups through PSM also can be used to stabilize water-sensitive MOFs. In 2010, Cohen's team successfully proved that the hydrophobicity of MOFs could be introduced by PSM.[171] According to the PSM strategy, they prepared two types of isoreticular MOFs (IRMOF series and MIL series). For IRMOFs, their water contact angles could increase to 116° after being modified with long alkyl

substituents, and this value could be compatible with common hydrophobic materials. After being modified with different alkyl substituents, the water contact angles of MILs could even reach 150°, demonstrating that their hydrophobicity can be comparable with that of superhydrophobic materials. Based on the PSM method, Bradshaw and co-workers also realized the enhancement of the structural stability of UiO-66-NH_2.[172] They used the diazotization reaction of UiO-66-NH_2 to prepare a more stable MOF (UiO-66-N=N-ind). The modified UiO-66-N=N-ind could retain its structural integrity in a pH = 12 aqueous solution, while the unmodified UiO-66-NH_2 only resisted a weaker basic solution (pH = 9).

In addition to organic ligands, the hydrophobic groups also can be introduced into the metal nodes of MOFs through the PSM strategy. For example, different hydrophobic groups were introduced into the Zr_6-oxo nodes of NU-1000 through the solvent-assisted ligand incorporation (SALI) method by Farha, Hupp, and co-workers.[173,174] The water resistance of Zr_6-oxo nodes could be efficiently improved after being modified with organic carboxylates. Notably, the perfluorodecanoic acid functionalized NU-1000 exhibited remarkable water stability; it could maintain the crystallinity and porosity even after 20 cycles of water vapor adsorption. By introducing hydrophobic phenylsilane into the metal-oxo nodes of NH_2-UiO-66, Kim's group realized the controllable construction of a super-hydrophobic MOF NH_2-UiO-66(Zr)-shp (Fig. 21).[169] NH_2-UiO-66(Zr)-shp not only retained the acid resistance of NH_2-UiO-66(Zr) (*e.g.*, resisted 12 M HCl and 16 M HNO_3) but also exhibited highly improved base stability (resisted 0.1 M NaOH solution at least for 5 hours).

2.4.4.3. Enhancing the kinetic stability by forming hybrid composites. Introducing hydrophobic groups into the pores of MOFs indeed can significantly improve their kinetic stability toward water. However, additional hydrophobic groups in the pores usually reduce the porosity of MOFs. Direct compositing of metastable MOFs and hydrophobic materials can also effectively improve the water stability of MOFs but can maintain their pore structure as much as possible. Many water-stable hybrid composites based on water-instable MOFs have been reported. For example, by coating a thin hydrophobic polydimethylsiloxane (PDMS) layer on the surface of initial MOFs, Yu, Jiang, and colleagues developed a universal approach to improve the water-resistance of MOFs. In addition to improving their water resistance, the fragile MOFs (MOF-5, HKUST-1, and ZnBT) coated with PDMS also inherited their original crystalline structure and pore properties.[175] In addition, Queen's team constructed a series of extremely hydrophobic and stable MOF

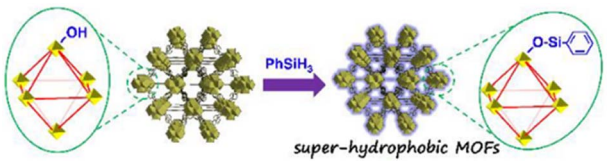

Fig. 21 Preparation of super-hydrophobic NH_2-UiO-66(Zr)-shp. Reproduced from ref. 169 with permission from Wiley, Copyright 2019.

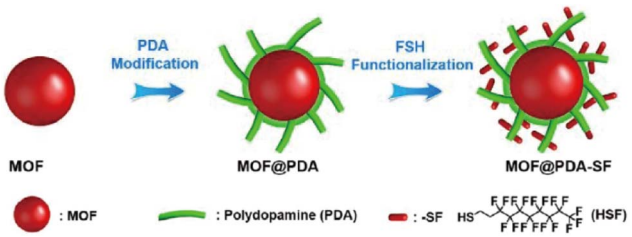

Fig. 22 The modification process used to prepare hydrophobic MOF@PDA-SF composites. Reproduced from ref. 170 with permission from the Royal Society of Chemistry, Copyright 2019.

composites utilizing a post-synthetic polymerization strategy (Fig. 22).[170] Here, polydopamine was first coated on the surface of MOFs and hydrophobic molecules were introduced by Michael addition. Notably, a range of MOFs (*e.g.*, HKUST-1 (Cu), Cu-TDPAT (Cu), and Mg-MOF-74 (Mg)) after modification demonstrated outstanding stability even under strongly acidic or basic conditions. In 2018, Cohen's group successfully incorporated UiO-66-NH_2 into nylon (PA-66) polymer fibers to give a hybrid composite by an interfacial polymerization method, which displayed improved stability.[176] Through interfacial polymerization, the UiO-66-NH_2 MOF was copolymerized with polyamide fiber (PA-66) to produce a hybrid composite with 29% MOF (mass fraction). Compared to MOF particles that were merely physically confined in the polymer, the covalently linked hybrid material exhibited better stability.

Recently, the Pd/UiO-66 nanocomposite surface was successfully covered with a thin layer of hydrophobic polydimethylsiloxane (PDMS) using a chemical vapor deposition (CVD) method by Jiang's group (Fig. 23).[177] The enhanced stability and retained porosity of Pd/UiO-66@PDMS were further confirmed by PXRD and N_2 sorption analysis. Moreover, the modified catalyst (Pd/UiO-66@PDMS) exhibited significantly enhanced surface wettability and recycling stability, paving a new way for developing new catalysts with high activity and stability. Similarly, by combining hydrophobic polymer polystyrene-*block*-polybutadiene-*block*-polystyrene (SBS) with epn-functionalized Mg_2(dobpdc) (epn-MOF) and various

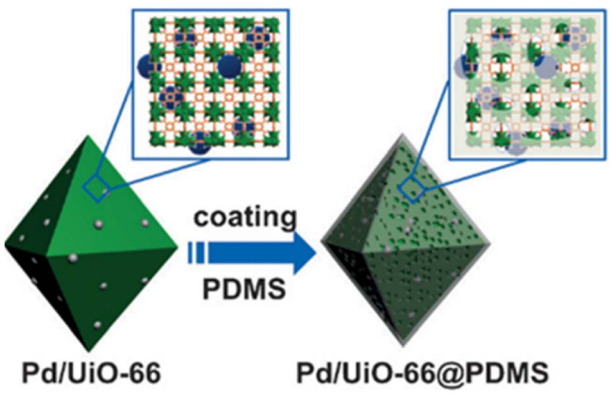

Fig. 23 Preparative route for Pd/UiO-66@PDMS. Reproduced from ref. 177 with permission from Wiley, Copyright 2016.

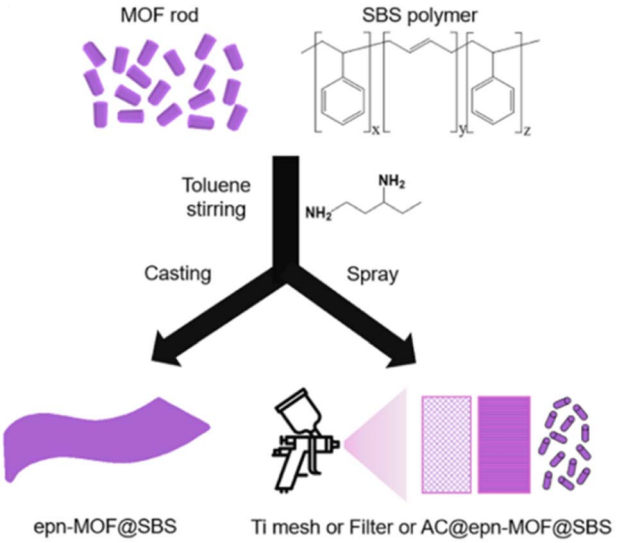

Fig. 24 Fabrication of epn-MOF@SBS, Ti mesh@epn-MOF@SBS, Filter@epn-MOF@SBS, and AC@epn-MOF@SBS composites. Reproduced from ref. 178 with permission from Elsevier, Copyright 2022.

supports (*e.g.*, Ti mesh, HEPA filter, and granular AC), Hong and co-workers prepared a series of epn-MOF@SBS composites on different supports, including Ti mesh@epn-MOF@SBS, Filter@epn-MOF@SBS, and AC@epn-MOF@SBS (Fig. 24).[178] The as-prepared hybrid materials could maintain their stability and activity even after a long time of exposure to 60% RH.

To encapsulate HKUST-1 within polystyrene, Maspoch *et al.* developed a facile spray-drying technique, which could produce water-resistant HKUST-1@polystyrene spheres.[179] Although HKUST-1 is very sensitive to water, the as-prepared hybrid composite (HKUST-1@polystyrene) could also maintain its water uptake capability even after three consecutive cycles. Very recently, Zhao's group realized the controllable construction of a super hydrophobic MOF membrane on polymer substrates through controlling the growth of ZIF-8 and using the surface coating technique.[180] In comparison to its pristine, the as-prepared hybrid composite (PDMS/MOF-NS/PVDF) displayed significantly enhanced hydrophobicity.

Besides hydrophobic polymers, carbon nanotubes could also be incorporated into MOFs, affording a hybrid composite with significantly improved water stability. The growth of Hf_{12}-porphyrin metal–organic frameworks on carbon nanotubes (CNTs) was reported by Lin's group in 2018.[181] The as-synthesized Hf_{12}-CoDBP/CNT hybrid composite could remain inert even in a pH = 1 aqueous solution. The same improved effects could also be achieved in other hybrid composites (*e.g.*, MOFMC, C-CNT, IM-CNT, and LM-CNT) based on MOFs and carbon nanotubes.[182,183]

3. Water-stable MOFs for carbon dioxide capture

3.1. Background of MOFs for carbon capture

Due to the rapid increase of population and the acceleration of urbanization, human's demand for fossil energy has increased dramatically, which leads to excessive emissions of CO_2. It is reported that the concentration of CO_2 in the air has increased from 310 ppm in 1960 to 415 ppm in 2021. Excess CO_2 in the atmosphere leads to a series of serious environmental problems, such as global warming, sea level rise, ocean acidification, and extreme weather. More than half of global CO_2 emissions come from the flue gas of power plants; thus, CO_2 emissions should be greatly reduced if unwanted CO_2 can be effectively captured from flue gas. At present, organic amine solution is mainly used in power plants to capture CO_2 from flue gas, but the desorption of CO_2 from organic amine requires a lot of energy; in addition, organic amine can cause serious corrosion of equipment. Therefore, there is an urgent need to develop more energy-efficient and green technologies for capturing CO_2 from flue gas.

Although CO_2 from flue gas can be captured by decarbonizing devices installed in power plants, about 27% of global CO_2 emissions are difficult to capture effectively. So, it is necessary to develop technologies that can be used to capture trace CO_2 from the air. Direct air capture (DAC) is a negative emission technology in which chemical processes are used to capture CO_2 from ambient air, which can be used to not only reduce the excessive CO_2 (>415 ppm) in the atmosphere to the optimal level below 350 ppm, but also compensate for the CO_2 emissions from economic activities that are difficult to decarbonize. Currently, there are a few absorbents available for DAC, including alkaline aqueous solutions (such as NaOH and KOH) and porous solids loaded with amines. These technologies also have the problem of a high recovery energy, and more energy-efficient DAC technologies should be developed.

Natural gas has been considered as a promising clean energy due to its high energy-conversion efficiency and low environmental impact. Unfortunately, crude natural gas usually contains a large amount of CO_2, which not only sharply reduces the burning heat of methane, but also causes serious corrosion to the transmission pipelines. In order to capture CO_2 from crude natural gas, alkali adsorption technology has been widely used in industry, which also requires a high recovery energy. Thus, more energy-efficient technologies for purifying natural gas are urgently needed.

Alkali solution can indeed efficiently capture unwanted CO_2, but it requires a large amount of energy to recover and tends to corrode equipment. Using suitable porous materials to capture CO_2 can overcome these challenges and achieve more energy-efficient carbon capture. Compared with traditional porous materials such as activated carbon, mesoporous silica, and zeolite, the pore size and pore environment of MOFs can be precisely regulated, which enables them to capture CO_2 more efficiently and selectively. To achieve efficient carbon capture of MOFs in various scenarios (*e.g.*, flue gas decarbonization, direct air capture, and natural gas upgrading), many MOFs with different active sites and pore sizes have been designed and synthesized. Ideally, a practical carbon capture adsorbent should have not only excellent adsorption performance, such as high adsorption capacity, high adsorption selectivity, and low adsorption enthalpy; but also excellent chemical stability, recyclability, and high cost-effectiveness. However, developing

such a MOF remains a huge challenge, as it is very difficult to achieve these functions simultaneously through one MOF.

3.2. Physical and chemical properties of carbon dioxide

To achieve efficient and selective capture of CO_2 by MOFs, it is necessary to fully understand the physical and chemical properties of CO_2 and its competing gases (*e.g.*, N_2 and CH_4) (Scheme 4). CO_2 is a linear molecule with strong polarity, composed of one sp hybrid carbon atom and two sp^2 hybrid oxygen atoms. The as-formed carbon–oxygen bond has the characteristics of both carbon–oxygen double bond and carbon–oxygen triple bond. The carbon atom in the middle is electrically deficient, while the oxygen atoms at both ends are electrically rich. The size and kinetic diameter of CO_2 are $3.19 \times 3.34 \times 5.39$ Å^3 and 3.3 Å respectively. Due to its specific structure, CO_2 can not only coordinate with metal ions providing empty orbitals, but also generate dipole interactions with various polar atoms (*e.g.*, H, N, and O) as well as π–π interactions with conjugated molecules (*e.g.*, benzene ring). In this regard, by introducing suitable active sites that can interact with CO_2 into a MOF, its CO_2 adsorption performance can be improved thermodynamically, and the construction of pores matched with CO_2 (about 3.3 Å) is kinetically conducive to CO_2 capture. N_2, the main component of flue gas and air, may compete with CO_2 in the process of flue gas decarbonization and direct air capture; therefore, inhibiting the competitive adsorption of N_2 is conducive to improving the efficiency of CO_2 capture. N_2 is a spherical, non-polar molecule with a size and kinetic diameter of $3.6 \times 3.6 \times 3.6$ Å^3 and 3.64 Å, respectively. As the main component of natural gas, CH_4 is a spherical molecule with weak polarity, whose size and kinetic diameter are $3.7 \times 3.7 \times 3.7$ Å^3 and 3.758 Å, respectively. By inhibiting the competitive adsorption of CH_4, the purification efficiency of natural gas can be significantly improved. Therefore, by increasing the pore polarity of MOFs and controlling its pore size (smaller than the kinetic diameter of N_2/CH_4), the competitive adsorption of N_2/CH_4 can be significantly inhibited.

3.3. The adsorption mechanisms and characterization of MOFs for carbon dioxide

When a fluid comes into contact with a porous solid, its components accumulate on the surface of the solid, which is called adsorption. If the interactions between the adsorbate and the adsorbent are weak intermolecular interactions (*e.g.*, van der Waals forces, hydrophobic interactions, electrostatic forces, and hydrogen bonding), this process can be defined as physical adsorption, also known as physisorption, which usually exhibits low adsorption heat but fast adsorption and high desorption kinetics. When an adsorption process involves one or more chemical reactions, it can be defined as chemical adsorption (chemisorption), which is an irreversible adsorption process with a high adsorption enthalpy. If the interaction between a specific MOF and CO_2 is relatively weak (*e.g.*, the adsorption enthalpy is less than 40 kJ mol^{-1}), then its adsorption of CO_2 is undoubtedly physical adsorption. In contrast, the adsorption between CO_2 and a MOF that can react with CO_2 while producing new species should be a chemical adsorption process. Despite having a strong interaction with CO_2 (*e.g.*, the adsorption enthalpy is greater than 50 kJ mol^{-1}), a particular MOF does not react with the adsorbed CO_2 or generate new species. We still discuss it according to physical adsorption, even though the real situation may be the coexistence of physical and chemical adsorption.

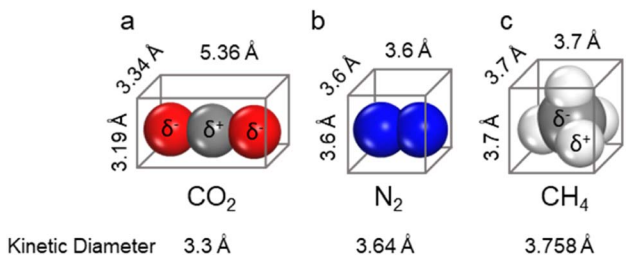

Scheme 4 Physical and chemical properties of CO_2 (a), N_2 (b), and CH_4 (c).

When CO_2 enters the pores of MOFs and interacts with the active sites, not only will the charge distribution or strength of carbon–oxygen bonds be changed, but potential new species may also be formed. All of these can be detected by NMR and infrared absorption spectroscopy (IR). In addition, when the adsorbed CO_2 molecules are orderly distributed in the pores of MOFs, their adsorption sites can be accurately located through SCXRD, PXRD, and neutron powder diffraction (NPD) analyses. Therefore, the adsorption character of MOFs for CO_2 can be analyzed in detail. In addition, due to the determinacy of the structure of MOFs, molecular simulation (MS) is also a useful supplement to understanding the adsorption mechanism of MOFs for CO_2. Next, we briefly introduce the reported adsorption mechanisms and characterization of MOFs for CO_2, hoping to provide a useful guidance for designing MOF-based CO_2 adsorbents with better performance.

3.3.1. Physical adsorption of carbon dioxide in MOFs. Due to the potential of coordination between metal ions and CO_2, various open metal sites (OMSs) were widely introduced into MOFs for improving CO_2 adsorption, with many different types of metal–CO_2 interactions observed. For example, through the coordination between Ni(II) ions and CO_2, Dietzel and co-authors used SCXRD to observe the adsorption sites of CO_2 in MOFs for the first time, where CO_2 was directly attached to the Ni(II) site of CPO-27-Ni (known as Ni-MOF-74) with a Ni–O distance of 2.29 Å (Fig. 25a).[184] In isomorphic MOFs containing harder Co(II) ions, Long and collaborators used *in situ* SCXRD to confirm that open Co(II) ions were the preferential adsorption sites for CO_2 while finding other CO_2 adsorption sites inside the pores (Fig. 25b).[185] For the isomerized MOF (UTSA-74) containing softer Zn(II) ions, Chen's group found that the adsorbed CO_2 molecules could be stabilized by two neighbouring Zn(II) ions synergically (Fig. 25c).[186] In addition, we proved that the Cu(II) ions with planar four-coordination were highly efficient adsorption sites for CO_2 through *in situ* IR, GCMC simulation and DFT optimization (Fig. 25d),[137] which have been widely introduced into MOFs for CO_2 capture.

In addition to various open metal sites, polar atoms that can form strong dipole interactions with CO_2 are another type of

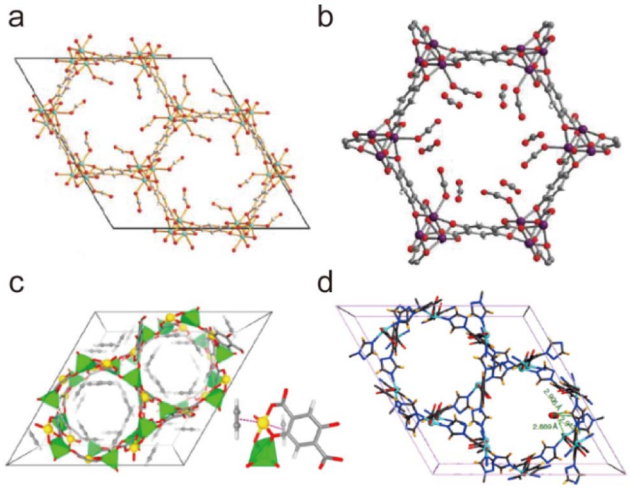

Fig. 25 Carbon dioxide adsorption on open metal ions through coordination interactions. (a) The Ni(II)–CO_2 interactions in CPO-27-Ni. Reproduced from ref. 184 with permission from the Royal Society of Chemistry, Copyright 2008. (b) The Co(II)–CO_2 interactions in Co-MOF-74. Reproduced from ref. 185 with permission from the Royal Society of Chemistry, Copyright 2017. (c) The Zn(II)–CO_2 interactions in UTSA-74. Reproduced from ref. 186 with permission from the American Chemical Society, Copyright 2016. (d) The Cu(II)–CO_2 interactions in FJI-H14. Reproduced from ref. 136 with permission from Springer Nature, Copyright 2017.

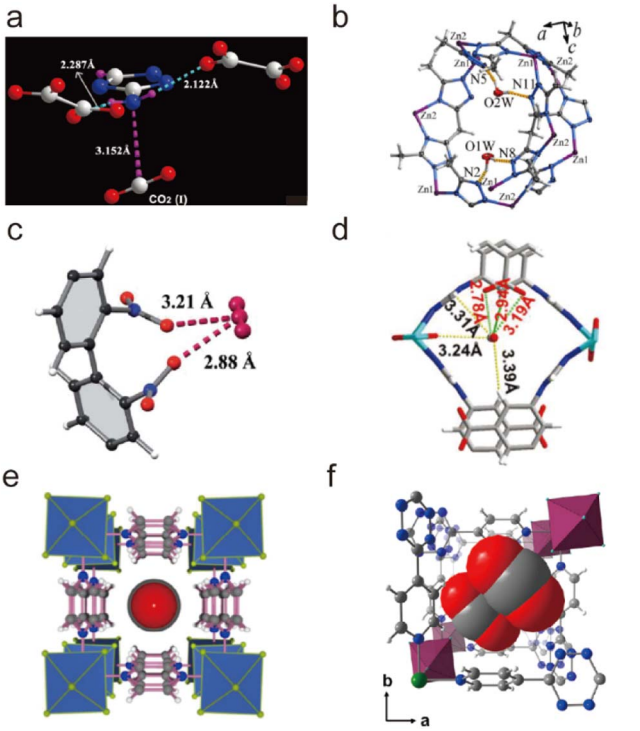

Fig. 26 Carbon dioxide adsorption on electrically rich atoms through dipole interactions. (a) The N···CO_2 dipole interactions in $Zn_2(Atz)_2(ox)$. Reproduced from ref. 187 with permission from the American Association for the Advancement of Science, Copyright 2010. (b) The N···CO_2 dipole interactions in $[Zn_2(btm)_2]$. Reproduced from ref. 188 with permission from the American Chemical Society, Copyright 2012. (c) The O···CO_2 dipole interactions in MFM-102-NO_2. Reproduced from ref. 189 with permission from the Royal Society of Chemistry, Copyright 2020. (d) The O···CO_2 dipole interactions in FJI-H38. Reproduced from ref. 190 with permission from Wiley, Copyright 2023. (e) The F···CO_2 dipole interactions in NbOFFIVE-1-Ni. Reproduced from ref. 191 with permission from the American Chemical Society, Copyright 2016. (f) The F···CO_2 dipole interactions in dptz-$CuTiF_6$. Reproduced from ref. 192 with permission from Elsevier, Copyright 2019.

adsorption site for CO_2, which have also been widely introduced into MOFs for carbon capture, and a variety of polar groups are proved to stabilize the adsorbed CO_2 molecules. For instance, in the MOF ($Zn_2(Atz)_2(ox)$, Atz = 3-amino-1,2,4-triazole, ox = oxalate) containing aromatic amine groups, Shimizu and co-workers observed the bonding of adsorbed CO_2 and aromatic amine groups for the first time, where the electrically deficient C atoms could be stabilized by the electrically rich N atoms. The distance between them was about 3.152 Å, less than the sum of van der Waals radii of N and C atoms (Fig. 26a).[187] Based on the uncoordinated triazole groups, Chen and Zhang also observed strong N···C dipole interactions (Fig. 26b),[188] where the adsorbed CO_2 molecules were synergistically stabilized by two adjacent N atoms (C15–N8, 3.178(8) Å; C15–N2, 3.011(8) Å; C16–N11, 3.15(1) Å; C16–N5, 3.26(1) Å), resulting in a high adsorption enthalpy. Polar oxygen atoms can also be served as adsorption sites for CO_2 capture. For example, Schröder and Yang used nitro groups to achieve an efficient promotion of CO_2 adsorption. Through NPD analyses, they further found that there were strong C···O dipole interactions between the adsorbed CO_2 and nitro groups with a distance of 2.88 Å and 3.21 Å, respectively (Fig. 26c).[189] Recently, our group proved that the carboxylic acid group could well adsorb and stabilize CO_2 through SCXRD. In the structure of CO_2@FJI-H38, the adsorbed CO_2 is simultaneously stabilized by two O atoms of the carboxylic acid group, with the shortest C–O distance of only 2.78 Å, far below the sum of van der Waals radii of C and O atoms (Fig. 26d).[190] Like N and O atoms, the more electronegative fluorine atoms can also adsorb CO_2 effectively. As confirmed by Eddaoudi's group, the CO_2 adsorbed in the pores of NbOFFIVE-1-Ni can be efficiently stabilized by four different $(NbOF_5)^{2-}$ with a C···F distance of 3.050(8) Å, lower than the sum of the van der Waals radii of C and F atoms (Fig. 26e).[191] In another isomorphic MOF (dptz-$CuTiF_6$), the CO_2 located in the pore was also stabilized by the surrounding TiF_6^{2-} ions, where the distance between the F and C atoms was only 2.512 Å, indicating that a stronger C···F dipole interaction is formed (Fig. 26f).[192]

Since electron-rich oxygen atoms easily form hydrogen bonding with electron-deficient hydrogen atoms, active hydrogen atoms can also serve as adsorption sites for CO_2. In 2012, Chen's group found that a MOF (UTSA-16) without OMS could also efficiently capture CO_2. Through SCXRD analysis, they found that the coordinated H_2O on the framework was the adsorption site of CO_2 (O3w–H···O72 = 2.971(1) Å and O3w–H···O71 = 3.067(1) Å) (Fig. 27a).[193] In the same year, Schröder and Yang confirmed that the hydroxyl group was also an efficient adsorption site for CO_2 through PXRD. In the structure of CO_2@NOTT-300, the adsorbed CO_2 and hydroxyl group formed

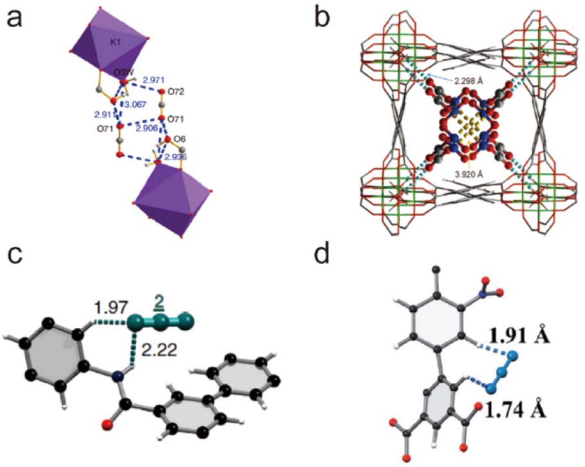

Fig. 27 Carbon dioxide adsorption on electron-deficient H atoms through hydrogen-bonding interactions. (a) The OH···O hydrogen-bonding interactions in UTSA-16. Reproduced from ref. 193 with permission from Springer Nature, Copyright 2012. (b) The OH···O hydrogen-bonding interactions in NOTT-300. Reproduced from ref. 194 with permission from Springer Nature, Copyright 2012. (c) The NH/CH···O hydrogen-bonding interactions in MFM-188a. Reproduced from ref. 195 with permission from Springer Nature, Copyright 2017. (d) The CH···O hydrogen-bonding interactions in MFM-102-NO_2. Reproduced from ref. 189 with permission from the Royal Society of Chemistry, Copyright 2020.

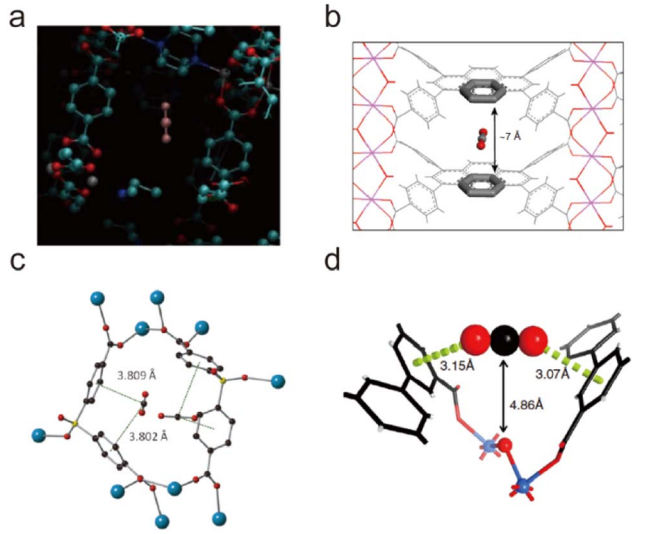

Fig. 28 Carbon dioxide adsorption on phenyl groups through π–π interaction. (a) and (b) The potential π–π interaction between adsorbed CO_2 and phenyl rings based on MS. Reproduced from ref. 196 with permission from the American Chemical Society, Copyright 2013. Reproduced from ref. 197 with permission from Springer Nature, Copyright 2019. (c) The π–π/p–π interactions between adsorbed CO_2 and phenyl groups in CaSDB. Reproduced from ref. 198 with permission from Wiley, Copyright 2013. (d) The π–π/p–π interactions between adsorbed CO_2 and phenyl groups in MFM-300(V^{IV}). Reproduced from ref. 199 with permission from Springer Nature, Copyright 2017.

a stronger hydrogen-bonding interaction than that between CO_2 and UTSA-16, with a distance of only 2.298 Å between H and O atoms (Fig. 27b).[194] In 2017, they confirmed that the active hydrogen on the amide group and phenyl group could also form strong hydrogen-bonding interactions with adsorbed CO_2 through NPD experiments. The distance of the adsorbed CO_2 from the H atoms of the amide group and the phenyl group was 2.22 and 1.97 Å, respectively (Fig. 27c).[195] In the structure of CO_2@MFM-102-NO_2, they further found that the adsorbed CO_2 was only 1.91 and 1.74 Å away from the H atoms of the phenyl group, implying the formation of stronger hydrogen-bonding based on CH and CO_2 (Fig. 27d).[189]

Due to the presence of π bonds and p electrons, π–π or p–π interactions can be formed between CO_2 and suitable conjugated molecules. Therefore, molecules containing conjugated groups (*e.g.*, phenyl groups) can also serve as adsorption sites of CO_2. Both Walton and Smit's group used MS to confirm that the phenyl rings could indeed serve as an effective adsorption site of CO_2 (Fig. 28a and b).[196,197] However, due to its weak strength and the lack of clear directionality, it is difficult to directly characterize the π–π interactions between adsorbed CO_2 and MOFs. So far, only very limited examples that can directly reveal the π–π interactions between CO_2 and MOFs have been reported. In 2013, Li and Paris first observed the π–π/p–π interactions between adsorbed CO_2 and phenyl groups through SXCRD analysis, where the adsorbed CO_2 was located between two centroids of the phenyl groups, with an average distance of 3.81 Å (Fig. 28c).[198] Later, Schröder and Yang discovered another type of interaction between adsorbed CO_2 and phenyl groups through NPD analysis. In the structure of the CO_2-adsorbed MFM-300(V^{IV}), CO_2 bound with the two adjacent phenyl rings in a 'sandwich' form, and the distance between the O atom of CO_2 and the phenyl group was 3.069(2) and 3.146(3) Å respectively (Fig. 28d).[199]

In short, OMSs that can provide empty orbitals for CO_2, polar atoms (*e.g.*, N, O, and F) that can generate dipole interactions with CO_2, H atoms that can form hydrogen-bonding with CO_2, and conjugated molecules can all serve as effective sites for the physical adsorption of CO_2. It should also be pointed out that multiple CO_2 adsorption sites can exist simultaneously in MOFs, and adsorbed CO_2 molecules can be synergistically stabilized by multiple adsorption sites.

3.3.2. Chemical adsorption of carbon dioxide in MOFs. As a weak acidic gas, CO_2 can react with aliphatic amines and their derivatives to form ammonium carbamates/ammonium bicarbonates, which can be reversibly decomposed into CO_2 and free amines under the induction of suitable external stimuli (*e.g.* temperature). Therefore, amino groups that can reversibly react with CO_2 can be introduced into MOFs as chemisorption sites for CO_2 capture. Although Long's group had already achieved the chemisorption of CO_2 using an ethylenediamine functionalized MOF as early as 2009,[208] it was not until 2015 that he and collaborators directly observed the interactions between adsorbed CO_2 and aliphatic amines using high-resolution PXRD. In the adsorbed CO_2 MOF (mmen-Mn_2(dobpdc) (mmen = *N*,*N*′-dimethylethylenediamine, $dobpdc^{4-}$ = 4,4′-dioxidobiphenyl-3,3′-dicarboxylate)), the reaction between adsorbed CO_2 and the coordinated mmen can be promoted by the adjacent

mmen, thus achieving the rapid formation of ammonium carbamate at a low pressure. When CO_2 adsorption was saturated, these newly formed ammonium carbamate would form an infinite ammonium carbamate chain (Fig. 29a).[200] Through ^{13}C solid-state NMR analyses, Yaghi's group found that the carbon capture product of primary alkylamine functionalized MOFs (IRMOF-74-III-$(CH_2NH_2)_2$) under dry conditions was carbamic acid (the signal at 160.3 ppm) rather than ammonium carbamate, which is the major product of other primary amine functionalized MOFs. However, in the presence of water vapor, the as-formed carbamic acid could effectively convert into ammonium carbamate (the signal at 164.0 ppm) (Fig. 29b).[201] Through the regulation of metal ions and ligands, Long and co-workers realized the regulation of CO_2 chemisorbed products in diamine-M_2(dobpdc) MOFs. For example, the chemisorbed products of a Zn-based MOF (dmpn-Zn_2(dobpdc), dmpn = 2,2-dimethyl-1,3-diaminopropane) could be ammonium carbamate and carbamate pairs (the signal at 161.1 ppm) (Fig. 29c),[202] which was confirmed using ^{13}C solid-state NMR and SCXRD analyses. For an isomorphic Mg-based MOF (dmpn-Mg_2(-dobpdc)), an unusual mixture of carbamic acid and ammonium carbamate at a ratio of 1 : 1 would be formed (Fig. 29d).[203]

In addition to aliphatic amines, O-containing alkaline groups (*e.g.*, hydroxyl anions and alcohol anions) can also react reversibly with CO_2 to produce carbonates. Thus, suitable O-containing groups that can react reversibly with CO_2 can also be introduced into MOFs as chemisorption sites of CO_2. Due to the strong alkalinity of O-containing alkaline groups, only MOFs with an excellent base tolerance can introduce them. So only very limited examples of CO_2 adsorption based on O-containing alkaline groups have been reported. In 2011, Stoddart and Yaghi used CD-MOF-2 to achieve the chemisorption of CO_2 in MOFs for the first time, where free primary alcohol groups could react with adsorbed CO_2 to form alkyl carbonates, which can be monitored through ^{13}C solid-state NMR (the signal at 158 ppm) (Fig. 30a).[204] In 2015, Zhang and Chen achieved another mode of CO_2 chemisorption using a MOF (MAF-X25ox, [$Mn^{II}M$-n^{III}(OH)Cl_2(bbta)], H_2bbta = 1*H*,5*H*-benzo(1,2-*d*:4,5-*d*′)bis-triazole) containing monodentate hydroxide. The newly formed bicarbonate could be determined by IR spectroscopy, where multiple new adsorption peaks (the peaks at 3682/1224/1050 cm^{-1}) attributed to bicarbonate were generated simultaneously (Fig. 30c).[206] By mimicking the active centre of carbonic anhydrase, both Wade and Dincă's groups synthesized different MOFs containing active ZnN_3OH units by introducing hydroxide anions into Zn(II) metal nodes, separately realizing their chemical adsorption of CO_2.[209] Here, the Zn–OH group also reacts with the adsorbed CO_2 to produce bicarbonate, which can be confirmed by *in situ* IR and diffuse reflectance infrared Fourier transform spectroscopy respectively (Fig. 30d).[207] Recently, Milner and collaborators also achieved the chemical adsorption of CO_2 using a MOF (KOH CD-MOF), which was isomorphic to CD-MOF-2 but less alkaline. Here, the adsorbed CO_2 reacted with the hydroxyl anions in the pores of the MOF to form bicarbonate, which could be confirmed using solid ^{13}C NMR (the signal at 159.6 ppm) and IR spectra (the peak at 1663 cm^{-1}) simultaneously (Fig. 30b).[205]

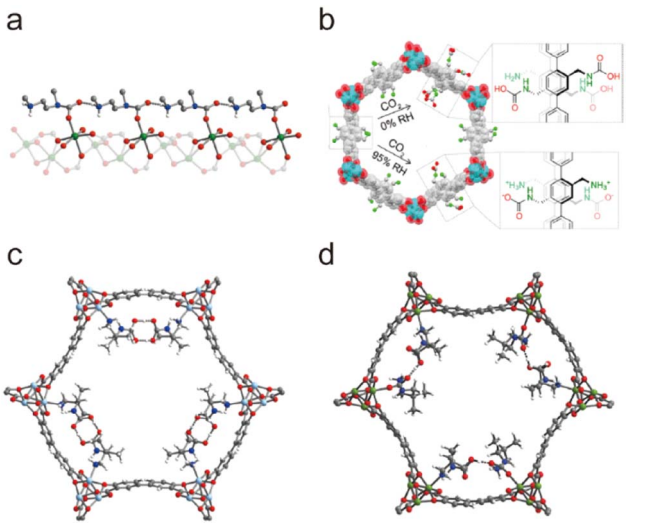

Fig. 29 Carbon dioxide adsorption on nitrogen atoms through the formation of ammonium carbamate/carbamic acid. (a) The ammonium carbamate chain in mmen-Mn_2(dobpdc). Reproduced from ref. 200 with permission from Springer Nature, Copyright 2015. (b) The carbamic acid and ammonium carbamate in IRMOF-74-III-$(CH_2NH_2)_2$. Reproduced from ref. 201 with permission from the American Chemical Society, Copyright 2017. (c) The carbamate pairs in dmpn-Zn_2(dobpdc). Reproduced from ref. 202 with permission from the American Chemical Society, Copyright 2017. (d) The mixture of carbamic acid and ammonium carbamate in dmpn-Mg_2(dobpdc). Reproduced from ref. 203 with permission from the American Chemical Society, Copyright 2018.

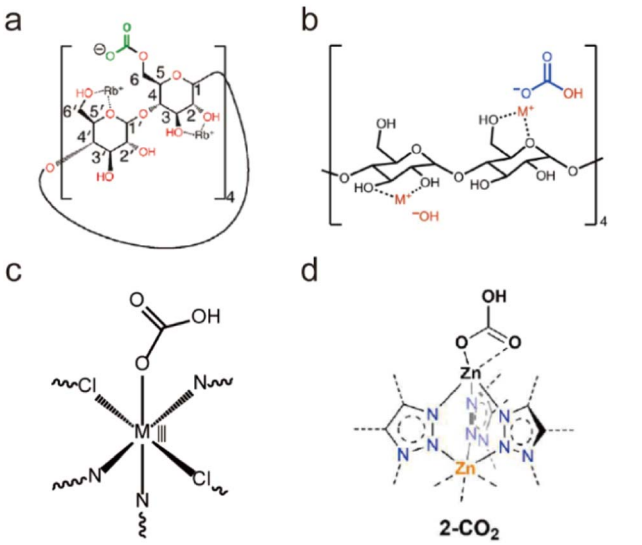

Fig. 30 Carbon dioxide adsorption on oxygen atoms through the formation of carbonate. (a) The alkyl carbonates in CD-MOF-2. Reproduced from ref. 204 with permission from the American Chemical Society, Copyright 2011. (b) The bicarbonate in KOH CD-MOF. Reproduced from ref. 205 with permission from Wiley, Copyright 2022. (c) The bicarbonate in MAF-X25ox. Reproduced from ref. 206 with permission from the Royal Society of Chemistry, Copyright 2015. (d) The bicarbonate in [$Zn(ZnOH)_4$(bibta)$_3$]. Reproduced from ref. 207 with permission from the American Chemical Society, Copyright 2018.

Table 2 The performances of some representative MOFs for CO_2 capture from flue gas

MOFs	Stability	CO_2 adsorption amount at 1 bar (mmol g^{-1})	CO_2 adsorption amount at 0.15 bar (mmol g^{-1})	IAST selectivity at 1 bar (15/85) CO_2/N_2	Q_{st} (kJ mol^{-1})	Temperature (K)	Ref.
UiO-66	pH = 0–12	1.79	0.37	19.4	24.5	298K	234
UiO-66-NH_2	Water-stable	3	~0.11	~57	28	298	235
UiO-66-$(OPr)_2$	pH = 1–11	~2.6	1.19	39.1	~34.5	298	236
UiO-66-$(OH)_2$	Water-stable	~4.6	1.92	66	34.5	298	236
UiO-66-SO_3H-0.15	pH = 1–12	2.23	0.51	16.3	26.6	298	234
UiO-66-SO_3Li-0.15	pH = 1–12	3.28	0.93	39.7	25.4	298	234
UiO-66-$(COOLi)_4$-EX	Water-stable	2.34	0.7	26.62	27.5	298	237
UiO-66(Zr)-$(COOLi)_2$	Water-stable	1.36	0.44	50.8	34.7	298	238
UiO-66-EA	Water-stable	1.7	1.05	365	66	298	239
UiO-66(Hf)-$(OH)_2$	pH = 1–10	4.06	1.81	93	28.4	298	240
NOTT-300	Water-stable	7.0	2.64	815[e]	27–30	273	194
$Al(HCOO)_3$	(HCl 12M-pH 14)	~4	2.7	368	47.9	320	210
MIP-207	Water-stable	2.11	0.89	52.8	—	298	101
CPM-74	pH = 3–10	~2.91	—	72–77 (10 : 90)	33	198	160
NOTT-140	Water-stable	20.72[c]	—	—	24.7	283	246
La-BTN	pH = 2–12	3.904	—	93	28.5	273	109
NKMOF-3-Eu	Moisture-stable (90% RH)	1.9	—	~160	47	298	212
NJU-Bai53	pH = 2–11	5.01	—	—	88.3	298	233
ZIF-301	Moisture-stable (80% RH)	1.47[f]	—	19[e]	~30	298	247
ZIF-300	Moisture-stable (80% RH)	1.32[f]	—	22[e]	~28	298	247
ZIF-1001	pH = 3–14	~0.67	0.328	19.7	26.4	298	248
ZIF-1002	pH = 3–14	~0.50	0.268	21.5	26.9	298	248
ZIF-1003	pH = 3–14	~0.49	0.265	21.6	28.4	298	248
ZIF-1004	pH = 3–14	~0.65	0.348	24.4	28.1	298	248
ZnF(daTZ)	pH = 1–12	~1.8	0.96	120	33	298	249
ZnF(aTZ)	pH = 2–12	~1.85	0.56	46	32.3	298	249
ZnF(TZ)	pH = 3–12	~1.63	0.27	13	23.6	298	249
SIFSIX-3-Zn	Moisture-stable (74% RH)	2.55	—	1818	45	298	214
SIFSIX-2-Cu-i	Moisture-stable (95% RH)	5.41	—	140	31.9	298	213
UTSA-120	Moisture-stable (80% RH)	5.0	3.56	~600	27–31	296	215
dptz-$CuTiF_6$	Moisture-stable	4.52	2.93[i]	—	38.2	298	192
Cu-BTTri	Water-stable	3.24	0.277[d]	21	21	298	130
SIFSIX-3-Cu	Moisture-stable (74% RH)	~2.50	—	—	54	298	214
Qc-5-Cu-sql-β	Water-stable	2.16	—	40 000	36	293	216
Cu–F-pymo	pH = 1–14	1.19	—	$>10^7$	29.1	298	250
TIFSIX-Cu-TPA	Water-stable	2.1	—	910	39.2	298	251
SIFSIX-18-Ni-β	Moisture-stable (90% RH)	~3	~2.8	—	52	298	230
SIFSIX-3-Ni	Moisture-stable (75% RH)	2.7	~2.5[i]	—	50.9	298	231
TIFSIX-3-Ni	Moisture-stable (75% RH)	~2.42	2.39	—	50	298	229
NbOFFIVE-1-Ni	Moisture-stable (95% RH)	2.2	—	—	54	298	191
CALF-20	Water-stable	4.07[a]	—	230 (10 : 90)	39	293	217
FJI-H14	pH = 2–12	6.52	2.3	51	26.6	298	136
FJI-H29	pH = 2–13	1.79	0.92	146	34	298	138
ZU-301	pH = 2–12	2.44	—	~850	38	298	252
PCN-200	pH = 2–12	~1.56	~1.69	60	38.5	273	253
MOF-808-DL-Lys	Water-stable	—	1.04	—	80	298	211
MOF-808-Gly	Water-stable	—	0.54[g] 0.69[h]	—	46	298	211
een-Mg_2(dobpdc)	Moisture-stable (100% RH)	5.05	4.04	—	70–74	313	226
en-Mg_2(dobpdc)	Moisture-stable (100% RH)	4.57	3.62	230	49–51	298	219
ipen-Mg_2(dobpdc)	Moisture-stable (100% RH)	4.05	3.47	—	76–85	313	226 and 242
een-MOF/Al–Si–C17-200	Moisture-stable	~3.47	2.82	342(15 : 75)	52−66	313	220
Mg_2(dobpdc)(3-4-3)	Moisture-stable	~3.4[b]	—	—	99	363	243
en-CuBTTri	Water-stable	1.27	0.366[d]	25	90	298	130
MAF-X25ox	Water-stable	7.14	4.08	250	120	298	206
MAF-X27ox	Water-stable	6.70	4.06	262	124	298	206
$KHCO_3$ CD-MOF	Water-stable	2.50	0.63	81	49.5 ± 1.8	313	205
PN@MOF-5	Moisture-stable (40% RH)	3.48	—	212(14 : 86)	29	273	222

[a] 1.2 bar. [b] At 40 mbar. [c] At 20 bar. [d] 0.06 bar. [e] Calculated from Henry's law constant. [f] 800 torr. [g] Dry air. [h] RH 10%. [i] 0.1 bar.

In short, suitable alkaline groups (*e.g.*, aliphatic amines, hydroxyl anions, and alcohol anions) that can react reversibly with CO_2 can be used as chemisorption sites of CO_2, and the newly formed species based on adsorbed CO_2 can be characterized through solid-state NMR and IR spectroscopy. It is worth mentioning that physical adsorption can also coexist even if an MOF has a high density of chemisorption sites.

3.4. Carbon capture based on water stable MOFs

As mentioned previously, since the pore size and pore environment of MOFs can be precisely controlled through structural design, they have better prospects in the field of carbon capture than traditional porous materials such as mesoporous silicon and zeolite. Indeed, the carbon capture performance of some MOFs has surpassed that of commercial zeolite materials. Considering that water vapor is widely present in flue gas, air, and crude natural gas, a practical carbon adsorbent should first have a good water vapor resistance. Although there have been many reviews on the progress of MOFs in the field of carbon capture, these articles are mainly focused on carbon capture performance and mechanisms. Here, we focus on the progress of water-stable (at least moisture stable) MOFs in flue gas decarbonization, direct air capture, and natural gas purification, hoping to provide a useful reference for the development of practical and excellent carbon adsorbents.

3.4.1. Carbon dioxide capture from flue gas. The total pressure of flue gas produced by a coal-fired power plant is about 1 atm, which contains 73–77% N_2, 15–16% CO_2, 5–7% H_2O, 3–4% O_2. This means that a practical MOF should have a high adsorption capacity and CO_2/N_2 adsorption selectivity, as well as a good water stability. In order to achieve flue gas decarbonization, many MOFs with various CO_2 active sites or matching CO_2 pores have been reported, and in this section, only MOFs that are at least wet resistant are discussed (Table 2).

As mentioned above, water-stable MOFs can be directly constructed from hard metal ions and carboxylate ligands. Then, using this strategy, many water-stable MOFs have been synthesized and used for carbon capture. For example, based on the cheap Al(III) ions and formate ligands, Cheetham, Zhao, and co-workers prepared a chemically stable MOF (ALF), which could retain its framework in both strong base solutions (1 M NaOH) and acidic solutions (12 M HCl) (Fig. 31a).[210] Due to its polar ultramicro-pores, ALF could selectively capture CO_2 from N_2 with a high CO_2/N_2 (85 : 15) selectivity of 368 (Fig. 31b). Notably, ALF could be used to effectively extract CO_2 from simulated flue gas (15/85 CO_2/N_2 binary gas at 323 K) (Fig. 31c) with a high adsorption capacity (0.80 mmol g^{-1}) and adsorption selectivity (75) (Fig. 31c), and such excellent separation performance could remain for at least 130 cycles (Fig. 31d). Furthermore, ALF could be prepared on a large scale, making it a potential carbon capture reagent for flue gas decarbonization.

Due to the excellent water stability of Zr–O clusters, many functionalized Zr-MOFs have been synthesized for carbon capture.[234–240] For example, Yaghi's group prepared a series of amino acid (AA) functionalized MOFs (MOF-808-AA) based on a highly stable MOF-808 [$Zr_6O_4(OH)_4(BTC)_2(HCOO)_6$], which

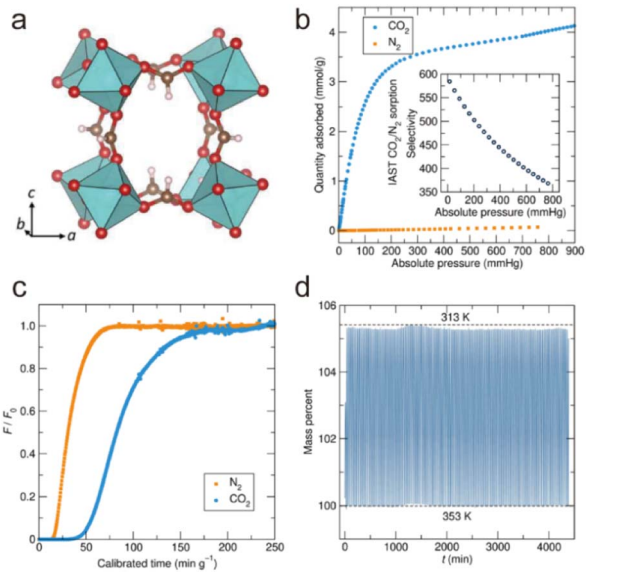

Fig. 31 The structure and CO_2 adsorption performance of ALF. Reproduced from ref. 210 with permission from the Advancement of Science, Copyright 2022. (a) The structure of ALF. (b) The CO_2/N_2 sorption isotherms of ALF at 298 K. (c) The breakthrough curves of ALF at 323 K. (d) 130 cycles of adsorption and desorption.

could effectively capture CO_2 from simulated flue gas in the presence of water.[211] The CO_2 uptake performances of MOF-808AAs varied from 0.277 to 1.040 mmol g^{-1} at 15 kPa (15% CO_2 in 1 atm gas mixture, relevant to flue gas). According to the binary CO_2/H_2O adsorption isotherms, the CO_2 uptake of MOF-808-Gly in the presence of water was significantly higher than that under dry conditions. This might be because the amine residues in the pores enabled MOF-808-AA to have enough affinity for CO_2 to form bicarbonate. Moreover, the adsorbed CO_2 could be released *via* vacuum swing adsorption instead of heating. By introducing ethanolamine (EA) into water-stable UiO-66, Zhang and co-workers also realized an efficient CO_2 capture under humid conditions.[239] Due to the strong interactions between amino groups and CO_2, the newly formed UiO-66-EA displayed higher adsorption enthalpy (66 kJ mol^{-1}) and adsorption selectivity (356) than the original UiO-66 (30 kJ mol^{-1} and 15), and such excellent CO_2 adsorption performance could be completely maintained even at 82% RH.

Water-stable lanthanide MOFs can also serve as efficient CO_2 adsorbents. For example, Zhang's team synthesised a series of robust ultramicroporous Ln-MOFs (NKMOF-3-Ln) (Fig. 32a), which could maintain their framework intact after being exposed to humid air with 90% RH for 7 days.[212] Due to its enzyme-like channels, NKMOF-3-Ln could be used to realize molecular sieving of CO_2 from N_2 (Fig. 32b and c), in which the CO_2 adsorption capacity and adsorption enthalpy would be enhanced gradually with the contraction of the ionic radius of lanthanide elements (Fig. 32d).

As described previously, thermodynamically stable MOFs could also be constructed using soft metal ions and soft N-containing ligands. Many water/moisture-stable MOFs based on this strategy have been used for carbon capture. For example,

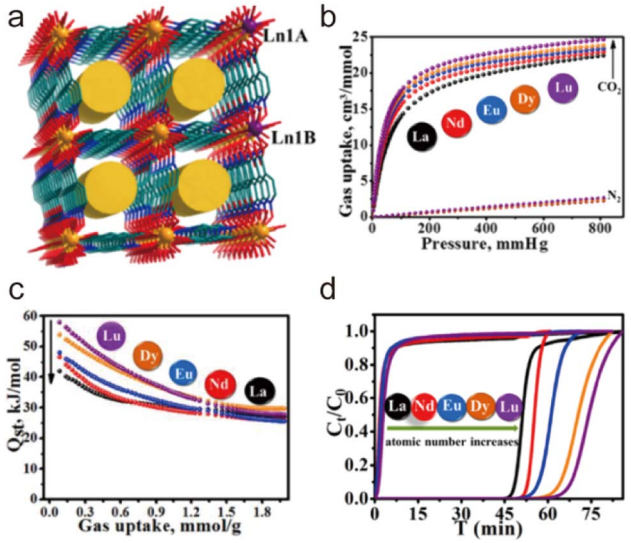

Fig. 32 (a) The structure of NKMOF-3-Ln. (b)–(d) The CO_2/N_2 adsorption isotherms, CO_2 adsorption enthalpy, and breakthrough curves of CO_2/N_2 (15/85) mixtures at 298 K. Reproduced from ref. 212 with permission from the American Chemical Society, Copyright 2019.

Zaworotko, Eddaoudi and co-workers used moisture-stable ultramicroporous frameworks (SIFSIX-2-Cu-i and SIFSIX-3-Zn) to realize an efficient and selective CO_2 capture (Fig. 33a). Due to the matched pore size (5.15 Å and 3.84 Å) and strong polar F^- anions, both of them could be used to effectively and selectively capture CO_2 at a relatively low CO_2 partial pressure (0.1 bar) (Fig. 33c and d).[213,214] Notably, SIFSIX-2-Cu-i could maintain its CO_2 adsorption capacity in the presence of water vapour (Fig. 33b). Such excellent CO_2 adsorption performance makes SIFSIX-2-Cu-i a promising absorbent for capturing CO_2 from flue gas.

To further enhance CO_2 capture, Chen *et al.* synthesized another ultramicroporous MOF (UTSA-120) using 3, 6-di(4-pyridyl)-1,2,4,5-tetrazine ligand, which had a similar pore to SIFSIX-2-Cu-i but with abundant N atoms.[215] Compared with SIFSIX-2-Cu-i, UTSA-120 not only displayed a better CO_2 sorption capacity (3.56 mmol g^{-1} at 296 K) at a low pressure (0.15 bar), but also exhibited a higher CO_2/N_2 adsorption selectivity. Notably, the IAST selectivity of UTSA-120 for simulated flue gas was 4 times higher than that of SIFSIX-2-Cu-i. Such an enhanced CO_2 sorption capacity at a low pressure was thought to have resulted from the high density of nitrogen sites. Even after an exposure of the UTSA-120 sample to air for 1 month, its carbon capture performance could be completely maintained.

As mentioned previously, the crystallinity and stability of MOFs can be optimized using self-assembling ligands containing both soft and hard coordination atoms with soft metal ions. Based on this strategy, many water-stable MOFs have been developed and used for CO_2 capture. For instance, Zaworotko, Zhang and co-workers prepared a water-stable MOF (Qc-5-Cu-sql-β) based on quinoline-5-carboxylic acid (HQc) and Cu(II) salts,[216] which had a very small pore that could match with CO_2 very well (3.3 Å). Notably, Qc-5-Cu-sql-β could maintain its structural integrity not only in water for 21 days but also in air with 75% RH for 14 days. Due to the well-matched pores, Qc-5-Cu-sql-β could be used to realize the molecular sieving of CO_2 with a very high IAST selectivity of 40 000. Dynamic breakthrough experiments further demonstrated that the CO_2 separation capacity of Qc-5-Cu-sql-β could also be maintained even at 75% RH.

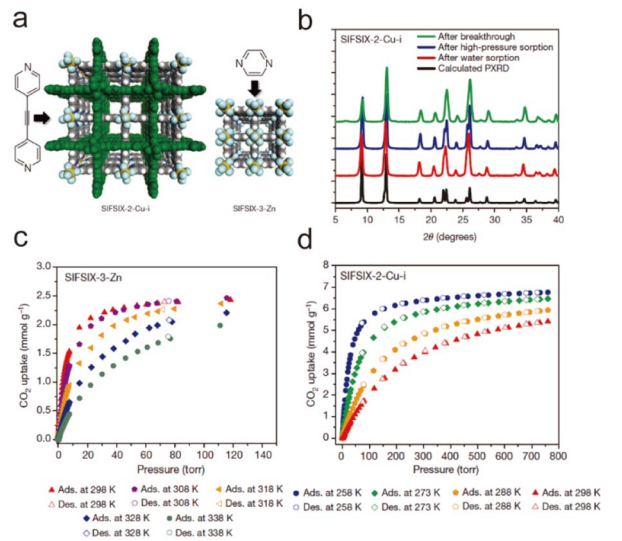

Fig. 33 (a) The structure of SIFSIX-2-Cu-i and SIFSIX-3-Zn. (b) PXRD patterns of SIFSIX-2-Cu-i after breakthrough experiments, high-pressure absorption, and water adsorption. (c) and (d) The CO_2 sorption isotherms of SIFSIX-3-Zn (c) and SIFSIX-2-Cu-i at different temperatures. Reproduced from ref. 213 and 214 with permission from Springer Nature, Copyright 2015.

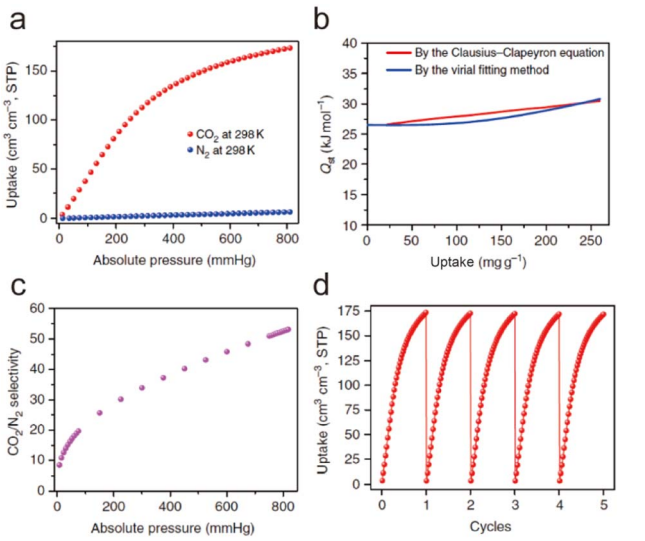

Fig. 34 (a) The CO_2 and N_2 adsorption isotherms for FJI-H14 at 298 K. (b) The isosteric heat of CO_2 adsorption (Q_{st}) for FJI-H14. (c) The IAST selectivity of FJI-H14 for CO_2/N_2 (15 : 85). (d) 5 Cycles of CO_2 adsorption for FJI-H14 at 298 K. Reproduced from ref. 136 with permission from Springer Nature, Copyright 2017.

Based on the H_2BTTA ligand containing both N and O atoms, our group also realized the controlled construction of an acid/base-resistant MOF (FJI-H14) (Fig. 12g) and its efficient carbon capture.[136] FJI-H14 exhibited a very high CO_2 adsorption capacity of 6.52 mmol g^{-1} while only with a relatively low adsorption enthalpy (the Q_{st} at a low coverage is 26.6 kJ mol^{-1}) (Fig. 34a and b). Its IAST selectivity for a CO_2/N_2 (15 : 85) mixture was calculated to be 51 at 298 K and 1 bar (Fig. 34c). Even after 5 cycles, FJI-H14 still retained almost 100% adsorption capacity, suggesting its excellent CO_2 tolerance (Fig. 34d). Mechanistic studies indicated that such excellent CO_2 adsorption performance (*e.g.*, very high adsorption capacity and high adsorption selectivity) came from the synergy of the confined pores and high density of open metal sites.

Using 1,2,4-triazolate, oxalate, and Zn(II) as coordination units, Shimizu and co-workers prepared another highly stable MOF ([Zn_2(1,2,4-triazolate)$_2$(oxalate)], CALF-20) (Fig. 35a).[217] Even after being exposed to steam at 150 °C for a week, CALF-20 could well maintain its structure. The uptake of CALF-20 for CO_2 was up to 4.07 mmol g^{-1} at 1.2 bar and 293 K, and its IAST selectivity for a CO_2/N_2 mixture (10 : 90) was calculated to be 230 (Fig. 35b). Such excellent CO_2 adsorption capacity could also be retained in the presence of water vapor due to different adsorption sites of CO_2 and H_2O. Furthermore, CALF-20 was resistant to wet acid gases and could be reused (>450 000 cycles) without the loss of adsorption capacity. In addition, the kg-scale of CALF-20 could be mildly prepared. All of these make CAL-20 a potential adsorbent for decarbonization in power plants.

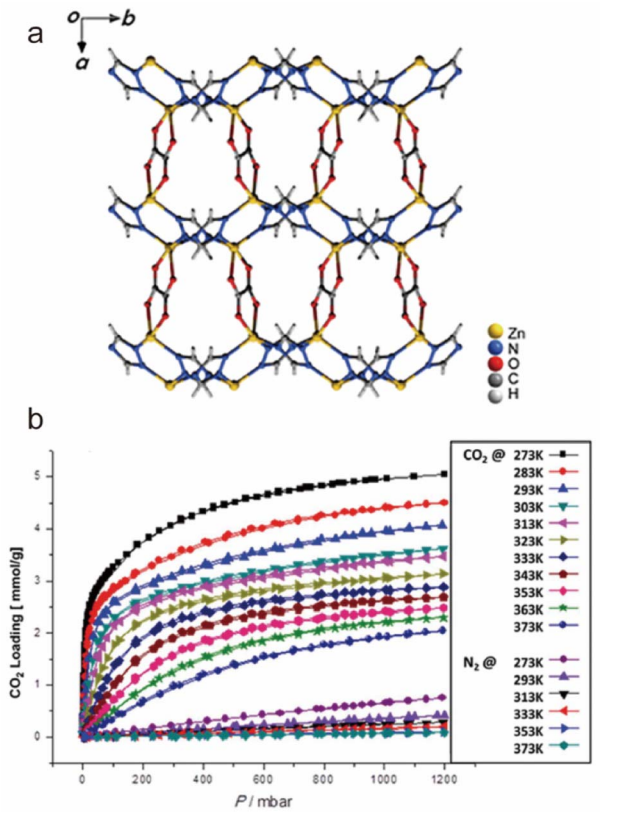

Fig. 35 (a) The structure of CALF-20. (b) The CO_2 and N_2 isotherms of CALF-20 at different temperatures. Reproduced from ref. 217 with permission from the Advancement of Science, Copyright 2021.

Active sites (*e.g.*, amines and hydroxides) that can strongly interact with CO_2 are often also able to coordinate with metal ions, so it is difficult to directly synthesize MOFs containing these active sites. By introducing these functional groups into water-stable MOFs, CO_2 adsorption can be promoted while also maintaining their stability. For example, through introducing ethylenediamine (en) into a water-stable MOF (CuBTTri) constructed from soft N-containing ligands, Long and co-workers successfully prepared an en-functionalized MOF (en-CuBTTri) and realized an enhanced CO_2 capture.[130] After ethylenediamine grafting, the selectivity of CO_2 over N_2 increased from 21 to 25 at 1 bar; and the adsorption enthalpy of CO_2 significantly rose from 21 kJ mol^{-1} to 90 kJ mol^{-1}, especially at extremely low loadings. Such enhanced adsorption performance could be attributed to the affinity of alkylamine for carbon dioxide. To further improve CO_2 adsorption capacity, *N*,*N*′-dimethylethylenediamine (mmen) was also introduced into the framework of CuBTTri by Long's group.[218] In comparison to unmodified CuBTTri, modified mmen-CuBTTri was able to adsorb 4.2 mmol g^{-1} of CO_2 at 298 K and 1 bar, showing an increase of 15% in adsorption capacity. According to ideal adsorbed solution theory, mmen-CuBTTri exhibited a relatively high selectivity of 327 for the CO_2/N_2 gas mixture (15 : 85) at 298 K. The extremely high Q_{st} for CO_2 (96 kJ mol^{-1} at zero coverage) was considered to be the main drive for the enhanced adsorption capacity and adsorption selectivity. Furthermore, even after 72 cycles of use, mmen-CuBTTri could also retain its adsorption capacity for CO_2. Besides Long's group, Hong and co-workers also reported several amine-functionalized MOFs, which exhibited enhanced CO_2 adsorption capacity.[219,220]

Through introducing a hydroxide group into water-resistant MOFs (MAF-X25/27) based on N-containing ligands,[221] Chen's group also realized enhanced CO_2 adsorption by synthesizing two hydroxide-functionalized isostructural frameworks [$Mn^{II}Mn^{III}$(OH)Cl_2(bbta)] (MAF-X25ox, 1′) and [$Co^{II}Co^{III}$(OH)Cl_2(bbta)] (MAF-X27ox, 2′).[206] In comparison to unmodified precursors, their CO_2 adsorption capacities at 1 bar and 298 K increased from 5.4 and 4.2 mmol g^{-1} to 7.1 and 6.7 mmol g^{-1}, respectively. At 0.15 bar and 298 K, the adsorption capacity of 1′ and 2′ was 410% and 540% larger than that of their precursors, reaching 4.08 and 4.06 mmol g^{-1}, respectively. Moreover, the CO_2/N_2 selectivity of 1′ and 2′ at 298 K was calculated to be 250 and 264, 8.6 and 9.2 times higher than that of their precursors, respectively. The significant increase in Q_{st} (from 38 and 28 kJ mol^{-1} to 99 and 110 kJ mol^{-1}) demonstrated the ultrahigh CO_2 affinity of 1′ and 2′. Notably, the breakthrough curves of 2′ were nearly the same in both dry and high-humidity environments, while its precursor almost could not capture CO_2 from the wet mixture of CO_2 and N_2. Based on a hydroxide-functionalized MOF ($KHCO_3$ CD-MOF), Milner and co-workers also realized the enhancement of CO_2 adsorption capacity.[205]

In addition to enhancing the kinetic water stability of MOFs, hydrophobic engineering can also be used to improve their CO_2 capture performance. For instance, Wang's group successfully realized the improvement of water stability and CO_2 adsorption

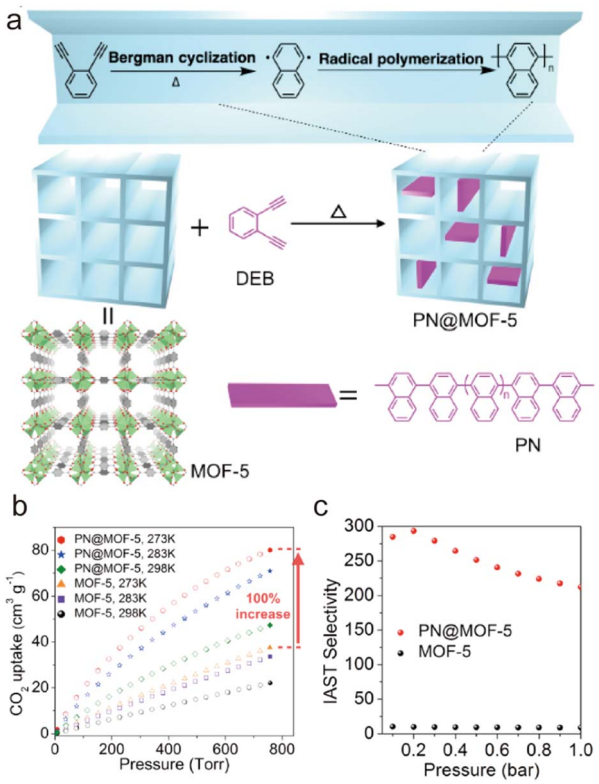

Fig. 36 (a) Introducing hydrophobic polynaphthylene (PN) into MOF-5 through the polymerization of DEB. (b) The CO_2 adsorption isotherms of MOF-5 and PN@MOF-5 at different temperatures. (c) The IAST selectivity of MOF-5 and PN@MOF-5 for a CO_2/N_2 mixture (14 : 86) at 273 K. Reproduced from ref. 222 with permission from the American Chemical Society, Copyright 2016.

by introducing hydrophobic polynaphthylene (PN) into MOF-5 (Fig. 36a).[222] In contrast to water-sensitive MOF-5, hydrophobically modified PN@MOF-5 could retain its crystallinity and porosity upon exposure to humid air (40% RH) for 40 h. Due to the smaller pores and the hydrophobic aromatic groups, PN@MOF-5 exhibited significantly enhanced CO_2 capture performance (Fig. 36b). Compared with the original MOF-5, the adsorption capacity was doubled and the adsorption selectivity for CO_2/N_2 (14 : 86) at 1 bar and 273 K increased by 23-fold (Fig. 36c). Such excellent CO_2 adsorption performance could be largely maintained at 65% RH.

To achieve efficient decarbonization of flue gas, many water-stable MOFs based on different synthetic strategies were prepared. Water-stable MOFs based on the Hard–Soft-Acid–Base strategy can not only be directly used for CO_2 adsorption (*e.g.*, ALF), but also be used as potential precursors for PSM to achieve more efficient CO_2 capture (*e.g.*, MOF 808 and CuBTTri). In addition, molecular sieving of CO_2 can be achieved by using MOFs with matched pores (*e.g.*, SIFSIX-2-Cu-I and UTSA-120), exhibiting very high adsorption selectivity but relatively low adsorption enthalpy. The self-assembly of ligands containing both N and O atoms with soft metals is beneficial for constructing MOFs with high performance, stability, and economy, such as CLAF-20. It is worth mentioning that CLAF-20 can be directly used for the decarbonization of flue gas and can be also mass-produced by BASF, making it a promising industrial CO_2 adsorbent.

3.4.2. Carbon dioxide capture from air. Compared with flue gas, the CO_2 concentration in the air is much lower. Currently, the concentration of CO_2 in the atmosphere is about 400 ppm while that in some confined spaces may reach 1000–10000 ppm. Therefore, developing MOFs that can capture trace CO_2 is more challenging than MOFs for flue gas. As far as we know, only limited MOFs that have very effective active sites (*e.g.*, amino groups and hydroxide groups) or highly matched pores for CO_2 can be used to capture trace CO_2, and several water-stable MOFs with excellent trace CO_2 capture performance are covered in this session (Table 3).[191,192,207,214,219,223–232]

Based on hard metals/ligands, Bai's group successfully synthesised two isostructural MOFs, $[Fe_3O(TPBTM^{6-})(Cl)(H_2O)_2]_n$ (NJU-Bai52) and $[Sc_3O(TPBTM^{6-})(OH)(H_2O)_2]_n$(NJU-Bai53) (TPBTM = *N*,*N*′,*N*″-tris(isophthalyl)-1,3,5-benzenetricarboxamide) (Fig. 37a).[233] Due to the strong Fe–O/Sc–O units, both of them could maintain their structural integrity in H_2O for two months. Notably, NJU-Bai53 could not only preserve its framework in aqueous solutions (pH = 2 to 11) but also maintain its porosity after water treatment (Fig. 37b). Due to the presence of monodentate hydroxide, NJI-Bai53 displayed higher CO_2 adsorption capacity than NJI-Bai52. At 298 K and 0.4 mbar, it could adsorb 0.64 mmol g^{-1} of CO_2, which was 50 times higher than that of NJU-Bai52 (0.013 mmol g^{-1}) (Fig. 37c). At zero-coverage, the adsorption enthalpy of NJU-Bai53 for CO_2 was up to 88.3 kJ mol^{-1}, demonstrating the presence of strong chemisorption interactions (Fig. 37d). According to the simple selectivity equation $S = (q_1/q_2)/(p_1/p_2)$, the CO_2/N_2 (0.4/800) selectivity of NJU-Bai53 at 298 K was calculated to be 6397. All of these make NJU-Bai53 a potential adsorbent for CO_2 capture from the air.

Besides hard metals/ligands, soft metals/ligands are also widely used to construct water/moisture MOFs for direct air capture. For instance, Eddaoudi's group prepared a moisture-stable ultramicroporous MOF (SIFSIX-3-Cu) based on the pyrazine ligand and $CuSiF_6$.[214] SIFSIX-3-Cu had not only very narrow pores (3.5 Å) suitable for CO_2 but also high-density F^- anions that could form strong interactions with CO_2. Due to its polar ultramicroporous pores, SIFSIX-3-Cu displayed not only a very high trace CO_2 adsorption capacity (1.24 mmol g^{-1} at 0.4 mbar and 298 K) but also extremely high adsorption selectivity (10 500 for CO_2/N_2 (1/999)). Further breakthrough experiments demonstrated that such excellent adsorption performance could be retained under humid conditions (74% RH). By replacing $(SiF_6)^{2-}$ with $(NbOF_5)^{2-}$, Eddaoudi's group synthesized another hydrolytically stable ultramicroporous MOF (NbOFFIVE-1-Ni) with a similar but smaller pore (about 3.2 Å) than SIFSIX-3-Cu (Fig. 38a).[191] Due to the more matched pore (pore size and pore environment). NbOFFIVE-1-Ni displayed a higher trace CO_2 adsorption capacity (1.3 mmol g^{-1} at 0.4 mbar and 298 K) than SIFSIX-3-Cu, meaning that NbOFFIVE-1-Ni was the most efficient physical adsorbent for direct air capture (Fig. 38b). Single-crystal X-ray diffraction studies demonstrated that such excellent adsorption capacity resulted

Table 3 The performances of some representative MOFs for carbon dioxide capture from ambient air

MOFs	Stability	CO_2 uptake at different pressures (mmol g^{-1}) 390 ppm	10 000 ppm	Q_{st} (kJ mol^{-1})	Temperature (K)	Ref.
NJU-Bai51	pH = 1–12	0.13	—	33.3	298	269
NJU-Bai53	pH = 2–11	0.64[a]	—	88.3	298	233
$[Zn(ZnOH)_4(bibta)_3]$	Moisture-stable	2.2	—	71	298	207
SIFSIX-3-Cu	Moisture-stable (74% RH)	1.24[a]	2.34	54	298	214
dptz-$CuTiF_6$	Moisture-stable	—	2.1	38.2	298	192
TIFSIX-3-Co	Moisture-stable	1.05[a]	2.63	—	298	228
NbOFFIVE-1-Ni	Moisture-stable (95% RH)	1.30[a]	~2.15	54	298	191
TIFSIX-3-Ni	Moisture-stable (75% RH)	1.12[a]	1.75	50.9	298	229
SIFSIX-18-Ni-β	Moisture-stable (90% RH)	0.4[b]	2.2	52	298	230
SIFSIX-3-Ni	Moisture-stable (75% RH)	0.35[a]	1.9	45	298	231
GeFSIX-3-Ni	Moisture-stable	1.07[a]	2.41	55.5	298	270
FJI-H38	pH = 2–12	—	2.33	27	298	190
$Mg_2(dobdc)(N_2H_4)_{1.8}$	Moisture-stable (82% RH)	3.89	—	118	298	223
en-Mg_2(dobpdc)	Moisture-stable (100% RH)	2.83		49–51	298	219
ED-Mg-MOF-74	Moisture-stable	1.5	—	—	298	268
epn-MOF80@SBS	Moisture-stable (60% RH)	—	2.8[c]	67	298	178

[a] 400 ppm. [b] 500 ppm. [c] 1000 ppm.

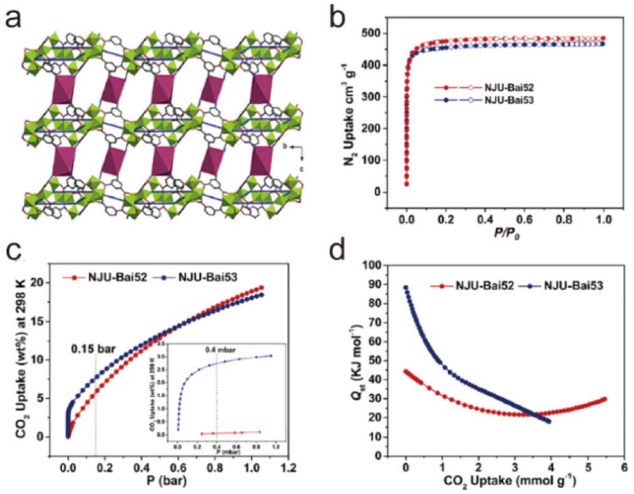

Fig. 37 (a) The structure of NJU-Bai52 and NJU-Bai53. (b) The N_2 sorption isotherms of NJU-Bai53 (77 K) before and after water treatment. (c) The CO_2 adsorption isotherms of NJU-Bai52 and NJU-Bai53 at 298 K. (d) The adsorption enthalpy of NJU-Bai52 and NJU-Bai53 for CO_2. Reproduced from ref. 233 with permission from the American Chemical Society, Copyright 2019.

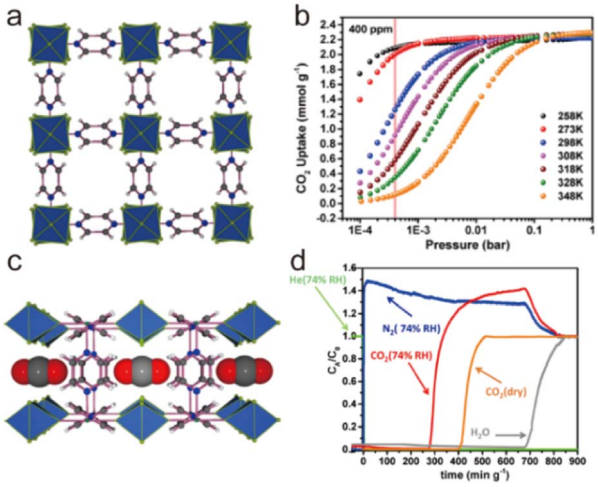

Fig. 38 (a) The structure of NbOFFIVE-1-Ni. (b) The CO_2 sorption isotherms of NbOFFIVE-1-Ni at different temperatures. (c) The CO_2 adsorption sites in NbOFFIVE-1-Ni. (d) The breakthrough curves with the mixed-gas CO_2/N_2 (1/99) at 1 bar and 298 K in both dry and humid environments. Reproduced from ref. 191 with permission from the American Chemical Society, Copyright 2016.

from the good match between the adsorbed CO_2 and the pores of NbOFFIVE-1-Ni (Fig. 38c).

Furthermore, the adsorption capacity of NbOFFIVE-1-Ni for CO_2 could be maintained even at high humidity (Fig. 38d) and the adsorbed CO_2 could be completely desorbed at 328 K under vacuum. All of these make NbOFFIVE-1-Ni a promising adsorbent for capturing CO_2 in the atmosphere.

Using a methylated dipyrazolyl ligand (3,3′,5,5′-tetramethyl-1*H*,1′*H*-4,4′-bipyrazole) and $NiSiF_6$ as coordination units, Zaworotko's group realized the controlled construction of a more hydrophobic ultramicroporous framework (SIFSIX-18Ni-β).[230] Due to its ultramicropores, SIFSIX-18-Ni-β also exhibited high adsorption capacity for trace CO_2 (*e.g.*, 0.4 mmol g^{-1} at 500 ppm and 2.2 mmol g^{-1} at 10 000 ppm). More importantly, due to the introduction of hydrophobic methyl groups, SIFSIX-18-Ni-β displayed a very low H_2O uptake (1.6 mmol g^{-1}) even at 95% RH, which allowed SIFSIX-18-Ni-β to preferentially adsorb CO_2 from nitrogen and water in any case. This work not only provides a potential trace CO_2 adsorbent for confined spaces but also offers a useful strategy for developing efficient trace CO_2 adsorbents resisting water vapor.

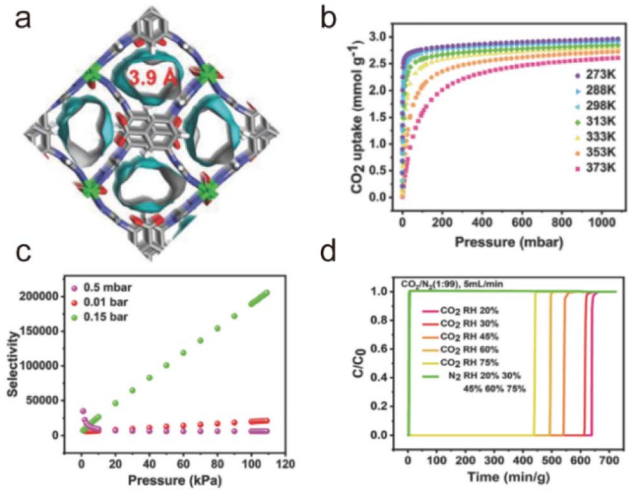

Fig. 39 (a) The structure of FJI-H38. (b) The CO_2 sorption isotherms of FJI-H38 at different temperatures. (c) The IAST selectivity of FJI-H38 for CO_2/N_2 at various partial pressures. (d) The breakthrough curves of FJI-H38 for CO_2/N_2 (1 : 99) under different humid conditions. Reproduced from ref. 190 with permission from Wiley, Copyright 2023.

Very recently, through the reaction of a soft N-containing ligand (3, 5-di(4*H*-1, 2, 4-triazol-4-yl) benzoic acid, HDTBA) with Co(II) salts, our group reported an acid/base-resistant ultramicroporous MOF (FJI-H38), which could capture trace CO_2 from humid air (Fig. 39a).[190] Due to the stable CoN_4O nodes, FJI-H38 could retain its framework in aqueous solutions with a pH of 2–12. It could capture trace CO_2 from air with the high adsorption capacity (0.57 mmol g^{-1} at 0.5 mbar and 2.33 mmol g^{-1} at 0.01 bar) and the very high adsorption selectivity (6469 at 0.5 mbar) but a relatively low adsorption enthalpy (27 kJ mol^{-1}) (Fig. 39b and c). Such outstanding CO_2 adsorption performance could be largely maintained even at high humidity (75 RH%) (Fig. 39d). Mechanistic studies demonstrated that this excellent adsorption performance came from the synergism of flexible frameworks, ultramicropores, and different adsorption sites of H_2O and CO_2. Furthermore, FJI-H38 could be prepared on a large scale and reused without losing adsorption capacity, making it a potential adsorbent for trace CO_2 in industry.

By introducing amino groups into MOFs through pore engineering not only can their CO_2 capture capacity be improved, but their water resistance is also enhanced. For example, Chen, Zhang and co-workers introduced a very small amine molecule (N_2H_4) into the pores of Mg_2(dobdc), preparing a amine-functionalized MOF (Mg_2(dobdc)(N_2H_4)$_{1.8}$) (Fig. 40a).[223] Due to the extremely high concentration of amine groups (7.08 mmol cm^{-3} or 6.01 mmol g^{-1}), the as-synthesized Mg_2(dobdc)(N_2H_4)$_{1.8}$ could capture 3.89 mmol g^{-1} of CO_2 at 0.4 mbar and 298 K, demonstrating its excellent trace CO_2 adsorption capacity (Fig. 40b). Even at high humidity, such excellent CO_2 adsorption performance could also be retained (Fig. 40c), which might be because the grafted N_2H_4 was not substituted by H_2O. In addition to (Mg_2(dobdc)(N_2H_4)$_{1.8}$), there were several amine-functionalized MOFs (*e.g.*, dmpn-Mg_2(dobpdc) and nmen-Mg_2(dobpdc)) that could realize efficient capture of trace CO_2.[202,226]

Hydrophobic engineering can be used to simultaneously improve the water stability and trace CO_2 adsorption of MOFs. For example, based on water-resistant Mg_2(dobpdc) hybrids after hydrophobic modification (Fig. 24), Hong's group realized enhanced trace CO_2 capture performance.[178] Especially, epn-MOF80@SBS demonstrated an impressive CO_2 adsorption of

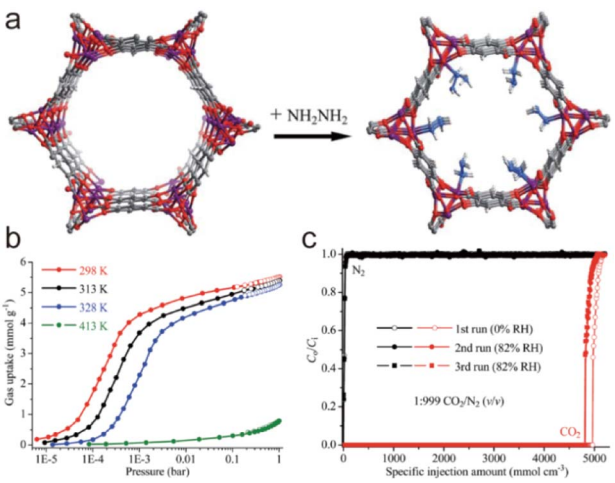

Fig. 40 (a) Introducing N_2H_4 into pores of Mg_2(dobdc). (b) The CO_2 sorption isotherms of (Mg_2(dobdc)(N_2H_4)$_{1.8}$) at different temperatures. (c) The breakthrough curves of (Mg_2(dobdc)(N_2H_4)$_{1.8}$) for CO_2/N_2 (1 : 999) under different humid conditions. Reproduced from ref. 223 with permission from the Royal Society of Chemistry, Copyright 2016.

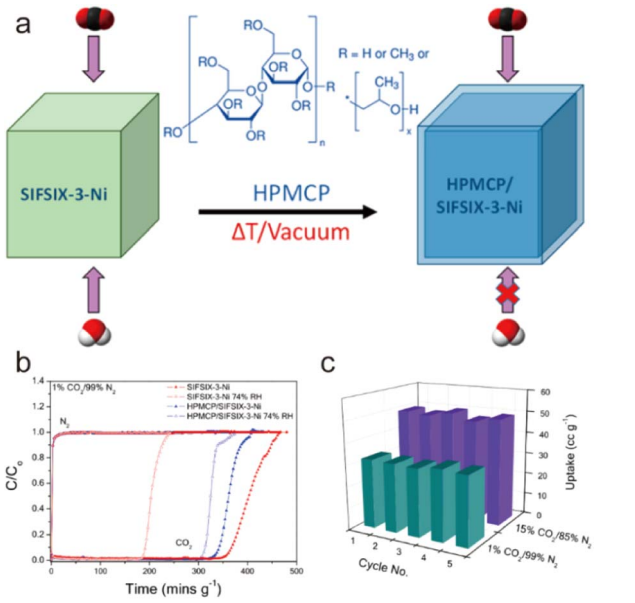

Fig. 41 (a) Coating HPMCP on SIFSIX-3-Ni. (b) The breakthrough curves of SIFSIX-3-Ni and HPMCP/SIFSIX-3 for CO_2/N_2 (1 : 99) under different humid conditions. (c) The HPMCP/SIFSIX-3-Ni recyclability tests for humid 1% CO_2/99% N_2 and 15% CO_2/85% N_2 gas mixtures (regeneration at 80 °C). Reproduced from ref. 254 with permission from the American Chemical Society, Copyright 2020.

Table 4 The performances of some representative MOFs for purification of crude natural gas[a]

MOFs	Stability	CO_2 adsorption amount at 1 atm (mmol g^{-1})	IAST selectivity at 1 bar (50/50) CO_2/CH_4	Q_{st} (kJ mol^{-1})	Temperature (K)	Ref.
UiO-66-SO_3Li-0.15	pH = 1–12	3.28	12.7	25.4	298	234
UiO-66-SO_3Rb-1	pH = 1–12	0.54	54.2	35.0	298	234
UiO-66-SO_3H-0.64	pH = 1–12	1.54	15.2	33.2	298	234
UiO-66-SO_3Na-0.64	pH = 1–12	0.94	46.2	35.1	298	234
UiO-66-SO_3K-1	pH = 1–12	0.91	18	31.9	298	234
UiO-66(Hf)	Water-stable	1.50	12	22.8	298	240
UiO-66(Hf)-$(OH)_2$	pH = 1–10	4.06	30	28.4	298	240
UiO-66(Hf)-NH_2	Water-stable	2.80	15	25.6	298	240
UiO-66(Hf)-$(COOH)_2$	Water-stable	1.20	13	28.2	298	240
UiO-66(Hf)-$(F)_4$	Water-stable	0.82	16	23.4	298	240
PCN-222	Water-stable	1.16	4.3	18.3	298	134
NJU-Bai52	Water-stable	5.3	13.5	44.2	298	233
NJU-Bai51	pH = 1–12	—	10.7	33.3	298	269
NJU-Bai50	pH = 1–12	—	4.4	26.6	298	269
CPM-231	Moisture-stable (75% RH)	6.77	2.65	20.4	298	258
ee-2-Mg_2(dobpdc)	Water-stable	~4.5	—	-65 ± 1	298	260
UTSA-280	Water-stable	3.0	—	42.9	298	267
[$Zn_3(OH)_2$(pzdc)(atz)]	pH = 2–12	2.1	1.3×10^7	48	273	263
SIFSIX-3-Zn	Moisture-stable	2.55	231	45	298	214
UTSA-49	Moisture-stable	3.08	33.7	27	298	273
UTSA-120	Moisture-stable	5.0	100	27–31	296	215
UTSA-121	Moisture-stable	2.65	10	21.9	298	274
Qc-5-Cu-sql-β	Water-stable	2.16	3300	36	293	216
SIFSIX-2-Cu-i	Moisture-stable	5.41	33	31.9	298	213
Cu(MTABA)	Water-stable	1.5	9.9	38.4	298	276
Cu–F-pymo	pH = 1–14	1.19	$>10^7$	29.1	298	250
Co-btz-ht	pH = 1–12	2.16	63	38	273	125
Ni-btz-ht	pH = 1–12	4.24	54	~38	273	125
GeFSIX-3-Co	Moisture-stable	2.65	160	39.1	298	270
GeFSIX-3-Ni	Moisture-stable	2.61	930	55.5	298	270
WOFOUR-1-Ni	pH = 2–13	2.32	26	65.5	298	277
NbOFFIVE-1-Ni	Moisture-stable (95% RH)	2.2	6528	54	273	191
CSMCRI-9	pH = 4–10	3.34	5.39	28.21	273	278
CSMCRI-3	pH = 5–10	2.4	11.7	27	273	279
MUF-16	Water-stable	2.13	6690	32.3	293	265
MUF-16(Ni)	Water-stable	2.14	1220	37.3	293	265
MUF-16(Mn)	Water-stable	2.25	470	36.6	293	265
IITKGP-6	Water-stable	1.67	5.1	23	295	280
[Co_2(4,4′-bpy)(STBZ)]	Water-stable	1.63	9.9	29–31	298	281
FJI-H29	pH = 2–13	1.79	25	34	298	138
ZJNU-27	Water-stable	3.54	5.4	26.7	298	282
ZJNU-28	Water-stable	3.43	9.6	32.1	298	282
ZJNU-26	Water-stable	3.06	4.3	30.4	298	282
SNNU-52	pH = 3–11	2.64	7.3	28.3	298	257
SNNU-53	pH = 3–11	1.96	7.1	34.2	298	257
SNNU-55	pH = 3–11	1.49	10	33.6	298	257
SNNU-56	pH = 3–11	2.49	6.2	32.5	298	257
SNNU-54	Water-stable	2.31	7.5	38	298	257
SNNU-51	Water-stable	2.4	15.2	23.3	298	257
MOF-508b	Water-stable	1.85	3	19.2	303	283
Zn(BDC)$(BPY)_{0.5}$	Water-stable	0.32	12.3	10.0–37.2	298	284
QI-Cu	Water-stable	4.56	6.1	23.75 ± 0.49	293	271
UTSA-16GO	Water-stable	3.62	114.4	42.1	296	259
MOF-505@GO	Moisture-stable	3.94	8.6	—	298	275

[a] Calculated from Henry's law constant.

2.8 mmol g^{-1} at 1000 ppm. Under the conditions with 60% RH, it could maintain consistent CO_2 removal performance after over 10 cycles and even 7 days of exposure.

Through polymer coating, Zaworotko's group also improved the water resistance of SIFSIX-3-Ni and its adsorption for trace CO_2 adsorption (Fig. 41a). Compared with uncoated SIFSIX-3-

Ni, the HPMCP-coated HPMCP/SIFSIX-3-Ni displayed a significantly enhanced water resistance. After coating, the water contact angle increased by 8 times, and the framework could be preserved after being exposed to moisture for a long time. In high humid environments, HPMCP/SIFSIX-3-Ni could also display excellent gas separation performance while SIFSIX-3-Ni could not (Fig. 41b). Such excellent CO_2 separation performance could be retained for at least 5 cycles (Fig. 41c), suggesting that it could be used to control indoor air quality.[254]

Compared to flue gas decarbonization, there are very few water-stable MOFs available for direct air capture. These MOFs either have strong active sites (*e.g.*, NJI-Bai53, and Mg_2(dobdc)$(N_2H_4)_{1.8}$) that can chemically adsorb CO_2 or have ultramicropores that match well with CO_2 (*e.g.*, SIFSIX-3-Cu, NbOFFIVE-1-Ni, SIFSIX-18-Ni-β, and FJI-H38). Compared with chemisorption, physical adsorption based on matched pores has lower recovery energy and is more conducive to the recycling of adsorbents.[244] It is worth mentioning that the capture capacities of SIFSIX-3-Cu, NbOFFIVE-1-Ni, and FJI-H38 exceed that of commercial zeolite 13X. Among these materials, FJI-H38 has lower adsorption enthalpy and better stability, indicating that it is a more practical adsorbent for trace CO_2 capture.

3.4.3. Carbon dioxide capture from crude natural gas. As mentioned previously, CO_2 from flue gas and the air can be captured efficiently and selectively through reasonably designed MOFs. Compared with CO_2, both N_2 and CH_4 have larger kinetic diameters but less polarity, which means that MOFs efficient at capturing CO_2 from flue gas can also be used to capture CO_2 from crude natural gas. While many MOFs that can selectively capture CO_2 from CH_4 have been reported, only those that have both water/wet stability and excellent CH_4 purification performance are discussed in this section (Table 4).[189,191,213,214,216,232,241,255–264]

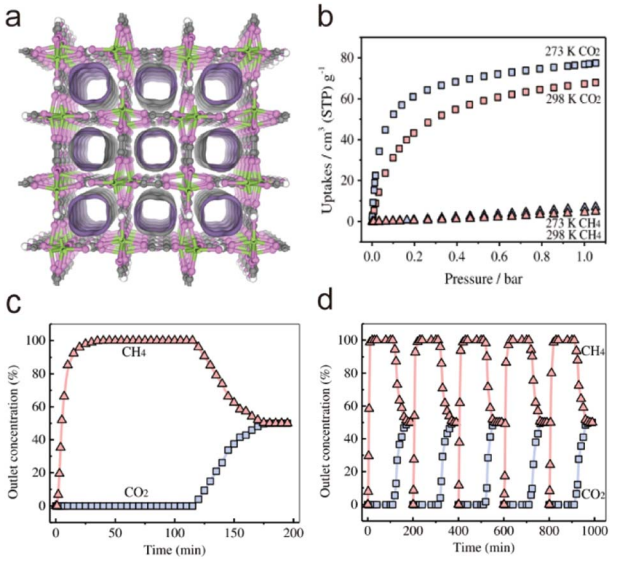

Fig. 42 (a) The structure of UTSA-280. (b) The CO_2/CH_4 sorption isotherms of UTSA-280 at 273 and 298 K. (c) and (d) The breakthrough curves and cycles of UTSA-280 for CO_2/CH_4 (1 : 1). Reproduced from ref. 245 with permission from Wiley, Copyright 2020.

Like flue gas decarbonization, many water-stable MOFs based on hard metal/carboxylate ligands have been prepared and used to purify natural gas. For instance, based on the hard Ca(II) ion and squaric acid ligand, Chen's group also achieved the controlled synthesis of a water-stable MOF ([$Ca(C_4O_4)(H_2O)$] UTSA-280) and its efficient purification of CH_4 (Fig. 42a).[264,265] Due to the strong Ca–O bonds, the as-synthesized UTSA-280 could remain its framework and porosity even after being immersed in water for 1 month. Due to its matched pore, UTSA-280 exhibited a relatively high CO_2 adsorption capacity (3.0 mmol g^{-1}) but almost no CH_4 adsorption (Fig. 42b). Dynamic breakthrough experiments demonstrated that UTSA-280 could capture 1.918 mmol g^{-1} of CO_2 from a CO_2/CH_4 (50/50) mixture at 298 K, and such excellent separation performance could be completely retained for over 5 cycles (Fig. 42c and d). All of these make UTSA-280 a potential adsorbent for natural gas purification.

Water-stable MOFs based on soft metals/ligands have also been widely prepared and used to purify crude natural gas. For example, Eddaoudi's group prepared a moisture stable MOF (AlFFIVE-1-Ni, KAUST-8) based on the pyrazine ligand and $Ni(NO_3)_2$, which could maintain its framework integrity even after being exposed to humid air with 95% RH (Fig. 43a).[266,267] Due to its specific pore environment, AlFFIVE-1-Ni could effectively and equally adsorb CO_2 and H_2S from gas mixtures containing CO_2, H_2S and CH_4 in a wide temperature range. This unusual co-adsorption of CO_2 and H_2S was further proved by temperature-dependent desorption (Fig. 43b). Moreover, such excellent separation performance could be retained not only in the presence of water vapour, but also during multiple cycling

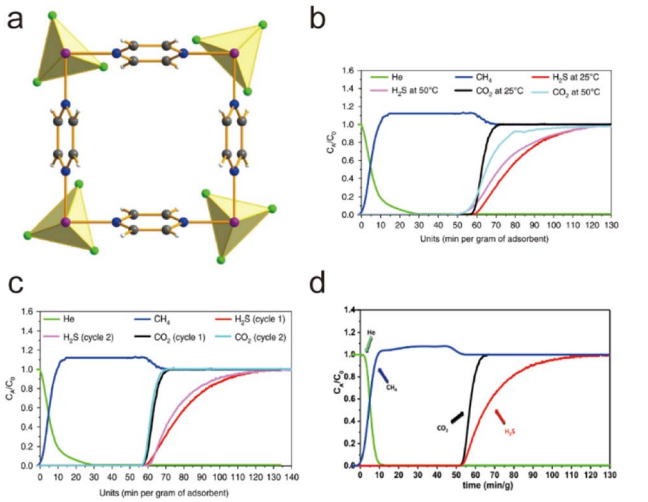

Fig. 43 (a) The framework of AlFFIVE-1-Ni. (b) The breakthrough experiments using a $CO_2/H_2S/CH_4$:5/5/90 gas mixture on AlFFIVE-1-Ni at 298 K and 323 K (1 bar). (c) The breakthrough trials using a fresh sample under the same parameters (298 K) after optimal activation (105 °C) and after five breakthrough cycles. (d) The breakthrough experiments under humid conditions (65% RH). Reproduced from ref. 266 with permission from the American Association for the Advancement of Science, Copyright 2017. Reproduced from ref. 267 with permission from Springer Nature, Copyright 2018.

tests (Fig. 43c and d). This work represents a simple and efficient method for the simultaneous removal of acid gases (*e.g.*, H_2S and CO_2) from crude natural gas.

Based on soft Cu(II) ions and 5-fluoropyrimidin-2-olate ligands, Chen's group also achieved the synthesis and natural gas purification of a water-stable MOF (Cu–F-pymo). Due to the stable CuN_4 nodes, Cu–F-pymo could preserve its framework in aqueous solutions with a pH of 1–14.[250] Due to its polar ultramicropores (about 3.3 Å), Cu–F-pymo could exclusively capture CO_2 over CH_4 and N_2. At 298 K and 1 atm, Cu–F-pymo exhibited a relatively high CO_2 adsorption capacity of 1.6 mmol g^{-1} but very low adsorption capacities for both CH_4 (0.042 mmol g^{-1}) and N_2 (0.0075 mmol g^{-1}). Such unusual size-sieving separation performance could be further confirmed by their IAST selectivity for both CO_2/CH_4 (50 : 50) (>10^7) and CO_2/N_2 (15 : 85) (>10^7) mixtures. Such excellent separation performance could be maintained for at least 5 cycling tests.

Through selecting soft N-containing ligands (5-aminoisophthalic acid, H_2aip), Telfer's team prepared a series of water-stable microporous MOFs ($M(Haip)_2$; M = Co, (MUF-16); M = Ni, MUF-16(Ni); M = Mn, MUF-16(Mn)), all of which could be used to purify natural gas effectively (Fig. 44a).[265] They could remain their frameworks after being immersed to water for two weeks. At 1 atm and 293 K, the CO_2 adsorption capacity of isomeric MUF-16, MUF-16(Ni) and MUF-16(Mn) was about 2.13 mmol g^{-1}, 2.13 mmol g^{-1} and 2.25 mmol g^{-1}, respectively (Fig. 44b). Meanwhile, MUF-16 could only capture a very small amount of CH_4 (0.054 mmol g^{-1}) under the same conditions. Notably, the IAST selectivity of MUF-16 for the mixture of CO_2 and CH_4 (50/50) was up to 6690 at 293 K and 1 bar (Fig. 44c). Mechanistic analysis showed that such excellent selectivity came from the match of its pore and CO_2 (from size to polarity). Moreover, such an excellent CO_2 adsorption capacity could be maintained even after being soaked in water for 24 h and being exposed to humid air (80% RH) for 12 months (Fig. 44d).

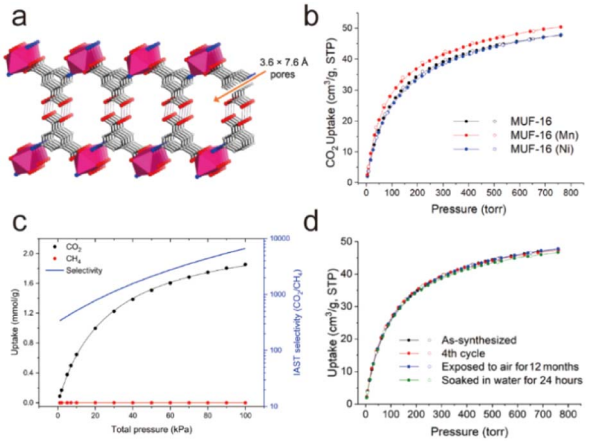

Fig. 44 (a) The structure of MUF-16. (b) The CO_2 adsorption isotherms of MUF-16s at 293 K. (c) The IAST selectivity of MUF-16 for CO_2/CH_4 (50 : 50) at 293 K. (d) The CO_2 adsorption isotherms of MUF-16 at 293 K, after 4 consecutive sorption cycles, 12 months of exposure to air with 80% RH, and 24 hours of immersion in water. Reproduced from ref. 265 with permission from Springer Nature, Copyright 2021.

Based on another soft N-containing ligand (3,5-pyrazoledicarboxylic acid, H_3pzdc), Zhang and co-workers also realized the controllable preparation and natural gas purification of a water-stable MOF ($[Zn_3(OH)_2(pzdc)(atz)]$, Hatz = 3-amino-1,2,4-trizole).[263] It could retain its framework in aqueous solutions (pH 3–12) and boiling water. Due to its polar ultramicropores, the activated $[Zn_3(OH)_2(pzdc)(atz)]$ displayed a relatively high CO_2 adsorption capacity of 2.1 mmol g^{-1} but a very low adsorption capacity for CH_4 (0.056 mmol g^{-1}), leading to a very high single-component selectivity for CO_2/CH_4 (50/50) (1.3×10^7). This means that $[Zn_3(OH)_2(pzdc)(atz)]$ is a very rare adsorbent, which can realize molecular sieving of CO_2 from CO_2/CH_4.

As mentioned above, hydrophobic engineering could enhance the water stability and CO_2 capture performance of MOFs simultaneously. Through introducing hydrophobic groups, Zhao and co-worker also realized the improvement of the water stability and CH_4 purification capacity of NOTT-101.[271] They prepared a new MOF QI-Cu through incorporating methyl and methylol groups into a famous MOF NOTT-101. Notably, the modified QI-Cu could remain its framework in water for at least 1 month while the framework of NOTT-101 would completely collapse in water within 24 h. Due to the reduced pores and increased groups, QI-Cu exhibited better CO_2 adsorption capacity and higher CO_2/CH_4 adsorption selectivity than NOTT-101.

Compared to direct air capture, there are more water-stable MOFs available for purifying natural gas. Due to the similar polarity and size of CH_4 and N_2, MOFs can be used for decarbonization of flue gas, as well as for purifying natural gas. Purifying natural gas is mainly to remove CO_2 impurities from CH_4, so the adsorption selectivity of MOFs for CO_2/CH_4 (1 : 1) is the most important indicator, and many recently reported MOFs display very high CO_2/CH_4 adsorption selectivity (*e.g.*, $[Zn_3(OH)_2(pzdc)(atz)]$, MUF-16, UTSA-280, and AlFFIVE-1-Ni). Among these MOFs, UTSA-280 and MUF-16 can be prepared from inexpensive building blocks and are expected to be used as potential adsorbents for natural gas purification.

4. Summary and perspective

In order to develop practical MOFs for the real world, increased studies have been carried out on the design and synthesis of water-resistant MOFs, with a series of water-stable MOFs constructed reasonably. In this review, we first briefly introduce the definition of water stability of MOFs and how to characterize their stability. To discuss the water stability of MOFs more fully, we divide it into thermodynamic stability and kinetic stability, and then introduce a method to improve their thermodynamic and kinetic stability. According to Hard–Soft-Acid–Base theory, thermodynamically stable MOFs can be reasonably constructed through directly selecting metal ions and ligands with matched softness/hardness. Therefore, we first discuss the reported water-stable MOFs directly constructed from coordination units with matched hardness, including (1) water-stable MOFs based on hard metal ions and ligands and (2) water-stable MOFs based on soft metal ions and ligands. In addition, other specific

strategies that can be used to improve the thermodynamic stability of MOFs (*e.g.*, interlocking of frameworks and improving their rigidity) are also introduced. The kinetic stability of MOFs to water can be improved by reducing the kinetics of their hydrolysis reaction. Therefore, a series of strategies that can inhibit the kinetics of MOF hydrolysis, including the direct use of hydrophobic ligands, the introduction of hydrophobic groups into the pores of MOFs, the coating of hydrophobic films on the surface of MOFs, and the increase of steric hindrance around metal nodes, are discussed in detail.

Although great advance has been made in this area, there are several challenges that still need to be overcome. For example, because the currently used PXRD technique only reflects the state of MOFs before and after exposure to water, the interactions between MOFs and water remain unclear at the microscopic level. If such microscopic interactions between water and MOFs can be revealed by combining various *in situ* characterization and computational simulations,[272] the water-stable MOFs that meet different application requirements (*e.g.*, carbon capture at high humidity and radioactive metal capture under strong acids) can be precisely designed and synthesized. In addition, balancing the water stability and activity of MOFs is another challenge. Metal ions and ligands with matched hardness can be used to directionally construct water-stable MOFs. However, the functions of MOFs are also achieved by introducing specific Lewis acid or base sites. Therefore, it is necessary to not only avoid the competitive active sites interfering with the assembly of MOFs, but also ensure that the active sites can be reasonably introduced into the channels of MOFs, which is a contradiction. The hydrophobic modification of MOFs may also affect the performance of MOFs, because the channels of MOFs can be changed. More importantly, if water-stable MOFs are to be widely used in industry, both their economy and processability need to be solved. For economy, first of all, cheap organic ligands and metal salts should be selected as the raw materials for a target MOF, and then large-scale synthesis should be realized through cheap reaction media (such as water and ethanol). Finally, the recovery of unreacted ligands/metals and reaction media should be achieved. In terms of processability, the controllable preparation of a target MOF with different sizes should be achieved first, and then appropriate devices (*e.g.*, fixed bed, thin film, *etc.*) should be made according to different application scenarios.

The controllable preparation of water-stable MOFs further expands the application scenarios of MOFs. Due to the necessity and urgency of carbon capture, we only introduce the progress of water-resistant MOFs in carbon capture in this review. We begin with a brief introduction to the background of carbon capture and then discuss the applications of water-stable MOFs to flue gas decarbonization, direct air capture, and the purification of crude natural gas. Considering that the carbon capture capacity of some reported MOFs has been superior to that of commercial molecular sieves, it is very possible to use appropriate MOFs to achieve carbon capture in industry. Before realizing industrialization, the following problems need to be solved. (1) The target MOFs need to be tested and cycled for a long time under real working conditions; (2) it is also necessary to solve the processability and economy of the target MOFs.

In a word, more and more water-stable MOFs are synthesized, and the understanding of the relationship between the water stability and structure of MOFs is getting deeper and deeper, and the use of water-stable MOFs is more and more extensive. Notably, the carbon capture capacity of some reported MOFs has been better than that of commercial molecular sieves. So, we believe that MOFs will eventually be widely used as a type of porous material for carbon capture in the real world. We hope that this review could accelerate the achievement of this goal.

Author contributions

Conceptualization: M. Hong and Q. Chen; writing – original draft: C. Xiao; validation: J. Tian; writing – review & editing: M. Hong and Q. Chen.

Conflicts of interest

The authors declare no conflicts of interest.

Acknowledgements

We gratefully acknowledge the financial support from the National Key Research and Development Program of China (2021YFA1500400 and 2018YFA0704500) and the Natural Science Foundation of Fujian Province (2023J06046).

References

1 S. R. Batten, N. R. Champness, X.-M. Chen, J. Garcia-Martinez, S. Kitagawa, L. Öhrström, M. O'Keeffe, M. Paik Suh and J. Reedijk, *Pure Appl. Chem.*, 2013, **85**, 1715–1724.
2 M. Eddaoudi, D. B. Moler, H. L. Li, B. L. Chen, T. M. Reineke, M. O'Keeffe and O. M. Yaghi, *Acc. Chem. Res.*, 2001, **34**, 319–330.
3 R. J. Hill, D. L. Long, N. R. Champness, P. Hubberstey and M. Schroder, *Acc. Chem. Res.*, 2005, **38**, 335–348.
4 Y. He, B. Li, M. O'Keeffe and B. Chen, *Chem. Soc. Rev.*, 2014, **43**, 5618–5656.
5 L. Feng, K.-Y. Wang, X.-L. Lv, T.-H. Yan and H.-C. Zhou, *Natl. Sci. Rev.*, 2020, **7**, 1743–1758.
6 J.-P. Zhang, Y.-B. Zhang, J.-B. Lin and X.-M. Chen, *Chem. Rev.*, 2012, **112**, 1001–1033.
7 Q.-G. Zhai, X. Bu, X. Zhao, D.-S. Li and P. Feng, *Acc. Chem. Res.*, 2017, **50**, 407–417.
8 Y. Bai, Y. Dou, L.-H. Xie, W. Rutledge, J.-R. Li and H.-C. Zhou, *Chem. Soc. Rev.*, 2016, **45**, 2327–2367.
9 S. Furukawa, J. Reboul, S. Diring, K. Sumida and S. Kitagawa, *Chem. Soc. Rev.*, 2014, **43**, 5700–5734.
10 G. Ferey, C. Mellot-Draznieks, C. Serre and F. Millange, *Acc. Chem. Res.*, 2005, **38**, 217–225.
11 J. J. I. V. Perry, J. A. Perman and M. J. Zaworotko, *Chem. Soc. Rev.*, 2009, **38**, 1400–1417.

12 V. Guillerm and M. Eddaoudi, *Acc. Chem. Res.*, 2021, **54**, 3298–3312.
13 Z. Chen, K. O. Kirlikovali, P. Li and O. K. Farha, *Acc. Chem. Res.*, 2022, **55**, 579–591.
14 H. Assi, G. Mouchaham, N. Steunou, T. Devic and C. Serre, *Chem. Soc. Rev.*, 2017, **46**, 3431–3452.
15 L. Chen, Q. Chen, M. Wu, F. Jiang and M. Hong, *Acc. Chem. Res.*, 2015, **48**, 201–210.
16 S. M. Cohen, *Chem. Rev.*, 2012, **112**, 970–1000.
17 T. Islamoglu, S. Goswami, Z. Li, A. J. Howarth, O. K. Farha and J. T. Hupp, *Acc. Chem. Res.*, 2017, **50**, 805–813.
18 J.-P. Zhang, P.-Q. Liao, H.-L. Zhou, R.-B. Lin and X.-M. Chen, *Chem. Soc. Rev.*, 2014, **43**, 5789–5814.
19 T. L. Easun, F. Moreau, Y. Yan, S. Yang and M. Schroeder, *Chem. Soc. Rev.*, 2017, **46**, 239–274.
20 Y. Inokuma, S. Yoshioka, J. Ariyoshi, T. Arai, Y. Hitora, K. Takada, S. Matsunaga, K. Rissanen and M. Fujita, *Nature*, 2013, **495**, 461–466.
21 R. Kubota, S. Tashiro, M. Shiro and M. Shionoya, *Nat. Chem.*, 2014, **6**, 913–918.
22 Y. Xie, Y. Shi, E. M. Cedeno Morales, A. El Karch, B. Wang, H. Arman, K. Tan and B. Chen, *J. Am. Chem. Soc.*, 2023, **145**, 2386–2394.
23 Y. Xiao, Y. Chen, A. N. Hong, X. Bu and P. Feng, *Angew. Chem., Int. Ed.*, 2023, **62**, e202300721.
24 X. W. Gu, E. Wu, J. X. Wang, H. M. Wen, B. Chen, B. Li and G. Qian, *Sci. Adv.*, 2023, **9**, eadh0135.
25 C. Yu, Z. Guo, L. Yang, J. Cui, S. Chen, Y. Bo, X. Suo, Q. Gong, S. Zhang, X. Cui, S. He and H. Xing, *Angew. Chem., Int. Ed.*, 2023, **62**, e202218027.
26 Z. Niu, Z. Fan, T. Pham, G. Verma, K. A. Forrest, B. Space, P. K. Thallapally, A. M. Al-Enizi and S. Ma, *Angew. Chem., Int. Ed.*, 2022, **61**, e202117807.
27 J. Pei, H.-M. Wen, X.-W. Gu, Q.-L. Qian, Y. Yang, Y. Cui, B. Li, B. Chen and G. Qian, *Angew. Chem., Int. Ed.*, 2021, **60**, 25068–25074.
28 Q. Dong, Y. Huang, J. Wan, Z. Lu, Z. Wang, C. Gu, J. Duan and J. Bai, *J. Am. Chem. Soc.*, 2023, **145**, 8043–8051.
29 J. W. Wang, S. C. Fan, H. P. Li, X. Bu, Y. Y. Xue and Q. G. Zhai, *Angew. Chem., Int. Ed.*, 2023, **62**, e202217839.
30 Y. Jiang, L. Wang, T. Yan, J. Hu, W. Sun, R. Krishna, D. Wang, Z. Gu, D. Liu, X. Cui, H. Xing and Y. Zhang, *Chem. Sci.*, 2023, **14**, 298–309.
31 B. Zhu, J.-W. Cao, S. Mukherjee, T. Pham, T. Zhang, T. Wang, X. Jiang, K. A. Forrest, M. J. Zaworotko and K.-J. Chen, *J. Am. Chem. Soc.*, 2021, **143**, 1485–1492.
32 M. Bonneau, C. Lavenn, J. J. Zheng, A. Legrand, T. Ogawa, K. Sugimoto, F. X. Coudert, R. Reau, S. Sakaki, K. I. Otake and S. Kitagawa, *Nat. Chem.*, 2022, **14**, 816–822.
33 V. I. Nikolayenko, D. C. Castell, D. Sensharma, M. Shivanna, L. Loots, K. A. Forrest, C. J. Solanilla-Salinas, K. I. Otake, S. Kitagawa, L. J. Barbour, B. Space and M. J. Zaworotko, *Nat. Chem.*, 2023, **15**, 542–549.
34 S. Zhou, O. Shekhah, A. Ramirez, P. Lyu, E. Abou-Hamad, J. Jia, J. Li, P. M. Bhatt, Z. Huang, H. Jiang, T. Jin, G. Maurin, J. Gascon and M. Eddaoudi, *Nature*, 2022, **606**, 706–712.
35 D. E. Jaramillo, A. Jaffe, B. E. R. Snyder, A. Smith, E. Taw, R. C. Rohde, M. N. Dods, W. DeSnoo, K. R. Meihaus, T. D. Harris, J. B. Neaton and J. R. Long, *Chem. Sci.*, 2022, **13**, 10216–10237.
36 W. Gong, Y. Xie, X. Wang, K. O. Kirlikovali, K. B. Idrees, F. Sha, H. Xie, Y. Liu, B. Chen, Y. Cui and O. K. Farha, *J. Am. Chem. Soc.*, 2023, **145**, 2679–2689.
37 H. Zeng, M. Xie, T. Wang, R.-J. Wei, X.-J. Xie, Y. Zhao, W. Lu and D. Li, *Nature*, 2021, **595**, 542–548.
38 T. He, X. J. Kong, Z. X. Bian, Y. Z. Zhang, G. R. Si, L. H. Xie, X. Q. Wu, H. Huang, Z. Chang, X. H. Bu, M. J. Zaworotko, Z. R. Nie and J. R. Li, *Nat. Mater.*, 2022, **21**, 689–695.
39 S. Sharma, A. V. Desai, B. Joarder and S. K. Ghosh, *Angew. Chem., Int. Ed.*, 2020, **59**, 7788–7792.
40 X. Wang, F. Ma, S. Liu, L. Chen, S. Xiong, X. Dai, B. Tai, L. He, M. Yuan, P. Mi, S. Gong, G. Li, Y. Tao, J. Wan, L. Chen, X. Sun, Q. Tang, L. He, Z. Yang, Z. Chai and S. Wang, *J. Am. Chem. Soc.*, 2022, **144**, 13634–13642.
41 T. Chen, J.-H. Dou, L. Yang, C. Sun, J. J. Oppenheim, J. Li and M. Dinca, *J. Am. Chem. Soc.*, 2022, **144**, 5583–5593.
42 G. Skorupskii, B. A. Trump, T. W. Kasel, C. M. Brown, C. H. Hendon and M. Dinca, *Nat. Chem.*, 2020, **12**, 131–136.
43 S. Kim, B. Joarder, J. A. Hurd, J. Zhang, K. W. Dawson, B. S. Gelfand, N. E. Wong and G. K. H. Shimizu, *J. Am. Chem. Soc.*, 2018, **140**, 1077–1082.
44 J. Tian, L. Liu, K. Zhou, Z. Hong, Q. Chen, F. Jiang, D. Yuan, Q. Sun and M. Hong, *Chem. Sci.*, 2020, **11**, 9818–9826.
45 L. Li, L. Guo, D. H. Olson, S. Xian, Z. Zhang, Q. Yang, K. Wu, Y. Yang, Z. Bao, Q. Ren and J. Li, *Science*, 2022, **377**, 335–339.
46 Y. Han, Y. Chen, Y. Ma, J. Bailey, Z. Wang, D. Lee, A. M. Sheveleva, F. Tuna, E. J. L. McInnes, M. D. Frogley, S. J. Day, S. P. Thompson, B. F. Spencer, M. Nikiel, P. Manuel, D. Crawshaw, M. Schroder and S. Yang, *Chem*, 2023, **9**, 738–754.
47 L. Yang, P. Cai, L. Zhang, X. Xu, A. A. Yakovenko, Q. Wang, J. Pang, S. Yuan, X. Zou, N. Huang, Z. Huang and H.-C. Zhou, *J. Am. Chem. Soc.*, 2021, **143**, 12129–12137.
48 Y. Wu, X. Wang, K. O. Kirlikovali, X. Gong, A. Atilgan, K. Ma, N. M. Schweitzer, N. C. Gianneschi, Z. Li, X. Zhang and O. K. Farha, *Angew. Chem., Int. Ed.*, 2022, **61**, e202117528.
49 S. Wang, H. G. T. Ly, M. Wahiduzzaman, C. Simms, I. Dovgaliuk, A. Tissot, G. Maurin, T. N. Parac-Vogt and C. Serre, *Nat. Commun.*, 2022, **13**, 1–8.
50 Q. Mo, L. Zhang, S. Li, H. Song, Y. Fan and C.-Y. Su, *J. Am. Chem. Soc.*, 2022, **144**, 22747–22758.
51 A. J. Howarth, Y. Y. Liu, P. Li, Z. Y. Li, T. C. Wang, J. Hupp and O. K. Farha, *Nat. Rev. Mater.*, 2016, **1**, 15018.
52 K. Wang, Y. Li, L.-H. Xie, X. Li and J.-R. Li, *Chem. Soc. Rev.*, 2022, **51**, 6417–6441.
53 T. He, X.-J. Kong and J.-R. Li, *Acc. Chem. Res.*, 2021, **54**, 3083–3094.
54 L.-H. Xie, M.-M. Xu, X.-M. Liu, M.-J. Zhao and J.-R. Li, *Adv. Sci.*, 2020, **7**, 1901758.
55 N. C. Burtch and K. S. Walton, *Acc. Chem. Res.*, 2015, **48**, 2850–2857.

56 N. C. Burtch, H. Jasuja and K. S. Walton, *Chem. Rev.*, 2014, **114**, 10575–10612.
57 X. Zhang, B. Wang, A. Alsalme, S. Xiang, Z. Zhang and B. Chen, *Coord. Chem. Rev.*, 2020, **423**, 213507.
58 M. Ding, X. Cai and H.-L. Jiang, *Chem. Sci.*, 2019, **10**, 10209–10230.
59 S. Yuan, L. Feng, K. Wang, J. Pang, M. Bosch, C. Lollar, Y. Sun, J. Qin, X. Yang, P. Zhang, Q. Wang, L. Zou, Y. Zhang, L. Zhang, Y. Fang, J. Li and H. C. Zhou, *Adv. Mater.*, 2018, **30**, e1704303.
60 J. Duan, W. Jin and S. Kitagawa, *Coord. Chem. Rev.*, 2017, **332**, 48–74.
61 K. Jayaramulu, F. Geyer, A. Schneemann, S. Kment, M. Otyepka, R. Zboril, D. Vollmer and R. A. Fischer, *Adv. Mater.*, 2019, **31**, e1900820.
62 S. Wang and C. Serre, *ACS Sustain. Chem. Eng.*, 2019, **7**, 11911–11927.
63 H. Lin, Y. Yang, Y.-C. Hsu, J. Zhang, C. Welton, I. Afolabi, M. Loo and H.-C. Zhou, *Adv. Mater.*, 2023, **35**, e2209073.
64 X. Yao, K. E. Cordova and Y. B. Zhang, *Small Struct.*, 2022, **3**, 2100209.
65 R. Sahoo, S. Mondal, D. Mukherjee and M. C. Das, *Adv. Funct. Mater.*, 2022, **32**, 2207197.
66 R. Custelcean, *Chem. Sci.*, 2021, **12**, 12518–12528.
67 X. Shi, H. Xiao, H. Azarabadi, J. Song, X. Wu, X. Chen and K. S. Lackner, *Angew. Chem., Int. Ed.*, 2020, **59**, 6984–7006.
68 D.-D. Zhou, X.-W. Zhang, Z.-W. Mo, Y.-Z. Xu, X.-Y. Tian, Y. Li, X.-M. Chen and J.-P. Zhang, *EnergyChem*, 2019, **1**, 100016.
69 R. L. Siegelman, P. J. Milner, E. J. Kim, S. C. Weston and J. R. Long, *Energy Environ. Sci.*, 2019, **12**, 2161–2173.
70 J. Liu, Y. Wei and Y. Zhao, *ACS Sustain. Chem. Eng.*, 2019, **7**, 82–93.
71 Z. G. Hu, Y. X. Wang, B. B. Shah and D. Zhao, *Adv. Sustainable Syst.*, 2019, **3**, 1800080.
72 M. Ding, R. W. Flaig, H.-L. Jiang and O. M. Yaghi, *Chem. Soc. Rev.*, 2019, **48**, 2783–2828.
73 Y. Belmabkhout, V. Guillerm and M. Eddaoudi, *Chem. Eng. J.*, 2016, **296**, 386–397.
74 Z. Zhang, Z.-Z. Yao, S. Xiang and B. Chen, *Energy Environ. Sci.*, 2014, **7**, 2868–2899.
75 G. Ferey, C. Serre, T. Devic, G. Maurin, H. Jobic, P. L. Llewellyn, G. De Weireld, A. Vimont, M. Daturi and J.-S. Chang, *Chem. Soc. Rev.*, 2011, **40**, 550–562.
76 G. Férey, C. Mellot-Draznieks, C. Serre, F. Millange, J. Dutour, S. Surblé and I. Margiolaki, *Science*, 2005, **309**, 2040–2042.
77 Z. Li, X. Liu, W. Jin, Q. Hu and Y. Zhao, *J. Colloid Interface Sci.*, 2019, **554**, 692–704.
78 I. J. Kang, N. A. Khan, E. Haque and S. H. Jhung, *Chem.–Euro. J.*, 2011, **17**, 6437–6442.
79 L. Liang, L. Liu, F. Jiang, C. Liu, D. Yuan, Q. Chen, D. Wu, H.-L. Jiang and M. Hong, *Inorg. Chem.*, 2018, **57**, 4891–4897.
80 K. Leus, T. Bogaerts, J. De Decker, H. Depauw, K. Hendrickx, H. Vrielinck, V. Van Speybroeck and P. Van Der Voort, *Microporous Mesoporous Mater.*, 2016, **226**, 110–116.
81 L. Z. Qin, X. H. Xiong, S. H. Wang, L. Zhang, L. L. Meng, L. Yan, Y. N. Fan, T. A. Yan, D. H. Liu, Z. W. Wei and C. Y. Su, *ACS Appl. Mater. Interfaces*, 2022, **14**, 45444–45450.
82 K. A. Cychosz and A. J. Matzger, *Langmuir*, 2010, **26**, 17198–17202.
83 P. Horcajada, S. Surble, C. Serre, D. Y. Hong, Y. K. Seo, J. S. Chang, J. M. Greneche, I. Margiolaki and G. Ferey, *Chem. Commun.*, 2007, **43**, 2820–2822.
84 C. Volkringer, D. Popov, T. Loiseau, G. Férey, M. Burghammer, C. Riekel, M. Haouas and F. Taulelle, *Chem. Mater.*, 2009, **21**, 5695–5697.
85 J. Lv, B. Wang, Y. B. Xie, P. L. Wang, L. Shu, X. O. Su and J. R. Li, *Environ. Sci.: Nano*, 2019, **6**, 2759–2766.
86 F. Yang, G. Xu, Y. Dou, B. Wang, H. Zhang, H. Wu, W. Zhou, J.-R. Li and B. Chen, *Nat. Energy*, 2017, **2**, 877–883.
87 J. H. Cavka, S. Jakobsen, U. Olsbye, N. Guillou, C. Lamberti, S. Bordiga and K. P. Lillerud, *J. Am. Chem. Soc.*, 2008, **130**, 13850–13851.
88 N.-X. Zhu, Z.-W. Wei, C.-X. Chen, X.-H. Xiong, Y.-Y. Xiong, Z. Zeng, W. Wang, J.-J. Jiang, Y.-N. Fan and C.-Y. Su, *Angew. Chem., Int. Ed.*, 2022, **61**, e202112097.
89 H. L. Jiang, D. W. Feng, T. F. Liu, J. R. Li and H. C. Zhou, *J. Am. Chem. Soc.*, 2012, **134**, 14690–14693.
90 D. W. Feng, Z. Y. Gu, Y. P. Chen, J. Park, Z. W. Wei, Y. J. Sun, M. Bosch, S. Yuan and H. C. Zhou, *J. Am. Chem. Soc.*, 2014, **136**, 17714–17717.
91 T. F. Liu, D. W. Feng, Y. P. Chen, L. F. Zou, M. Bosch, S. Yuan, Z. W. Wei, S. Fordham, K. C. Wang and H. C. Zhou, *J. Am. Chem. Soc.*, 2015, **137**, 413–419.
92 Y. X. Sun, Q. Sun, H. L. Huang, B. Aguila, Z. Niu, J. A. Perman and S. Q. Ma, *J. Mater. Chem. A*, 2017, **5**, 18770–18776.
93 B. Wang, X.-L. Lv, D. Feng, L.-H. Xie, J. Zhang, M. Li, Y. Xie, J.-R. Li and H.-C. Zhou, *J. Am. Chem. Soc.*, 2016, **138**, 6204–6216.
94 B. Wang, Q. Yang, C. Guo, Y. X. Sun, L. H. Xie and J. R. Li, *ACS Appl. Mater. Interfaces*, 2017, **9**, 10286–10295.
95 B. Wang, P. Wang, L.-H. Xie, R.-B. Lin, J. Lv, J.-R. Li and B. Chen, *Nat. Commun.*, 2019, **10**, 3861.
96 X.-J. Kong, Y.-Z. Zhang, T. He, X.-Q. Wu, M.-M. Xu, S.-N. Wang, L.-H. Xie and J.-R. Li, *CrystEngComm*, 2018, **20**, 6018–6025.
97 L. H. Xie, X. M. Liu, T. He and J. R. Li, *Chem*, 2018, **4**, 1911–1927.
98 W. Liang, H. Chevreau, F. Ragon, P. D. Southon, V. K. Peterson and D. M. D'Alessandro, *CrystEngComm*, 2014, **16**, 6530–6533.
99 O. V. Gutov, W. Bury, D. A. Gomez-Gualdron, V. Krungleviciute, D. Fairen-Jimenez, J. E. Mondloch, A. A. Sarjeant, S. S. Al-Juaid, R. Q. Snurr, J. T. Hupp, T. Yildirim and O. K. Farha, *Chem.–Euro. J.*, 2014, **20**, 12389–12393.
100 Z. Lu, J. Duan, H. Tan, L. Du, X. Zhao, R. Wang, S. Kato, S. Yang and J. T. Hupp, *J. Am. Chem. Soc.*, 2023, **145**, 4150–4157.

101 S. Wang, H. Reinsch, N. Heymans, M. Wahiduzzaman, C. Martineau-Corcos, G. De Weireld, G. Maurin and C. Serre, *Matter*, 2020, **2**, 440–450.
102 S. Wang, M. Cabrero-Antonino, S. Navalon, C.-c. Cao, A. Tissot, I. Dovgaliuk, J. Marrot, C. Martineau-Corcos, L. Yu, H. Wang, W. Shepard, H. Garcia and C. Serre, *Chem*, 2020, **6**, 3409–3427.
103 W.-B. Zhong, R.-X. Li, J. Lv, T. He, M.-M. Xu, B. Wang, L.-H. Xie and J.-R. Li, *Inorg. Chem. Front.*, 2020, **7**, 1161–1171.
104 H.-Q. Yin, K. Tan, S. Jensen, S. J. Teat, S. Ullah, X. Hei, E. Velasco, K. Oyekan, N. Meyer, X.-Y. Wang, T. Thonhauser, X.-B. Yin and J. Li, *Chem. Sci.*, 2021, **12**, 14189–14197.
105 F. C. Leng, H. Liu, M. L. Ding, Q. P. Lin and H. L. Jiang, *ACS Catal.*, 2018, **8**, 4583–4590.
106 H. L. Jiang, N. Tsumori and Q. Xu, *Inorg. Chem.*, 2010, **49**, 10001–10006.
107 D. Alezi, A. M. Peedikakkal, L. J. Weselinski, V. Guillerm, Y. Belmabkhout, A. J. Cairns, Z. Chen, L. Wojtas and M. Eddaoudi, *J. Am. Chem. Soc.*, 2015, **137**, 5421–5430.
108 D. X. Xue, A. J. Cairns, Y. Belmabkhout, L. Wojtas, Y. Liu, M. H. Alkordi and M. Eddaoudi, *J. Am. Chem. Soc.*, 2013, **135**, 7660–7667.
109 J. Duan, M. Higuchi, R. Krishna, T. Kiyonaga, Y. Tsutsumi, Y. Sato, Y. Kubota, M. Takata and S. Kitagawa, *Chem. Sci.*, 2014, **5**, 660–666.
110 J. G. Duan, M. Higuchi, S. Horike, M. L. Foo, K. P. Rao, Y. Inubushi, T. Fukushima and S. Kitagawa, *Adv. Funct. Mater.*, 2013, **23**, 3525–3530.
111 D. X. Xue, Y. Belmabkhout, O. Shekhah, H. Jiang, K. Adil, A. J. Cairns and M. Eddaoudi, *J. Am. Chem. Soc.*, 2015, **137**, 5034–5040.
112 S. Yuan, J. S. Qin, J. Li, L. Huang, L. Feng, Y. Fang, C. Lollar, J. Pang, L. Zhang, D. Sun, A. Alsalme, T. Cagin and H. C. Zhou, *Nat. Commun.*, 2018, **9**, 808.
113 K. Wang, D. Feng, T.-F. Liu, J. Su, S. Yuan, Y.-P. Chen, M. Bosch, X. Zou and H.-C. Zhou, *J. Am. Chem. Soc.*, 2014, **136**, 13983–13986.
114 K. S. Park, Z. Ni, A. P. Cote, J. Y. Choi, R. Huang, F. J. Uribe-Romo, H. K. Chae, M. O'Keeffe and O. M. Yaghi, *Proc. Natl. Acad. Sci. U. S. A.*, 2006, **103**, 10186–10191.
115 X. C. Huang, Y. Y. Lin, J. P. Zhang and X. M. Chen, *Angew. Chem., Int. Ed.*, 2006, **45**, 1557–1559.
116 Y. Wang, N.-Y. Huang, X.-W. Zhang, H. He, R.-K. Huang, Z.-M. Ye, Y. Li, D.-D. Zhou, P.-Q. Liao, X.-M. Chen and J.-P. Zhang, *Angew. Chem., Int. Ed.*, 2019, **58**, 7692–7696.
117 Z. S. Wang, M. Li, Y. L. Peng, Z. Zhang, W. Chen and X. C. Huang, *Angew. Chem., Int. Ed.*, 2019, **58**, 16071–16076.
118 H. J. Choi, M. Dinca, A. Dailly and J. R. Long, *Energy Environ. Sci.*, 2010, **3**, 117–123.
119 A. Phan, C. J. Doonan, F. J. Uribe-Romo, C. B. Knobler, M. O'Keeffe and O. M. Yaghi, *Acc. Chem. Res.*, 2010, **43**, 58–67.
120 R. Banerjee, A. Phan, B. Wang, C. Knobler, H. Furukawa, M. O'Keeffe and O. M. Yaghi, *Science*, 2008, **319**, 939–943.
121 M. Tonigold, Y. Lu, B. Bredenkotter, B. Rieger, S. Bahnmuller, J. Hitzbleck, G. Langstein and D. Volkmer, *Angew. Chem., Int. Ed.*, 2009, **48**, 7546–7550.
122 X.-F. Lu, P.-Q. Liao, J.-W. Wang, J. X. Wu, X.-W. Chen, C.-T. He, J.-P. Zhang, G.-R. Li and X.-M. Chen, *J. Am. Chem. Soc.*, 2016, **138**, 8336–8339.
123 J. Tian, C. Shi, C. Xiao, F. Jiang, D. Yuan, Q. Chen and M. Hong, *Inorg. Chem.*, 2020, **59**, 18264–18275.
124 D. Liu, J. Pei, X. Zhang, X. W. Gu, H. M. Wen, B. Chen, G. Qian and B. Li, *Angew. Chem., Int. Ed.*, 2023, **62**, e202218590.
125 S. Li, S. Zeng, Y. Tian, X. Jing, F. Sun and G. Zhu, *Nano Res.*, 2021, **14**, 3288–3293.
126 K. Wang, X.-L. Lv, D. Feng, J. Li, S. Chen, J. Sun, L. Song, Y. Xie, J.-R. Li and H.-C. Zhou, *J. Am. Chem. Soc.*, 2016, **138**, 914–919.
127 X.-L. Lv, K. Wang, B. Wang, J. Su, X. Zou, Y. Xie, J.-R. Li and H.-C. Zhou, *J. Am. Chem. Soc.*, 2017, **139**, 211–217.
128 V. Colombo, S. Galli, H. J. Choi, G. D. Han, A. Maspero, G. Palmisano, N. Masciocchi and J. R. Long, *Chem. Sci.*, 2011, **2**, 1311–1319.
129 T. He, Z. H. Huang, S. Yuan, X. L. Lv, X. J. Kong, X. D. Zou, H. C. Zhou and J. R. Li, *J. Am. Chem. Soc.*, 2020, **142**, 13491–13499.
130 A. Demessence, D. M. D'Alessandro, M. L. Foo and J. R. Long, *J. Am. Chem. Soc.*, 2009, **131**, 8784–8786.
131 J.-P. Zhang and X.-M. Chen, *J. Am. Chem. Soc.*, 2008, **130**, 6010–6017.
132 D. D. Zhou, P. Chen, C. Wang, S. S. Wang, Y. Du, H. Yan, Z. M. Ye, C. T. He, R. K. Huang, Z. W. Mo, N. Y. Huang and J. P. Zhang, *Nat. Mater.*, 2019, **18**, 994–998.
133 J.-H. Wang, M. Li and D. Li, *Chem.–Euro. J.*, 2014, **20**, 12004–12008.
134 D. Lv, R. Shi, Y. Chen, Y. Chen, H. Wu, X. Zhou, H. Xi, Z. Li and Q. Xia, *Ind. Eng. Chem. Res.*, 2018, **57**, 12215–12224.
135 Z. M. Ye, X. W. Zhang, P. Q. Liao, Y. Xie, Y. T. Xu, X. F. Zhang, C. Wang, D. X. Liu, N. Y. Huang, Z. H. Qiu, D. D. Zhou, C. T. He and J. P. Zhang, *Angew. Chem., Int. Ed.*, 2020, **59**, 23322–23328.
136 L. Liang, C. Liu, F. Jiang, Q. Chen, L. Zhang, H. Xue, H. L. Jiang, J. Qian, D. Yuan and M. Hong, *Nat. Commun.*, 2017, **8**, 1233.
137 J. Tian, F. Jiang, D. Yuan, L. Zhang, Q. Chen and M. Hong, *Angew. Chem., Int. Ed.*, 2020, **59**, 13101–13108.
138 D. Wu, C. Liu, J. Tian, F. Jiang, D. Yuan, Q. Chen and M. Hong, *Inorg. Chem.*, 2020, **59**, 13542–13550.
139 C. Montoro, F. Linares, E. Q. Procopio, I. Senkovska, S. Kaskel, S. Galli, N. Masciocchi, E. Barea and J. A. R. Navarro, *J. Am. Chem. Soc.*, 2011, **133**, 11888–11891.
140 Y. Hu, M. Ding, X.-Q. Liu, L.-B. Sun and H.-L. Jiang, *Chem. Commun.*, 2016, **52**, 5734–5737.
141 J. Tian, Q. Chen, F. Jiang, D. Yuan and M. Hong, *Angew. Chem., Int. Ed.*, 2023, **62**, e202215253.
142 C. Chen, Z. Yu, D. S. Sholl and K. S. Walton, *J. Phys. Chem. Lett.*, 2022, **13**, 4891–4896.
143 A. J. Rieth, A. M. Wright and M. Dinca, *Nat. Rev. Mater.*, 2019, **4**, 708–725.

144 S. Yuan, L. Feng, K. Wang, J. Pang, M. Bosch, C. Lollar, Y. Sun, J. Qin, X. Yang, P. Zhang, Q. Wang, L. Zou, Y. Zhang, L. Zhang, Y. Fang, J. Li and H.-C. Zhou, *Adv. Mater.*, 2018, **30**, e1704303.
145 A. Schaate, P. Roy, A. Godt, J. Lippke, F. Waltz, M. Wiebcke and P. Behrens, *Chem.–Euro. J.*, 2011, **17**, 6643–6651.
146 H. L. Jiang, D. W. Feng, K. C. Wang, Z. Y. Gu, Z. W. Wei, Y. P. Chen and H. C. Zhou, *J. Am. Chem. Soc.*, 2013, **135**, 13934–13938.
147 S. C. Li, C. P. Liu, Q. H. Chen, F. L. Jiang, D. Q. Yuan, Q. F. Sun and M. C. Hong, *Chem. Sci.*, 2022, **13**, 9016–9022.
148 F. Saraci, V. Quezada-Novoa, P. R. Donnarumma and A. J. Howarth, *Chem. Soc. Rev.*, 2020, **49**, 7949–7977.
149 H. Jasuja and K. S. Walton, *Dalton Trans.*, 2013, **42**, 15421–15426.
150 H. Jasuja, Y. Jiao, N. C. Burtch, Y. G. Huang and K. S. Walton, *Langmuir*, 2014, **30**, 14300–14307.
151 C.-T. He, P.-Q. Liao, D.-D. Zhou, B.-Y. Wang, W.-X. Zhang, J.-P. Zhang and X.-M. Chen, *Chem. Sci.*, 2014, **5**, 4755–4762.
152 D.-M. Chen, N.-N. Zhang, J.-Y. Tian, C.-S. Liu and M. Du, *J. Mater. Chem. A*, 2017, **5**, 4861–4867.
153 H. Yang, F. Peng, A. N. Hong, Y. Wang, X. Bu and P. Feng, *J. Am. Chem. Soc.*, 2021, **143**, 14470–14474.
154 Y. Ye, Z. Ma, R.-B. Lin, R. Krishna, W. Zhou, Q. Lin, Z. Zhang, S. Xiang and B. Chen, *J. Am. Chem. Soc.*, 2019, **141**, 4130–4136.
155 Y. X. Tan, Y. P. He and J. Zhang, *Inorg. Chem.*, 2012, **51**, 9649–9654.
156 D. M. Chen, J. Y. Tian, C. S. Liu and M. Du, *Chem. Commun.*, 2016, **52**, 8413–8416.
157 X.-L. Lv, S. Yuan, L.-H. Xie, H. F. Darke, Y. Chen, T. He, C. Dong, B. Wang, Y.-Z. Zhang, J.-R. Li and H.-C. Zhou, *J. Am. Chem. Soc.*, 2019, **141**, 10283–10293.
158 X.-J. Kong, T. He, J. Zhou, C. Zhao, T.-C. Li, X.-Q. Wu, K. Wang and J.-R. Li, *Small*, 2021, **17**, 2005357.
159 J. R. Karra, H. Jasuja, Y.-G. Huang and K. S. Walton, *J. Mater. Chem. A*, 2015, **3**, 1624–1631.
160 H. Yang, F. Peng, C. Dang, Y. Wang, D. Hu, X. Zhao, P. Feng and X. Bu, *J. Am. Chem. Soc.*, 2019, **141**, 9808–9812.
161 T. F. Liu, L. F. Zou, D. W. Feng, Y. P. Chen, S. Fordham, X. Wang, Y. Y. Liu and H. C. Zhou, *J. Am. Chem. Soc.*, 2014, **136**, 7813–7816.
162 J.-H. Wang, Y. Zhang, M. Li, S. Yan, D. Li and X.-M. Zhang, *Angew. Chem., Int. Ed.*, 2017, **56**, 6478–6482.
163 Z. J. Zhang, H. T. H. Nguyen, S. A. Miller, A. M. Ploskonka, J. B. DeCoste and S. M. Cohen, *J. Am. Chem. Soc.*, 2016, **138**, 920–925.
164 Y. Chen, B. Wang, X. Q. Wang, L. H. Xie, J. P. Li, Y. B. Xie and J. R. Li, *ACS Appl. Mater. Interfaces*, 2017, **9**, 27027–27035.
165 Z. R. Jiang, J. Ge, Y. X. Zhou, Z. Y. U. Wang, D. X. Chen, S. H. Yu and H. L. Jiang, *NPG Asia Mater.*, 2016, **8**, e253.
166 Y. Wang, T. Li, L. Li, R. B. Lin, X. Jia, Z. Chang, H. M. Wen, X. M. Chen and J. Li, *Adv. Mater.*, 2023, **35**, 2207955.
167 T. A. Makal, X. Wang and H. C. Zhou, *Cryst. Growth Des.*, 2013, **13**, 4760–4768.
168 D. Y. Ma, Y. W. Li and Z. Li, *Chem. Commun.*, 2011, **47**, 7377–7379.
169 D. Sun, P. R. Adiyala, S. J. Yim and D. P. Kim, *Angew. Chem., Int. Ed.*, 2019, **58**, 7405–7409.
170 S. Yang, L. Peng, D. T. Sun, M. Asgari, E. Oveisi, O. Trukhina, S. Bulut, A. Jamali and W. L. Queen, *Chem. Sci.*, 2019, **10**, 4542–4549.
171 J. G. Nguyen and S. M. Cohen, *J. Am. Chem. Soc.*, 2010, **132**, 4560–4561.
172 J. Aguilera-Sigalat and D. Bradshaw, *Chem. Commun.*, 2014, **50**, 4711–4713.
173 P. Deria, Y. G. Chung, R. Q. Snurr, J. T. Hupp and O. K. Farha, *Chem. Sci.*, 2015, **6**, 5172–5176.
174 J. Liu, R. Anderson, K. M. Schmalbach, T. R. Sheridan, Z. Wang, N. M. Schweitzer, A. Stein, N. A. Mara, D. Gomez-Gualdron and J. T. Hupp, *J. Mater. Chem. A*, 2022, **10**, 17307–17316.
175 W. Zhang, Y. Hu, J. Ge, H.-L. Jiang and S.-H. Yu, *J. Am. Chem. Soc.*, 2014, **136**, 16978–16981.
176 M. Kalaj, M. S. Denny Jr, K. C. Bentz, J. M. Palomba and S. M. Cohen, *Angew. Chem., Int. Ed.*, 2019, **58**, 2336–2340.
177 G. Huang, Q. H. Yang, Q. Xu, S. H. Yu and H. L. Jiang, *Angew. Chem., Int. Ed.*, 2016, **55**, 7379–7383.
178 Y. Seok Chae, S. Park, D. Won Kang, D. Won Kim, M. Kang, D. San Choi, J. Hyeak Choe and C. Seop Hong, *Chem. Eng. J.*, 2022, **433**, 133856.
179 A. Carne-Sanchez, K. C. Stylianou, C. Carbonell, M. Naderi, I. Imaz and D. Maspoch, *Adv. Mater.*, 2015, **27**, 869–873.
180 L.-H. Xu, S.-H. Li, H. Mao, Y. Li, A.-S. Zhang, S. Wang, W.-M. Liu, J. Lv, T. Wang, W.-W. Cai, L. Sang, W.-W. Xie, C. Pei, Z.-Z. Li, Y.-N. Feng and Z.-P. Zhao, *Science*, 2022, **378**, 308–313.
181 D. Micheroni, G. X. Lan and W. B. Lin, *J. Am. Chem. Soc.*, 2018, **140**, 15591–15595.
182 S. J. Yang, J. Y. Choi, H. K. Chae, J. H. Cho, K. S. Nahm and C. R. Park, *Chem. Mater.*, 2009, **21**, 1893–1897.
183 J. Noh, W. Chen, P. Wu, Y. Huang, J. Tan, H. C. Zhou and C. Yu, *Adv. Funct. Mater.*, 2021, **31**, 2104899.
184 P. D. C. Dietzel, R. E. Johnsen, H. Fjellvag, S. Bordiga, E. Groppo, S. Chavan and R. Blom, *Chem. Commun.*, 2008, **44**, 5125–5127.
185 M. I. Gonzalez, J. A. Mason, E. D. Bloch, S. J. Teat, K. J. Gagnon, G. Y. Morrison, W. L. Queen and J. R. Long, *Chem. Sci.*, 2017, **8**, 4387–4398.
186 F. Luo, C. Yan, L. Dang, R. Krishna, W. Zhou, H. Wu, X. Dong, Y. Han, T.-L. Hu, M. O'Keeffe, L. Wang, M. Luo, R.-B. Lin and B. Chen, *J. Am. Chem. Soc.*, 2016, **138**, 5678–5684.
187 R. Vaidhyanathan, S. S. Iremonger, G. K. H. Shimizu, P. G. Boyd, S. Alavi and T. K. Woo, *Science*, 2010, **330**, 650–653.
188 P. Q. Liao, D. D. Zhou, A. X. Zhu, L. Jiang, R. B. Lin, J. P. Zhang and X. M. Chen, *J. Am. Chem. Soc.*, 2012, **134**, 17380–17383.
189 T. D. Duong, S. A. Sapchenko, I. da Silva, H. G. W. Godfrey, Y. Cheng, L. L. Daemen, P. Manuel, M. D. Frogley,

G. Cinque, A. J. Ramirez-Cuesta, S. Yang and M. Schroeder, *Chem. Sci.*, 2020, **11**, 5339–5346.

190 D. Song, F. Jiang, D. Yuan, Q. Chen and M. Hong, *Small*, 2023, **19**, 2302677.

191 P. M. Bhatt, Y. Belmabkhout, A. Cadiau, K. Adil, O. Shekhah, A. Shkurenko, L. J. Barbour and M. Eddaoudi, *J. Am. Chem. Soc.*, 2016, **138**, 9301–9307.

192 W. Liang, P. M. Bhatt, A. Shkurenko, K. Adil, G. Mouchaham, H. Aggarwal, A. Mallick, A. Jamal, Y. Belmabkhout and M. Eddaoudi, *Chem*, 2019, **5**, 950–963.

193 S. Xiang, Y. He, Z. Zhang, H. Wu, W. Zhou, R. Krishna and B. Chen, *Nat. Commun.*, 2012, **3**, 954.

194 S. H. Yang, J. L. Sun, A. J. Ramirez-Cuesta, S. K. Callear, W. I. F. David, D. P. Anderson, R. Newby, A. J. Blake, J. E. Parker, C. C. Tang and M. Schroder, *Nat. Chem.*, 2012, **4**, 887–894.

195 F. Moreau, I. da Silva, N. H. Al Smail, T. L. Easun, M. Savage, H. G. Godfrey, S. F. Parker, P. Manuel, S. Yang and M. Schroder, *Nat. Commun.*, 2017, **8**, 14085.

196 N. C. Burtch, H. Jasuja, D. Dubbeldam and K. S. Walton, *J. Am. Chem. Soc.*, 2013, **135**, 7172–7180.

197 P. G. Boyd, A. Chidambaram, E. Garcia-Diez, C. P. Ireland, T. D. Daff, R. Bounds, A. Gladysiak, P. Schouwink, S. M. Moosavi, M. M. Maroto-Valer, J. A. Reimer, J. A. R. Navarro, T. K. Woo, S. Garcia, K. C. Stylianou and B. Smit, *Nature*, 2019, **576**, 253–256.

198 A. M. Plonka, D. Banerjee, W. R. Woerner, Z. J. Zhang, N. Nijem, Y. J. Chabal, J. Li and J. B. Parise, *Angew. Chem., Int. Ed.*, 2013, **52**, 1692–1695.

199 Z. Z. Lu, H. G. W. Godfrey, I. da Silva, Y. Q. Cheng, M. Savage, F. Tuna, E. J. L. McInnes, S. J. Teat, K. J. Gagnon, M. D. Frogley, P. Manuel, S. Rudic, A. J. Ramirez-Cuesta, T. L. Easun, S. H. Yang and M. Schroder, *Nat. Commun.*, 2017, **8**, 14212.

200 T. M. McDonald, J. A. Mason, X. Kong, E. D. Bloch, D. Gygi, A. Dani, V. Crocella, F. Giordanino, S. O. Odoh, W. S. Drisdell, B. Vlaisavljevich, A. L. Dzubak, R. Poloni, S. K. Schnell, N. Planas, K. Lee, T. Pascal, L. F. Wan, D. Prendergast, J. B. Neaton, B. Smit, J. B. Kortright, L. Gagliardi, S. Bordiga, J. A. Reimer and J. R. Long, *Nature*, 2015, **519**, 303–308.

201 R. W. Faig, T. M. O. Popp, A. M. Fracaroli, E. A. Kapustin, M. J. Kalmutzki, R. M. Altamimi, F. Fathieh, J. A. Reimer and O. M. Yaghi, *J. Am. Chem. Soc.*, 2017, **139**, 12125–12128.

202 P. J. Milner, R. L. Siegelman, A. C. Forse, M. I. Gonzalez, T. Runcevski, J. D. Martell, J. A. Reimer and J. R. Long, *J. Am. Chem. Soc.*, 2017, **139**, 13541–13553.

203 A. C. Forse, P. J. Milner, J. H. Lee, H. N. Redfearn, J. Oktawiec, R. L. Siegelman, J. D. Martell, B. Dinakar, L. B. Porter-Zasada, M. I. Gonzalez, J. B. Neaton, J. R. Long and J. A. Reimer, *J. Am. Chem. Soc.*, 2018, **140**, 18016–18031.

204 J. J. Gassensmith, H. Furukawa, R. A. Smaldone, R. S. Forgan, Y. Y. Botros, O. M. Yaghi and J. F. Stoddart, *J. Am. Chem. Soc.*, 2011, **133**, 15312–15315.

205 M. E. Zick, S. M. Pugh, J. H. Lee, A. C. Forse and P. J. Milner, *Angew. Chem., Int. Ed.*, 2022, **61**, e202206718.

206 P.-Q. Liao, H. Chen, D.-D. Zhou, S.-Y. Liu, C.-T. He, Z. Rui, H. Ji, J.-P. Zhang and X.-M. Chen, *Energy Environ. Sci.*, 2015, **8**, 1011–1016.

207 C. E. Bien, K. K. Chen, S.-C. Chien, B. R. Reiner, L.-C. Lin, C. R. Wade and W. S. W. Ho, *J. Am. Chem. Soc.*, 2018, **140**, 12662–12666.

208 A. Demessence, D. M. D'Alessandro, M. L. Foo and J. R. Long, *J. Am. Chem. Soc.*, 2009, **131**, 8784–8786.

209 A. M. Wright, Z. Wu, G. Zhang, J. L. Mancuso, R. J. Comito, R. W. Day, C. H. Hendon, J. T. Miller and M. Dinca, *Chem*, 2018, **4**, 2894–2901.

210 H. A. Evans, D. Mullangi, Z. Deng, Y. Wang, S. B. Peh, F. Wei, J. Wang, C. M. Brown, D. Zhao, P. Canepa and A. K. Cheetham, *Sci. Adv.*, 2022, **8**, eade1473.

211 H. Lyu, O. I.-F. Chen, N. Hanikel, M. I. Hossain, R. W. Flaig, X. Pei, A. Amin, M. D. Doherty, R. K. Impastato, T. G. Glover, D. R. Moore and O. M. Yaghi, *J. Am. Chem. Soc.*, 2022, **144**, 2387–2396.

212 L. Han, T. Pham, M. J. Zhuo, K. A. Forrest, S. Suepaul, B. Space, M. J. Zaworotko, W. Shi, Y. Chen, P. Cheng and Z. J. Zhang, *ACS Appl. Mater. Interfaces*, 2019, **11**, 23192–23197.

213 P. Nugent, Y. Belmabkhout, S. D. Burd, A. J. Cairns, R. Luebke, K. Forrest, T. Pham, S. Q. Ma, B. Space, L. Wojtas, M. Eddaoudi and M. J. Zaworotko, *Nature*, 2013, **495**, 80–84.

214 O. Shekhah, Y. Belmabkhout, Z. Chen, V. Guillerm, A. Cairns, K. Adil and M. Eddaoudi, *Nat. Commun.*, 2014, **5**, 4228.

215 H.-M. Wen, C. Liao, L. Li, A. Alsalme, Z. Alothman, R. Krishna, H. Wu, W. Zhou, J. Hu and B. Chen, *J. Mater. Chem. A*, 2019, **7**, 3128–3134.

216 K.-J. Chen, D. G. Madden, T. Pham, K. A. Forrest, A. Kumar, Q.-Y. Yang, W. Xue, B. Space, J. J. Perry, J.-P. Zhang, X.-M. Chen and M. J. Zaworotko, *Angew. Chem., Int. Ed.*, 2016, **55**, 10268–10272.

217 J.-B. Lin, T. T. T. Nguyen, R. Vaidhyanathan, J. Burner, J. M. Taylor, H. Durekova, F. Akhtar, R. K. Mah, O. Ghaffari-Nik, S. Marx, N. Fylstra, S. S. Iremonger, K. W. Dawson, P. Sarkar, P. Hovington, A. Rajendran, T. K. Woo and G. K. H. Shimizu, *Science*, 2021, **374**, 1464–1469.

218 T. M. McDonald, D. M. D'Alessandro, R. Krishna and J. R. Long, *Chem. Sci.*, 2011, **2**, 2022–2028.

219 W. R. Lee, S. Y. Hwang, D. W. Ryu, K. S. Lim, S. S. Han, D. Moon, J. Choi and C. S. Hong, *Energy Environ. Sci.*, 2014, **7**, 744–751.

220 J. H. Choe, H. Kim, M. Kang, H. Yun, S. Y. Kim, S. M. Lee and C. S. Hong, *J. Am. Chem. Soc.*, 2022, **144**, 10309–10319.

221 P.-Q. Liao, X.-Y. Li, J. Bai, C.-T. He, D.-D. Zhou, W.-X. Zhang, J.-P. Zhang and X.-M. Chen, *Chem.–Euro. J.*, 2014, **20**, 11303–11307.

222 N. Ding, H. Li, X. Feng, Q. Wang, S. Wang, L. Ma, J. Zhou and B. Wang, *J. Am. Chem. Soc.*, 2016, **138**, 10100–10103.

223 P.-Q. Liao, X.-W. Chen, S.-Y. Liu, X.-Y. Li, Y.-T. Xu, M. Tang, Z. Rui, H. Ji, J.-P. Zhang and X.-M. Chen, *Chem. Sci.*, 2016, **7**, 6528–6533.

224 H. Li, K. Wang, D. Feng, Y.-P. Chen, W. Verdegaal and H.-C. Zhou, *Chemsuschem*, 2016, **9**, 2832–2840.
225 T. M. McDonald, W. R. Lee, J. A. Mason, B. M. Wiers, C. S. Hong and J. R. Long, *J. Am. Chem. Soc.*, 2012, **134**, 7056–7065.
226 W. R. Lee, J. E. Kim, S. J. Lee, M. Kang, D. W. Kang, H. Y. Lee, V. Hiremath, J. G. Seo, H. Jin, D. Moon, M. Cho, Y. Jung and C. S. Hong, *ChemSusChem*, 2018, **11**, 1694–1707.
227 Z. Zhang, Q. Ding, S. B. Peh, D. Zhao, J. Cui, X. Cui and H. Xing, *Chem. Commun.*, 2020, **56**, 7726–7729.
228 Z. Zhang, Q. Ding, J. Cui, X. Cui and H. Xing, *Sci. China Mater.*, 2021, **64**, 691–697.
229 A. Kumar, C. Hua, D. G. Madden, D. O'Nolan, K. J. Chen, L. J. Keane, J. J. Perry and M. J. Zaworotko, *Chem. Commun.*, 2017, **53**, 5946–5949.
230 S. Mukherjee, N. Sikdar, D. O'Nolan, D. M. Franz, V. Gascon, A. Kumar, N. Kumar, H. S. Scott, D. G. Madden, P. E. Kruger, B. Space and M. J. Zaworotko, *Sci. Adv.*, 2019, **5**, eaax9171.
231 K.-J. Chen, H. S. Scott, D. G. Madden, T. Pham, A. Kumar, A. Bajpai, M. Lusi, K. A. Forrest, B. Space, J. J. Perry and M. J. Zaworotko, *Chem*, 2016, **1**, 753–765.
232 M. Jiang, B. Li, X. Cui, Q. Yang, Z. Bao, Y. Yang, H. Wu, W. Zhou, B. Chen and H. Xing, *ACS Appl. Mater. Interfaces*, 2018, **10**, 16628–16635.
233 X. H. Song, M. X. Zhang, C. Chen, J. G. Duan, W. W. Zhang, Y. Pan and J. F. Bai, *J. Am. Chem. Soc.*, 2019, **141**, 14539–14543.
234 Z. G. Hu, K. Zhang, M. Zhang, Z. G. Guo, J. W. Jiang and D. Zhao, *Chemsuschem*, 2014, **7**, 2791–2795.
235 G. E. Cmarik, M. Kim, S. M. Cohen and K. S. Walton, *Langmuir*, 2012, **28**, 15606–15613.
236 Y. X. Wang, Z. G. Hu, T. Kundu, Y. D. Cheng, J. Q. Dong, Y. H. Qian, L. Z. Zhai and D. Zhao, *ACS Sustainable Chem. Eng.*, 2018, **6**, 11904–11912.
237 Z. G. Hu, S. Faucher, Y. Y. Zhuo, Y. Sun, S. N. Wang and D. Zhao, *Chem.–Euro. J.*, 2015, **21**, 17245–17255.
238 Z. G. Hu, M. Khurana, Y. H. Seah, M. Zhang, Z. G. Guo and D. Zhao, *Chem. Eng. Sci.*, 2015, **124**, 61–69.
239 L.-J. Li, P.-Q. Liao, C.-T. He, Y.-S. Wei, H.-L. Zhou, J.-M. Lin, X.-Y. Li and J.-P. Zhang, *J. Mater. Chem. A*, 2015, **3**, 21849–21855.
240 Z. Hu, A. Nalaparaju, Y. Peng, J. Jiang and D. Zhao, *Inorg. Chem.*, 2016, **55**, 1134–1141.
241 W. L. Queen, M. R. Hudson, E. D. Bloch, J. A. Mason, M. I. Gonzalez, J. S. Lee, D. Gygi, J. D. Howe, K. Lee, T. A. Darwish, M. James, V. K. Peterson, S. J. Teat, B. Smit, J. B. Neaton, J. R. Long and C. M. Brown, *Chem. Sci.*, 2014, **5**, 4569–4581.
242 J. Park, J. R. Park, J. H. Choe, S. Kim, M. Kang, D. W. Kang, J. Y. Kim, Y. W. Jeong and C. S. Hong, *ACS Appl. Mater. Interfaces*, 2020, **12**, 50534–50540.
243 E. J. Kim, R. L. Siegelman, H. Z. H. Jiang, A. C. Forse, J.-H. Lee, J. D. Martell, P. J. Milner, J. M. Falkowski, J. B. Neaton, J. A. Reimer, S. C. Weston and J. R. Long, *Science*, 2020, **369**, 392–396.
244 A. Kumar, D. G. Madden, M. Lusi, K.-J. Chen, E. A. Daniels, T. Curtin, J. J. Perry and M. J. Zaworotko, *Angew. Chem., Int. Ed.*, 2015, **54**, 14372–14377.
245 A. R. Millward and O. M. Yaghi, *J. Am. Chem. Soc.*, 2005, **127**, 17998–17999.
246 C. Tan, S. Yang, N. R. Champness, X. Lin, A. J. Blake, W. Lewis and M. Schroder, *Chem. Commun.*, 2011, **47**, 4487–4489.
247 N. T. T. Nguyen, H. Furukawa, F. Gandara, H. T. Nguyen, K. E. Cordova and O. M. Yaghi, *Angew. Chem., Int. Ed.*, 2014, **53**, 10645–10648.
248 X. Zha, X. Li, A. A. Al-Omari, S. Liu, C. C. Liang, A. Al-Ghourani, M. Abdellatief, J. Yang, H. L. Nguyen, B. Al-Maythalony, Z. Shi, K. E. Cordova and Y. B. Zhang, *Angew. Chem., Int. Ed.*, 2022, **61**, e202207467.
249 Z. Shi, Y. Tao, J. Wu, C. Zhang, H. He, L. Long, Y. Lee, T. Li and Y.-B. Zhang, *J. Am. Chem. Soc.*, 2020, **142**, 2750–2754.
250 Y. Shi, Y. Xie, H. Cui, Z. A. Alothman, O. Alduhaish, R.-B. Lin and B. Chen, *Chem. Eng. J.*, 2022, **446**, 137101.
251 Y. Hu, Y. Jiang, J. Li, L. Wang, M. Steiner, R. F. Neumann, B. Luan and Y. Zhang, *Adv. Funct. Mater.*, 2023, **33**, 2213915.
252 C. Yu, Q. Ding, J. Hu, Q. Wang, X. Cui and H. Xing, *Chem. Eng. J.*, 2021, **405**, 126937.
253 M. Wriedt, J. P. Sculley, A. A. Yakovenko, Y. Ma, G. J. Halder, P. B. Balbuena and H.-C. Zhou, *Angew. Chem., Int. Ed.*, 2012, **51**, 9804–9808.
254 D. G. Madden, A. B. Albadarin, D. O'Nolan, P. Cronin, J. J. Perry, S. Solomon, T. Curtin, M. Khraisheh, M. J. Zaworotko and G. M. Walker, *ACS Appl. Mater. Interfaces*, 2020, **12**, 33759–33764.
255 S. R. Caskey, A. G. Wong-Foy and A. J. Matzger, *J. Am. Chem. Soc.*, 2008, **130**, 10870–10871.
256 Q. G. Zhai, X. Bu, C. Mao, X. Zhao, L. Daemen, Y. Cheng, A. J. Ramirez-Cuesta and P. Feng, *Nat. Commun.*, 2016, **7**, 13645.
257 Y.-Y. Xue, S.-N. Li, Y.-C. Jiang, M.-C. Hu and Q.-G. Zhai, *J. Mater. Chem. A*, 2019, **7**, 4640–4650.
258 R. L. Siegelman, J. A. Thompson, J. A. Mason, T. M. McDonald and J. R. Long, *Chem. Sci.*, 2022, **13**, 11772–11784.
259 Y. Shen, Z. Li, L. Wang, Y. Ye, Q. Liu, X. Ma, Q. Chen, Z. Zhang and S. Xiang, *J. Mater. Chem. A*, 2015, **3**, 593–599.
260 J. Lu, C. Perez-Krap, M. Suyetin, N. H. Alsmail, Y. Yan, S. Yang, W. Lewis, E. Bichoutskaia, C. C. Tang, A. J. Blake, R. Cao and M. Schroder, *J. Am. Chem. Soc.*, 2014, **136**, 12828–12831.
261 X.-W. Zhang, D.-D. Zhou and J.-P. Zhang, *Chem*, 2021, **7**, 1006–1019.
262 O. T. Qazvini, R. Babarao and S. G. Telfer, *Nat. Commun.*, 2021, **12**, 197.
263 J.-B. Lin, W. Xue, J.-P. Zhang and X.-M. Chen, *Chem. Commun.*, 2011, **47**, 926–928.
264 R.-B. Lin, L. Li, A. Alsalme and B. Chen, *Small Struct.*, 2020, **1**, 2000022.
265 R. B. Lin, L. Li, H. L. Zhou, H. Wu, C. He, S. Li, R. Krishna, J. Li, W. Zhou and B. Chen, *Nat. Mater.*, 2018, **17**, 1128–1133.

266 A. Cadiau, Y. Belmabkhout, K. Adil, P. M. Bhatt, R. S. Pillai, A. Shkurenko, C. Martineau-Corcos, G. Maurin and M. Eddaoudi, *Science*, 2017, **356**, 731–735.
267 Y. Belmabkhout, P. M. Bhatt, K. Adil, R. S. Pillai, A. Cadiau, A. Shkurenkol, G. Maurin, G. P. Liu, W. Koros and M. Eddaoudi, *Nat. Energy*, 2018, **3**, 1059–1066.
268 S. Choi, T. Watanabe, T. H. Bae, D. S. Sholl and C. W. Jones, *J. Phys. Chem. Lett.*, 2012, **3**, 1136–1141.
269 X. Song, M. Zhang, C. Chen, J. Duan, W. Zhang, Y. Pan and J. Bai, *Chem. Commun.*, 2019, **55**, 3477–3480.
270 Z. Q. Zhang, Q. Ding, S. B. Peh, D. Zhao, J. Y. Cui, X. L. Cui and H. B. Xing, *Chem. Commun.*, 2020, **56**, 7726–7729.
271 C. Wang, L. Li, S. Tang and X. Zhao, *ACS Appl. Mater. Interfaces*, 2014, **6**, 16932–16940.
272 N. C. Burtch, I. M. Walton, J. T. Hungerford, C. R. Morelock, Y. Jiao, J. Heinen, Y.-S. Chen, A. A. Yakovenko, W. Xu, D. Dubbeldam and K. S. Walton, *Nat. Chem.*, 2020, **12**, 186–192.
273 S. Xiong, Y. Gong, H. Wang, H. Wang, Q. Liu, M. Gu, X. Wang, B. Chen and Z. Wang, *Chem. Commun.*, 2014, **50**, 12101–12104.
274 O. Alduhaish, R.-B. Lin, H. Wang, B. Li, H. D. Arman, T.-L. Hu and B. Chen, *Cryst. Growth Des.*, 2018, **18**, 4522–4527.
275 Y. Chen, D. Lv, J. Wu, J. Xiao, H. Xi, Q. Xia and Z. Li, *Chem. Eng. J.*, 2017, **308**, 1065–1072.
276 P. Das and S. K. Mandal, *ACS Appl. Mater. Interfaces*, 2020, **12**, 37137–37146.
277 M. H. Mohamed, S. K. Elsaidi, T. Pham, K. A. Forrest, B. Tudor, L. Wojtas, B. Space and M. J. Zaworotko, *Chem. Commun.*, 2013, **49**, 9809–9811.
278 N. Seal, M. Singh, S. Das, R. Goswami, B. Pathak and S. Neogi, *Mater. Chem. Front.*, 2021, **5**, 979–994.
279 R. Goswami, N. Seal, S. R. Dash, A. Tyagi and S. Neogi, *ACS Appl. Mater. Interfaces*, 2019, **11**, 40134–40150.
280 A. Pal, S. Chand and M. C. Das, *Inorg. Chem.*, 2017, **56**, 13991–13997.
281 V. Gupta and S. K. Mandal, *Dalton Trans.*, 2019, **48**, 415–425.
282 L. Fan, S. Lin, X. Wang, L. Yue, T. Xu, Z. Jiang and Y. He, *Inorg. Chem.*, 2021, **60**, 2704–2715.
283 L. Bastin, P. S. Bárcia, E. J. Hurtado, J. A. C. Silva, A. E. Rodrigues and B. Chen, *J. Phys. Chem. C*, 2008, **112**, 1575–1581.
284 H. Liu, Y. Zhao, Z. Zhang, N. Nijem, Y. J. Chabal, H. Zeng and J. Li, *Adv. Funct. Mater.*, 2011, **21**, 4754–4762.